Calhoun
Institutional Archive of the Naval Postgraduate School

Calhoun: The NPS Institutional Archive

DSpace Repository

Theses and Dissertations | 1. Thesis and Dissertation Collection, all items

2015-12

Precision guidance of a rocket using Pseudospectral optimal control

Barton, Rachel M.

Monterey, California. Naval Postgraduate School

http://hdl.handle.net/10945/63151

Downloaded from NPS Archive: Calhoun

http://www.nps.edu/library

Calhoun is a project of the Dudley Knox Library at NPS, furthering the precepts and goals of open government and government transparency. All information contained herein has been approved for release by the NPS Public Affairs Officer.

Dudley Knox Library / Naval Postgraduate School
411 Dyer Road / 1 University Circle
Monterey, California USA 93943

NAVAL POSTGRADUATE SCHOOL

MONTEREY, CALIFORNIA

THESIS

PRECISION GUIDANCE OF A ROCKET USING PSEUDOSPECTRAL OPTIMAL CONTROL

by

Rachel M. Barton

December 2015

Thesis Advisor: Mark Karpenko
Second Reader: I. Michael Ross

Approved for public release; distribution is unlimited

THIS PAGE INTENTIONALLY LEFT BLANK

REPORT DOCUMENTATION PAGE			*Form Approved OMB No. 0704–0188*
Public reporting burden for this collection of information is estimated to average 1 hour per response, including the time for reviewing instruction, searching existing data sources, gathering and maintaining the data needed, and completing and reviewing the collection of information. Send comments regarding this burden estimate or any other aspect of this collection of information, including suggestions for reducing this burden, to Washington headquarters Services, Directorate for Information Operations and Reports, 1215 Jefferson Davis Highway, Suite 1204, Arlington, VA 22202–4302, and to the Office of Management and Budget, Paperwork Reduction Project (0704–0188) Washington DC 20503.			
1. AGENCY USE ONLY ***(Leave blank)***	**2. REPORT DATE** December 2015	**3. REPORT TYPE AND DATES COVERED** Master's thesis	
4. TITLE AND SUBTITLE PRECISION GUIDANCE OF A ROCKET USING PSEUDOSPECTRAL OPTIMAL CONTROL		**5. FUNDING NUMBERS**	
6. AUTHOR(S) Rachel M. Barton			
7. PERFORMING ORGANIZATION NAME(S) AND ADDRESS(ES) Naval Postgraduate School Monterey, CA 93943–5000		**8. PERFORMING ORGANIZATION REPORT NUMBER**	
9. SPONSORING /MONITORING AGENCY NAME(S) AND ADDRESS(ES) N/A		**10. SPONSORING / MONITORING AGENCY REPORT NUMBER**	
11. SUPPLEMENTARY NOTES The views expressed in this thesis are those of the author and do not reflect the official policy or position of the Department of Defense or the U.S. Government. IRB Protocol number ____N/A____.			
12a. DISTRIBUTION / AVAILABILITY STATEMENT Approved for public release; distribution is unlimited		**12b. DISTRIBUTION CODE**	

13. ABSTRACT (maximum 200 words)

Maximum range and minimum time maneuvers for a rocket are vital to the war fighter since weapons that can intercept targets faster or travel farther provide advantages that increase the chances of mission success. Yet, guidance laws for tactical rockets are based on principles that have been in use since World War II. This thesis applies Pseudospectral optimal control theory to assess the achievable performance of a guided rocket in the terminal stage of flight. The performance is compared to a baseline obtained using conventional control (proportional navigation). For a fictitious missile, an optimal control solution is shown to increase the range of the missile by nearly 300% in the mid-to-terminal phase of flight. A minimum time solution showed a reduction in flight time by about 40% compared to the conventional proportional navigation-based approach.

14. SUBJECT TERMS Optimal control, rocket, maximum range problem, minimum time problem, DIDO, trajectory optimization			**15. NUMBER OF PAGES** 127
			16. PRICE CODE
17. SECURITY CLASSIFICATION OF REPORT Unclassified	**18. SECURITY CLASSIFICATION OF THIS PAGE** Unclassified	**19. SECURITY CLASSIFICATION OF ABSTRACT** Unclassified	**20. LIMITATION OF ABSTRACT** UU

NSN 7540–01–280–5500 Standard Form 298 (Rev. 2–89)
Prescribed by ANSI Std. 239–18

THIS PAGE INTENTIONALLY LEFT BLANK

Approved for public release; distribution is unlimited

PRECISION GUIDANCE OF A ROCKET USING PSEUDOSPECTRAL OPTIMAL CONTROL

Rachel M. Barton
Lieutenant, United States Navy
B.S., United States Naval Academy, 2007

Submitted in partial fulfillment of the
requirements for the degree of

MASTER OF SCIENCE IN ASTRONAUTICAL ENGINEERING

from the

NAVAL POSTGRADUATE SCHOOL
December 2015

Approved by: Mark Karpenko
Thesis Advisor

I. Michael Ross
Second Reader

Garth V. Hobson
Chair, Department of Mechanical and Aerospace Engineering

THIS PAGE INTENTIONALLY LEFT BLANK

ABSTRACT

Maximum range and minimum time maneuvers for a rocket are vital to the war fighter since weapons that can intercept targets faster or travel farther provide advantages that increase the chances of mission success. Yet, guidance laws for tactical rockets are based on principles that have been in use since World War II. This thesis applies Pseudospectral optimal control theory to assess the achievable performance of a guided rocket in the terminal stage of flight. The performance is compared to a baseline obtained using conventional control (proportional navigation). For a fictitious missile, an optimal control solution is shown to increase the range of the missile by nearly 300% in the mid-to-terminal phase of flight. A minimum time solution showed a reduction in flight time by about 40% compared to the conventional proportional navigation-based approach.

THIS PAGE INTENTIONALLY LEFT BLANK

TABLE OF CONTENTS

LIST OF FIGURES

THIS PAGE INTENTIONALLY LEFT BLANK

LIST OF TABLES

THIS PAGE INTENTIONALLY LEFT BLANK

LIST OF ACRONYMS AND ABBREVIATIONS

3DOF	three degree-of-freedom
6DOF	six degree-of-freedom
AoA	angle of attack
BVP	boundary value problem
CG	center of gravity
CU	cost unit
DOF	degrees of freedom
DU	distance unit
EoM	equations of motion
GNC	guidance, navigation, and control
HMC	Hamiltonian Minimization Condition
IMU	inertial measurement unit
LOAL-LO	lock-on after launch- low
LOAL-HI	lock-on after launch- high
LOS	line of sight
NED	north, east, down
NPS	Naval Postgraduate School
OCP	optimal control problem
ODE	ordinary differential equation
rad	radian
TU	time unit

THIS PAGE INTENTIONALLY LEFT BLANK

LIST OF SYMBOLS

α	angle of attack (rad)
β	side slip angle (rad)
$\underline{\delta}$	fin deflection (rad)
μ	bank angle (rad)
γ	pitch angle (rad)
σ	heading angle (rad)
ρ	air density (kg/m^3)
λ	line-of-sight angle (rad)
λ	costate
φ	yaw (Euler angle, rad)
θ	pitch (Euler angle, rad)
ψ	roll (Euler angle, rad)
b	reference aerodynamic span (m)
$\bar{c}$	reference aerodynamic chord (m)
C_A	axial force coefficient along x-axis in body frame
C_N	normal force coefficient along z-axis in body frame
C_D	coefficient of drag
C_L	coefficient of lift
d	diameter (m)
D	drag force (N)
E	endpoint or event cost function
e	endpoint or event constraint function
g	acceleration due to gravity (m/s^2)
H	Hamiltonian value
I	moment of inertia ($kg\ m^2$)
J	scalar cost functional
l	length (m)
L	lift force (N)

L	rolling moment (kg m^2)
l_{fs}	fin span (m)
l_{ws}	wing span (m)
m	mass (kg)
M	Mach number
M	pitching moment (kg m^2)
N	yawing moment (kg m^2)
N’	effective navigation ratio
p	pitch rate (rad/s)
q	roll rate (rad/s)
r	yaw rate (rad/s)
R_{TM}	range of target to missile (m)
t	time (sec)
T	thrust (N)
u	control variable
u_α	AoA control (rad/s)
u_μ	bank angle control (rad/s)
v	velocity (m/s)
x	state vector
x	downrange distance (m)
X	axial force (N)
y	cross-range distance (m)
Y	side force (N)
z	altitude (m)
Z	normal force (N)

ACKNOWLEDGMENTS

I would like to extend my deepest gratitude to my thesis advisors, Dr. Mark Karpenko and Dr. Mike Ross, for your guidance, patience, and help throughout this process, and for providing me with an interesting topic that not only met the academic requirements but has real-world military applications.

Thank you to my classmates for your help throughout my time at NPS, for being a sounding board; for discussing ideas when one of us was stuck. I have learned something from every one of you and I am grateful that I was blessed with the opportunity to meet and work beside you.

Lastly, thank you to my family for your boundless love and support. Your unending encouragement has kept me going throughout this process, and I would not have been able to make it through without you.

THIS PAGE INTENTIONALLY LEFT BLANK

I. INTRODUCTION

A. BACKGROUND

One area that needs to be addressed prior to any discussion is: what is the difference between a missile and a rocket? While the exact definition varies from source to source, the general consensus throughout the aerospace community is that "a missile has a guidance system or brain to get it to its destination and a rocket just goes where it is initially pointed" [1]. The U.S. Bureau of Naval Personnel defines a guided missile as "an unmanned vehicle that travels above the earth's surface; it carries an explosive war head or other useful payload; and it contains within itself some means for controlling its own trajectory or flight path" [2]. The terms guided rocket and missile are used interchangeably throughout this thesis.

Prior to World War I, missiles and bombs were essentially shot or dropped on a certain trajectory, and there was no capability to control the device after its release. The concept for guided missiles was first conceived during World War I. The tactical use of aircraft in World War I raised the question as to whether a plane could be remotely controlled and used to bomb a target. The first guided missiles that emerged were small versions of the aircraft that were currently being flown by utilizing radio control [3]. It was not until World War II though, that tactical guided missiles began to emerge on the scene.

Today, guided missiles are an integrated part of the United States Order of Battle. The guidance system for a missile allows it to find a path to intercept the target "in spite of initial launching errors, in spite of wind or other forces acting on the missile, and in spite of any evasive actions the target may take" [2]. There are currently several types of guidance modes that are used in guided missiles, including command guidance, homing guidance, and navigational guidance. A missile may have more than one type of guidance system, with different systems engaging at different stages of flight.

1. Early Guided Rockets

The first guided missiles appeared in Germany during World War II. The most widely known missiles that were produced during this time were the V-1 and the V-2. The V-1 was a "pilotless, pulsejet, midwing, monoplane, lacking ailerons but using conventional airframe and tail construction" [2], shown in Figure 1. The guidance and control for the missile was done using an internally stabilized gyro and the existing compass guidance. These "missile fixed rate gyros were used to provide attitude rate signals for stabilization" [4]. The missile was not very accurate but its massive warhead caused significant damage if it hit the intended target. However, the V-1 was slow and approximately 95% of the missiles launched against England were brought down by anti-aircraft fire [2].

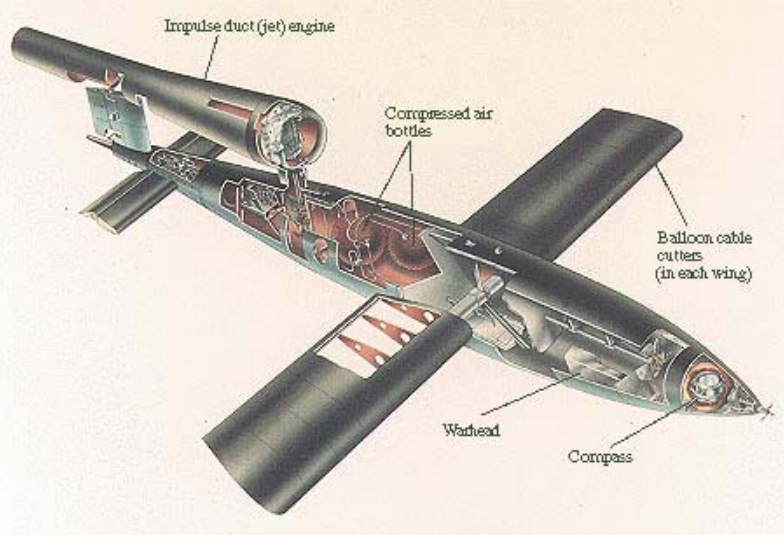

Figure 1. V-1 Missile

Source [5]: Warbirds Resource Group, "Fi-103/V-1 'Buzz Bomb'," 2015 (November 12).

The V-2, shown in Figure 2, was a much larger than the V-1 and had a liquid-fuel rocket propulsion system. The missile was launched using a vertical launch system. Prior to launch the system was loaded with a command angle that would cause the missile to rotate to a predetermined angle, between 41- to 47-degrees, shortly after launch. The launch speed required to reach the target would also be determined prior to launch and

when the missile reached the desired velocity, a radio command would be sent to the rocket and the propulsion system would be shut down. This was accomplished by utilizing the Doppler Effect to determine the missile velocity. The missile utilized a Wien bridge and the beat frequency of the return signal would be sent to the bridge in addition to the ground station's frequency second harmonic. Prior to launch a beat frequency would have been calculated corresponding to the desired cutoff velocity. When the received frequency matched the preset frequency, a command was transmitted to the missile to initiate the cutoff of the propulsion system [4]. Once the propulsion system was shut down, the range of the rocket was only about 320 km, it would reach speeds of approximately 1475 m/s. While the missile was not very accurate, its high speed made countermeasures impossible and "no V-2 missile was ever intercepted or shot down by anti-aircraft fire" [2].

Figure 2. German V-2 Rocket

Source [6]: Arkell, H., 2014, "Death from Above without Warning: 70 Years After the First One Fell, Interactive Map Reveals just Where Hitler's V2 Rockets Killed Thousands of British Civilians in Final Months of WW2," 2015 (November 12). Daily Mail.

On the other side of the Atlantic, the United States initiated the development of the Lark missile, shown in Figure 3, under a guided missile development program in

response to the effective Kamikaze attack against U.S. ships. In December of 1950, the first successful intercept of a guided missile against an unmanned aircraft was made [7]. The missile used an active continuous wave radar onboard the missile. Reflections from the target would be displaced in frequency by the Doppler Effect. However, the missile would also be receiving inputs from the ground, and once the stationary inputs were rejected, the missile would be left with the corresponding frequency to the moving target [8]. However, this type of guidance presented several fundamental problems. The first problem was that the Doppler shift from the target was not very large. The second problem was that there was a large amount of clutter in the return signal. The need for low-noise microwave sources became a critical part of the continuous wave radar development as a result of these issues [8]. At the end of World War II, the inertial sensors were limited in their accuracy due to the fiction in the ball and pivot bearings causing errors. Later, by utilizing cylindrical gas bearings that were externally pressurized, the accuracy of the internal sensors increased significantly [4]. These improvements paved the way for modern guidance systems.

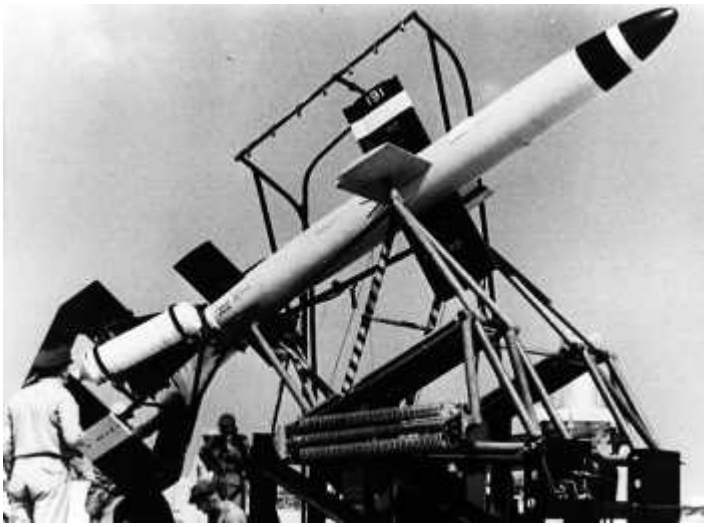

Figure 3. Lark Guided Missile

Source [9]: Parsch, A., "Lark," Encyclopedia Astronautica, 2015(November 14).

2. Modern Missile Guidance, Navigation, and Control Systems

A basic block diagram for a modern guidance, navigation, and control (GNC) system for a missile is shown in Figure 4. The main components include a weapon control system, sensors, flight controller, and airframe subsystems that control the missile. A more in-depth description of the GNC system is found in [10]. The weapon control system is ground or air based and allows the user to send commands to the missile and also receives flight data that is sent from the missile flight computer.

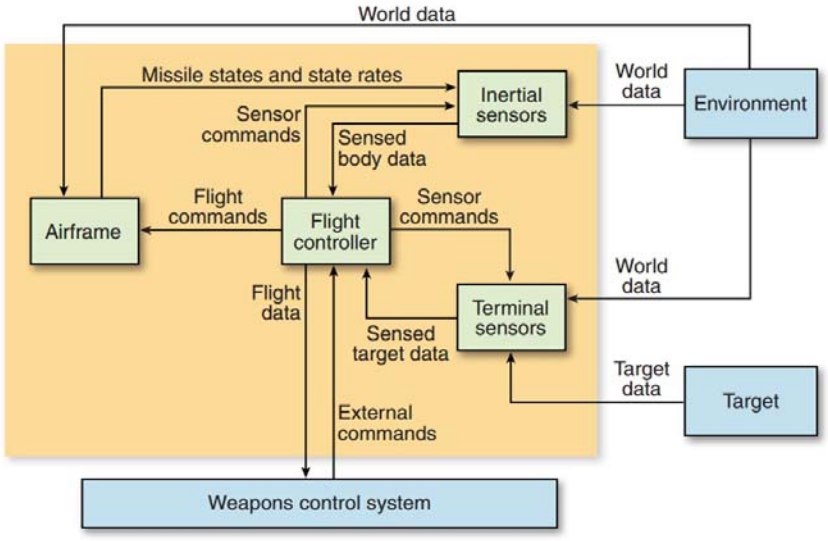

Figure 4. Basic GNC System for a Missile

Source [10]: Hawley, P. A., and Blauwkamp, R. A., 2010, "Six-Degree-of-Freedom Digital Simulations for Missile Guidance, Navigation, and Control," John Hopkins APL Technical Digest, Vol 29(No. 1) pp. 71–84.

The missile also contains two types of sensors, inertial sensors for determining where the missile is located in space and terminal sensors for determining where the target is in relation to the missile. The most commonly used inertial sensors include inertial measurement units, inertial reference units, and GPS. One or more of these sensors may be used to measure and/or help estimate the states of the missile. The terminal sensors for a missile will be based on the type of guidance system the missile

utilizes. Some of the more common sensors include radar, radio frequency seekers, and infrared seekers.

The flight controller is the brains of the missile and includes the navigation processor, guidance processor, and autopilot. The navigation processor uses external commands from the weapons control system and inertial sensor data to estimate the states and rates for the missile. This information is passed on to the guidance processor. The guidance processor receives inputs from the terminal sensor, the navigation processor and the weapons control system. It then computes and outputs a guidance command that is sent to the autopilot for implementation and sends sensor commands to the terminal sensors. The guidance law for a missile is implemented in the guidance processor, while the autopilot is used to convert the guidance signal into flight commands that will be sent to the airframe [10].

The flight commands from the autopilot are sent to either the propulsion system or the flight control actuators for the missile. The propulsion system will make any needed adjustments and the system may also output the mass of the propulsion that has been burned to determine the airframe mass changes. The flight control actuators adjust the flight control surfaces to produce an aerodynamic response. The propulsion forces and moments, airframe mass changes, and aerodynamic forces and moments are used to estimate the state and state rates for the missile. These states and state rates are used along with inertial sensors and environmental data to determine where the missile is located in space.

The U.S. Armed Forces currently has dozens of different types of guided rockets in their Order of Battle today that can be launched from land, sea, and the air. They range from ballistic guided missiles (e.g., Trident II D5), shown in Figure 5, to laser-guided rockets (e.g., APKWSTM), shown in Figure 6, to active radar homing (e.g. AIM-120 AMRAAM), anti-radiation homing (e.g., AGM-88 HARM), and GPS guided (e.g., UGM-133 Trident II). While tactical missiles that are used today are able to hit targets much more accurately, this is mainly due to improvements of the sensors in the missiles rather than the evolution of the overarching principles governing the guidance

control. In fact, the same guidance principals that were used for the Lark in 1950, are still being used today [7].

Figure 5. Trident II D5 Fleet Ballistic Missile

Source [11]: Lockheed Martin, 2014, "Trident II D5 Missile Reaches 150 Successful Test Flights," 2015(Nov 13).

Figure 6. Laser-Guided APKWS Rocket

Source [12]: Sax, L. R., 2015, "U.S. Army Acquires APKWS™ Laser-Guided Rockets for Immediate Deployment," 2015(Nov 13).

For example, consider the AGM-114A is the original Hellfire missile that was used by the Army. It was fired from the air and one of the delivery modes for the missile

was Lock-on After Launch (LOAL). The LOAL profile allowed the aircrew to fire a missile in the general direction of a target without having a line-of-sight lock on the target. Within this profile, there are two delivery modes where the aircraft is able to be masked behind terrain when firing to reduce the risk to the aircraft: low and high. In LOAL-LO, shown in Figure 7, the missile is to clear 79.25 m (260 ft) of terrain with the aircraft located 600 m behind the highest terrain point. In LOAL-HI, shown in Figure 8, the missile can clear 304.8 m (1000 ft) of terrain with a 1500 m aircraft standoff distance. The missile utilizes a laser seeker located in the missile nose, which is programed prior to launch, to identify a specific laser code and lock onto the laser emission. For this missile, the laser seeker is the terminal sensor and after the missile obtains a lock on the target, the information from the seeker is sent to the guidance processor which then determines the appropriate steering command to be sent to the flight controls and the missile then tracks to the target [13]. While the laser seeker allows for increased accuracy in hitting the target, compared to the missiles used in World War II, the guidance law for the missile remains unchanged.

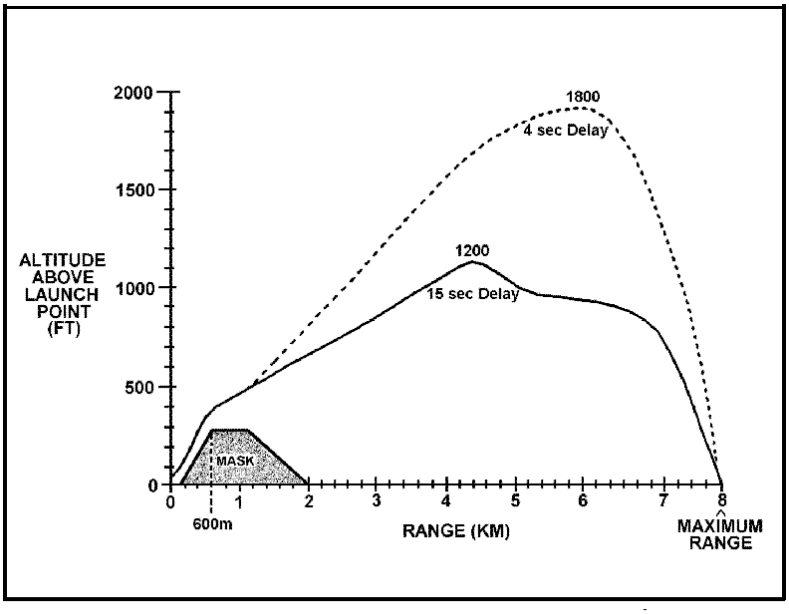

Figure 7. AGM-114A LOAL-LO Trajectory

Source [13]: Lange, A. W., 1998, "Hellfire: Getting the most from a Lethal Missile System," Armor, Jan-Feb, pp. 25–30.

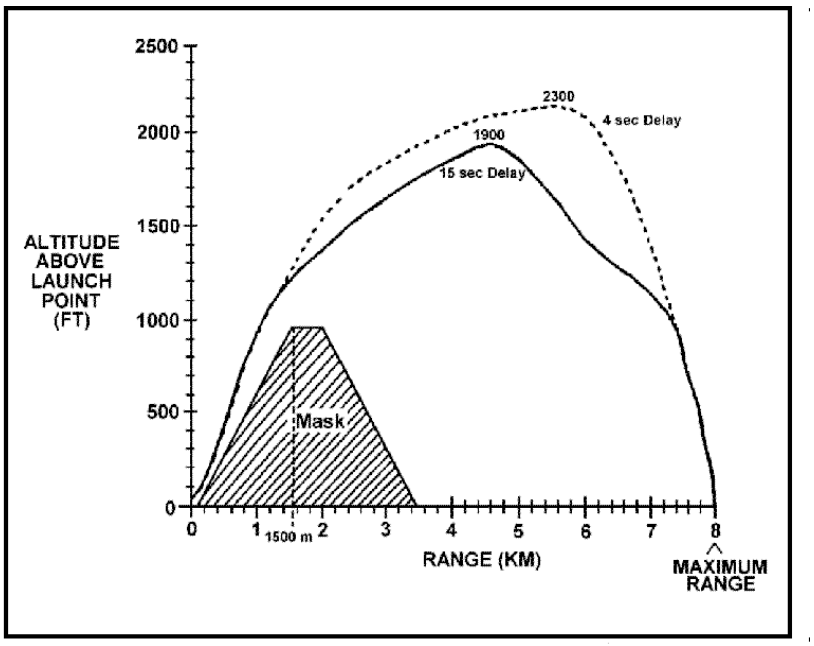

Figure 8. AGM 114-A LOAL-HI Trajectory

Source [13]: Lange, A. W., 1998, "Hellfire: Getting the most from a Lethal Missile System," Armor, Jan-Feb, pp. 25–30.

B. MOTIVATION AND SCOPE

A paper written by Lin [14], states:

Many long- and medium-range missile guidance studies have shown that optimal trajectory shaping promises an extended range with more favorable end-game conditions… However, in a three-dimensional, target-intercept flight, direct application of the optimal control theory will result in a two-point boundary value problem that involves several arbitrary parameters so that analytical solutions cannot be obtained without a lot of approximations. The problem can be further complicated with the lift, thrust and drag, and control constraints forced by structural and angle-of-attack limits. This increases the computational time so that it is not feasible to implement the resulting solutions of the missile performance within an onboard digital computer. In view of this complexity in the problem setup, either indirect methods or direct methods based on nonlinear programming are used to solve the sensitivity and convergence problems. However, both methods require very fast onboard microprocessor technology for real-time, on-line operation. [14]

It is now almost 30 years since this article was written, and the same challenges still exist today. The dynamic equations that govern a three-dimensional 6DOF model for a missile are complex. The equations consist of nonlinear trigonometric functions that present potential singularity problems. In addition, aerodynamic coefficients typically come in tables aerodynamic forces must be "built-up" so that the dynamics can be evaluated.

The boundary value problem for solving the optimal control contains a set of prescribed boundary conditions and also a set of constraints on the problem variables. The boundary conditions can be set values or functions. Airframes have limits that are applied to the angle of attack or acceleration, for example. The solution for the boundary value problem must therefore be constrained by these limits. In order to solve a boundary value problem, the underlying differential equations (e.g., the 6-DOF dynamics) need to be solved while simultaneously satisfying the constraints of the bounds [15]. The large number of constraints that are applied to the guidance of a missile, as described in the quote above, have led to difficulties in solving these boundary value problems in the past. Today, however, advanced tools are available to overcome these challenges, [15], [16].

As mentioned above, the principles that are used to control guided rockets today are the same principles used on some of the first guided rockets. The motivation behind this thesis is to examine how advances that have been made in optimal control theory might be used to change the way that guided rockets are controlled. The goal is to determine if a tactical advantage, such as enhanced range, can be obtained via a software solution only. Such a solution is advantageous in that its implementation would not change any of the physical characteristics of the missile.

In a warfighting environment, the difference between life and death for a solider comes down to being able to maintain a tactical advantage over the enemy. This advantage can come in many forms. For example, if applying an optimal control solution to the guidance of a rocket can increase the range or reduce the time of flight, it can provide our troops with an increased advantage in the battlefield.

The basic principles of the GNC that are used on tactical missiles, not only apply to missiles within the Earth's atmosphere but also apply to other systems such as intercontinental ballistic missiles, spacecraft performing close proximity rendezvous operations, and UAVs. Therefore, the results of this thesis could influence how guidance is done for these systems as well.

C. THESIS ORGANIZATION

The remainder of this thesis is organized as follows. Chapter II introduces the model of the fictitious rocket used in this work. In addition, the 3DOF and 6DOF models that can be used to simulate the flight of the guided rocket are introduced and the pros and cons of each are discussed. The software used to determine the coefficients of lift and drag is introduced, as well as the development of the coefficient of lift and drag equations. Chapter III presents the conventional proportional navigation approach that has long been used for guidance of the rockets. In addition, a maximum range maneuver is simulated to establish a baseline performance that can be used to compare against the results achieved through optimal control. In Chapter IV the Optimal Control Theory is introduced in order to provide the necessary background on the subject for the reader. In addition, this chapter introduces the optimal control software DIDO. This software package is used to solve the optimal missile trajectories. Chapter V discusses the maximum range problem and the steps that were taken in order to solve it. In addition, some of the challenges that were encountered when attempting to obtain the solution are discussed. Chapter VI presents some conclusions and suggestions for future work.

THIS PAGE INTENTIONALLY LEFT BLANK

II. GUIDED ROCKET MODEL

This chapter covers the development of the model for the tactical missile that will be used for simulations in this thesis. It introduces not only the physical characteristics of the model but also the assumptions that were made in regard to the model. The reference frames and equations of motion for the missile are also introduced. This chapter also shows the development of the coefficients of lift and drag for the missile using the Missile DATCOM software [17].

A. DEVELOPING THE MODEL

The first step in creating the model was to choose the physical configuration of a fictitious missile. In order to create a process that could be adapted to any missile, a generic rocket was created that is similar to the larger tactical missiles currently fired from aircraft, which are categorized as medium-range missiles. This size of missile was chosen with the intent that the model could later be scaled up or down in order to mimic different systems.

1. Guided Rocket Configuration

a. Physical Characteristics

The model for the rocket, shown in Figure 9, has a cylindrical body with a cone shaped nose and contains four wings and four tail fins.

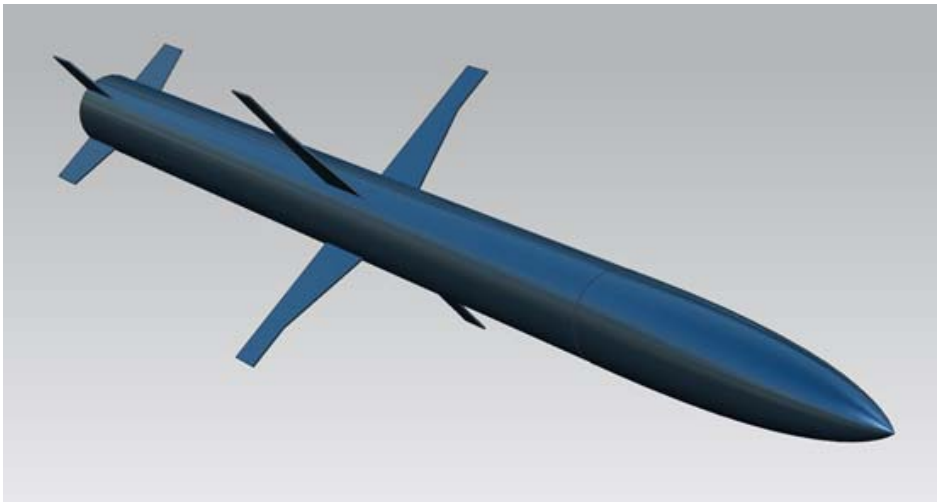

Figure 9. Image of a Fictitious Guided Missile

The fictitious guided rocket is 4.14 m in length with a wingspan of 1.01 m. The diameter of the rocket is 0.254 m around the tube, shown in Figure 10. The center of gravity for the guided rocket was placed at 2.08 m. The mass of the guided rocket is 360 kg. The guided rocket has two different sets of fins attached. The first set is a set of tail fins that are located on the tail end of the rocket and the second set is in the middle of the rocket and are referred to as the wings.

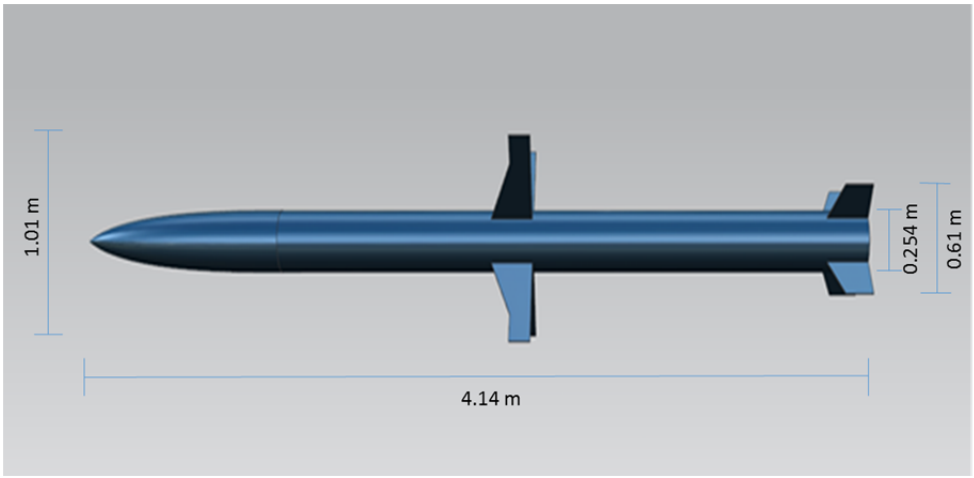

Figure 10. Image of the Model from the Side with Dimensions

Each wing of the guided rocket is 0.432 m with a width of 0.216 m where the wing attaches to the rocket body. The leading edge of the wing is tapered and has decreasing slope for the first two thirds of the wing span and then levels out for the last third. The width of the wing at the tail end is 0.108 m as shown in Figure 11. There are four wings on the missile that are mounted at 45° increments around the missile body (see Figure 12).

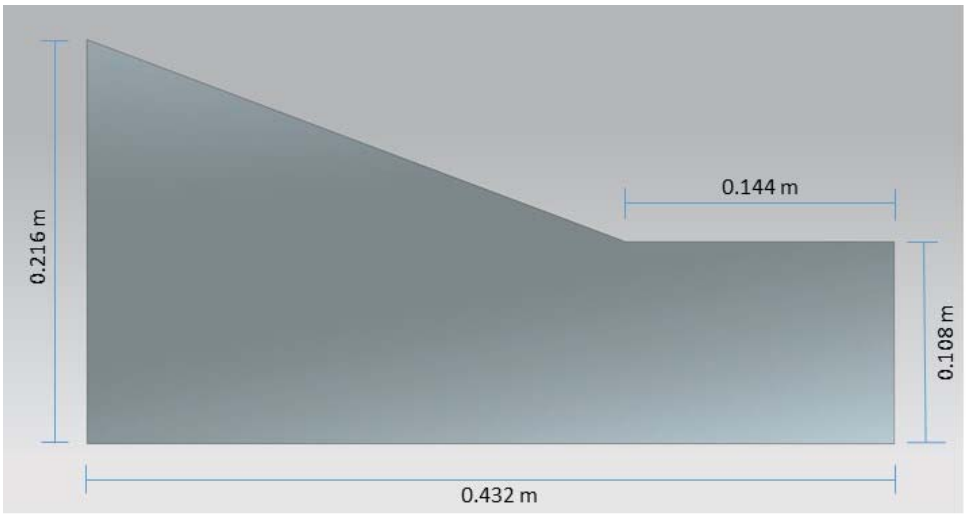

Figure 11. Missile Wing Dimensions

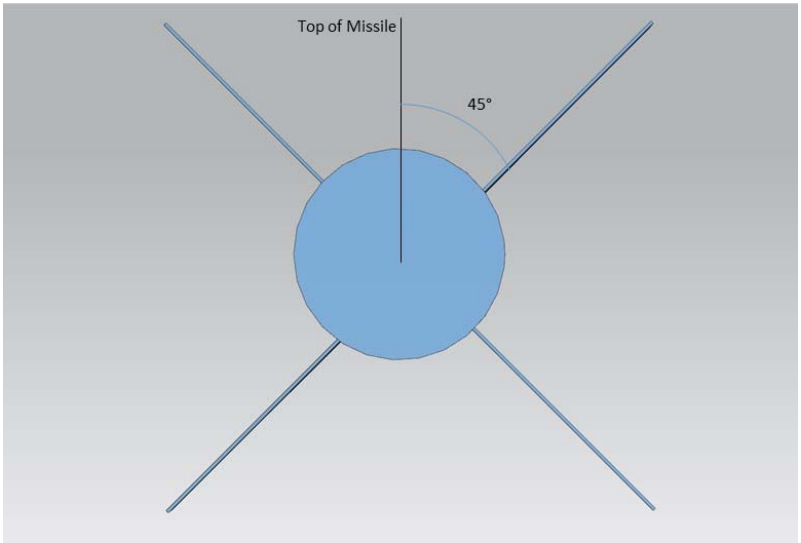

Figure 12. Orientation of Wings on the Missile

In addition, there are four tail fins that are mounted on the tail end of the missile. The fins are 0.178 m with a width of 0.216 m where the fin attaches to the body. The fins are tapered and at the outside edge are a width of 0.144 m, shown in Figure 13.

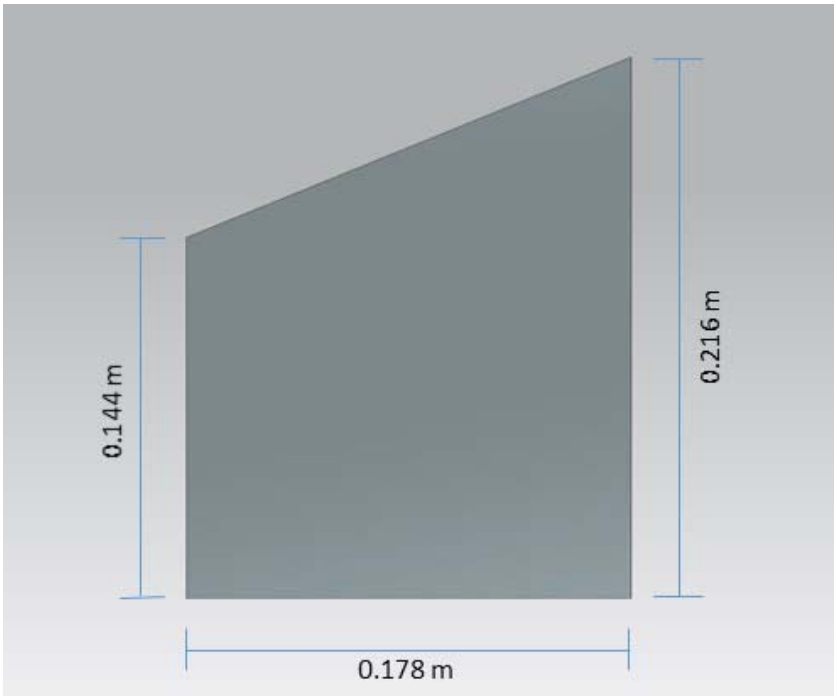

Figure 13. Missile Fins

The 6DOF equations of motion which are discussed in the next section of this chapter, also require a reference aerodynamic chord and reference aerodynamic span. These values are 0.063 m and 1.12 m, respectively. A summary of the physical characteristics of the missile is given in Table 1.

Table 1. Summary of Physical Characteristics for a Fictitious Missile

Parameter	Symbol	Value	Units
Mass	m	360	kg
Length	l	4.14	m
Diameter	d	0.83	m
Wing span	l_{ws}	1.01	m
Fin span	l_{fs}	0.61	m
Center of gravity	CG	2.08	m
Reference aerodynamic chord	$\bar{c}$	0.06	m
Reference aerodynamic span	b	1.12	m
Cross sectional area	S_{ref}	0.05	m^2

b. Performance Characteristics

In addition to designing the missile geometry, performance characteristics need to be created for the missile in order to be able to carry out control system design. These numbers were estimated by looking at a variety existing platforms and estimating values that would be in the same order of magnitude for a similar model. When the process described in this thesis is applied to an actual missile and more accurate numbers are available, the results that are produced from the control design and analysis will better reflect reality. The estimated performance values are listed in Table 2.

Table 2. Performance Characteristics for a Fictitious Missile

Parameter	Symbol	Value	Units
Minimum velocity	V_{min}	100	m/s
Maximum velocity	V_{max}	639	m/s
Minimum thrust	T_{min}	0.00	N
Maximum thrust	T_{max}	10000	N

2. 6DOF Dynamics Model

In a 6DOF dynamic model, all six degrees of freedom for the guided rocket are taken into account in regard to the rocket motion. There are three translational degrees of freedom and three rotational. The six degrees of freedom result in a total of twelve non-linear state equations.

a. Reference Frame

The 6DOF model uses a flat-Earth NED as a reference frame for position, as shown in Figure 14.

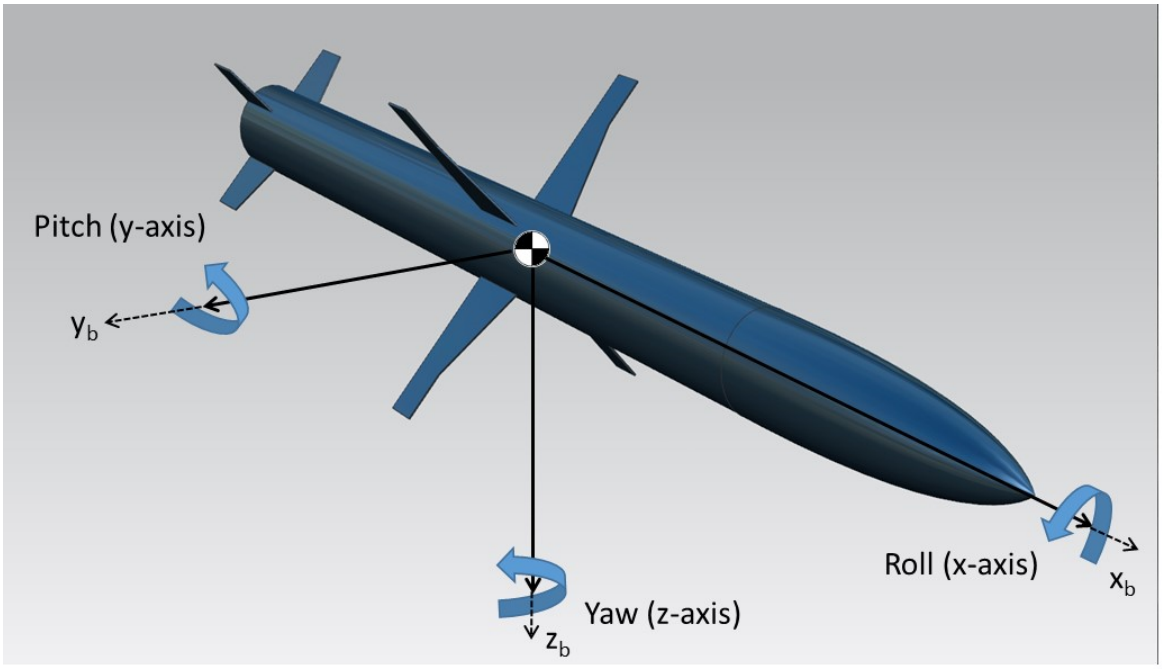

Figure 14. Body-Axis Reference Frame for Missile

All other states use a body-reference frame, as shown in Figures 15 and 16. The flight path angle, γ, illustrated in Figure 15, is the angle between the local horizon and the velocity vector. The angle of attack, α, is the angle between the velocity vector and the x-axis in the body-reference frame. The pitch angle, θ, is the angle between the local horizon and the x-axis in the body frame.

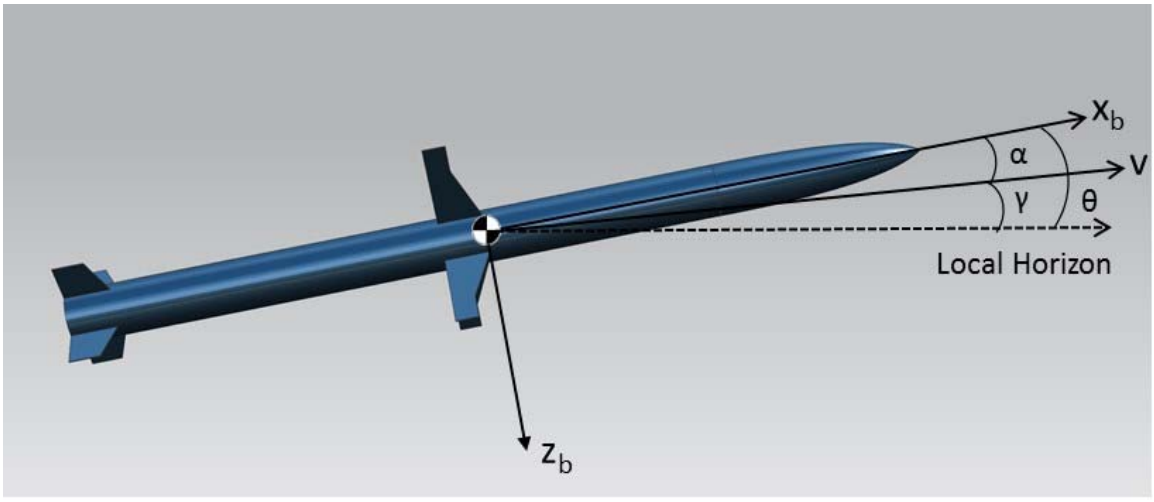

Figure 15. Flight Angles in the X-Z Body Reference Frame

The side-slip angle, β, shown in Figure 16, is the angle between the velocity vector and the x-axis in the body-reference frame. Yaw is the rotation of the x-y body-reference frame about the z-axis. The yaw angle, ψ, is the angle between the x-axis in the body-reference frame from a locally referenced position at the beginning of the rotation.

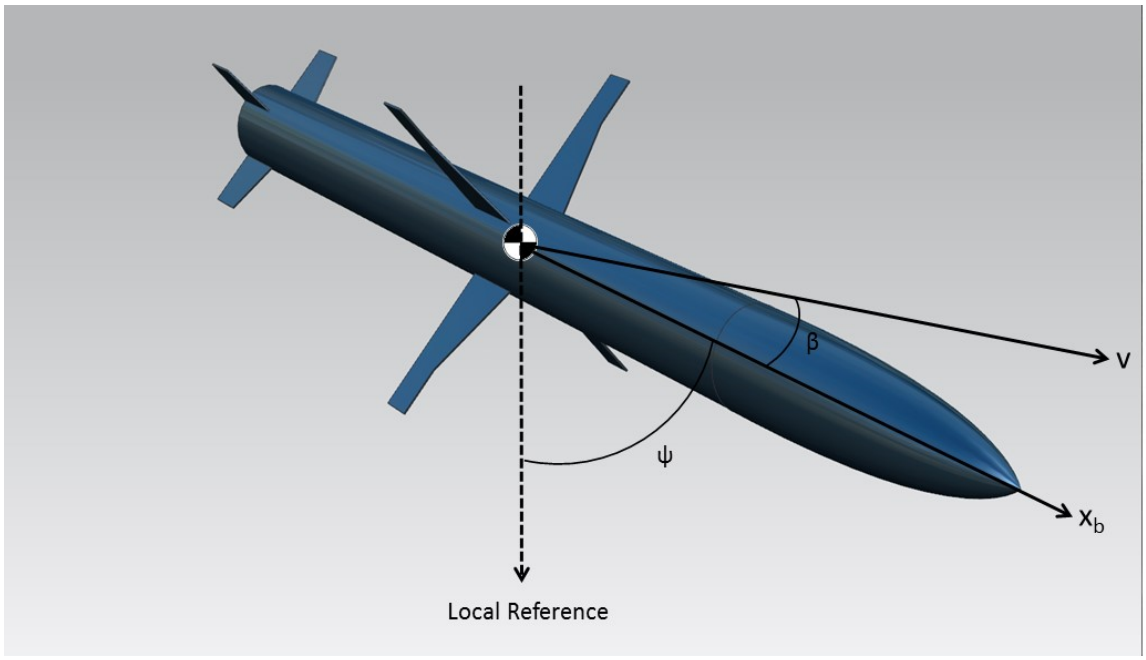

Figure 16. Flight Angles in the X-Y Body Reference Frame

The heading angle, σ, is the angle between the velocity vector and the x-axis in the x-y plane, where the velocity vector is in the direction of travel from the COG through the nose of the missile, shown in Figure 17.

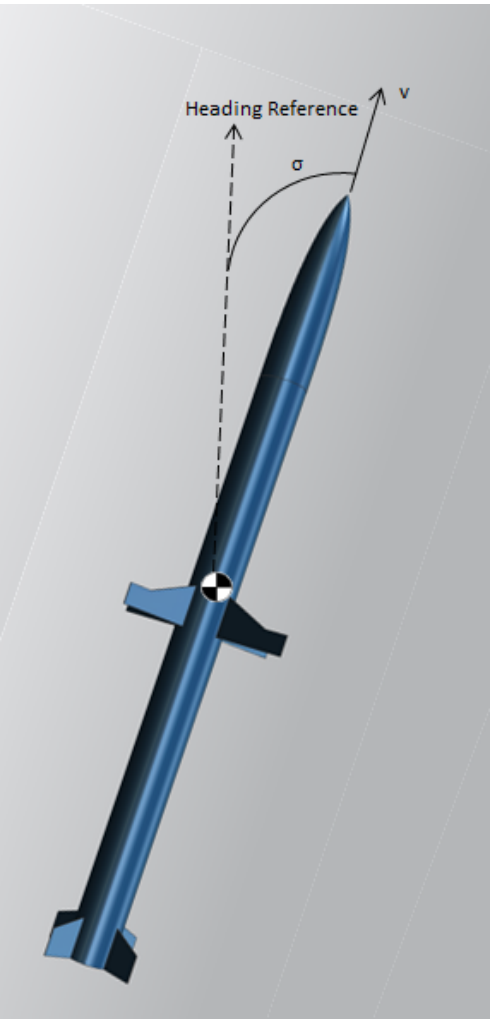

Figure 17. Definition of Flight Path Heading Angle

b. Dynamics Equations

For a 6DOF model, the equations of motion are a function of system states, forces, moments, and a number of parameters. The variables that represent the moment, forces, velocities, and parameters are listed in Table 3, while a representative set of states for the 6DOF model are listed in Table 4.

Table 3. 6DOF Forces, Moments, and Velocity Components

	Roll (x-axis)	Pitch (y-axis)	Yaw (z-axis)
Angular Rates	p	q	r
Velocity Components	u	v	w
Aerodynamic Force Components	X	Y	Z
Aerodynamic Moment Components	L	M	N
MOI about each axis	I_{xx}	I_{yy}	I_{zz}

Table 4. 6DOF States for Guided Rocket

Name	Symbol	Units
Velocity	V	m/s
Angle of Attack	α	rad
Sideslip Angle	β	rad
Roll rate	p	rad/sec
Pitch rate	q	rad/sec
Yaw rate	r	rad/sec
Roll angle	ψ	rad
Pitch angle	θ	rad
Yaw angle	ϕ	rad
X-coordinate (Earth Axes)	xe	m
Y-coordinate (Earth Axes)	ye	m
Altitude	ze	m

For each of the states that are listed in Table 4, there is an associated dynamic equation. The standard 6DOF equations of motion from [18], [19] include the position equations (2.1), the control rate equations (2.2), the angular velocity equations (2.3), the Euler angle rate equations (2.4), and the force and moment equations (2.5).

$$\dot{x}_e = (\cos\theta\cos\psi)\,\mathrm{V}\cos\alpha\cos\beta + (\sin\phi\sin\theta\cos\psi - \cos\phi\sin\psi)\,\mathrm{V}\sin\beta$$
$$+(\sin\phi\sin\psi + \cos\phi\sin\theta\cos\psi)\,\mathrm{V}\sin\alpha\cos\beta$$

$$\dot{y}_e = (\cos\theta\sin\psi)\,\mathrm{V}\cos\alpha\cos\beta + (\cos\phi\cos\psi + \sin\phi\sin\theta\sin\psi)\,\mathrm{V}\sin\beta \qquad (2.1)$$
$$+(\cos\phi\sin\theta\sin\psi - \sin\phi\cos\psi)\,\mathrm{V}\sin\alpha\cos\beta$$

$$\dot{z}_e = (-\sin\theta)\,\mathrm{V}\cos\alpha\cos\beta + (\sin\phi\cos\theta)\,\mathrm{V}\sin\beta + (\cos\phi\sin\theta)\,\mathrm{V}\sin\alpha\cos\beta$$

$$\dot{V} = (\frac{X}{m} - g\sin\theta)\cos\alpha\cos\beta + (\frac{Y}{m} + g\sin\phi\cos\theta)\sin\beta$$
$$+(\frac{Z}{m} + g\cos\phi\cos\theta)\sin\alpha\cos\beta$$
$$\dot{\alpha} = \frac{1}{mV\cos\beta}(Z\cos\alpha - X\sin\alpha) + \frac{g}{V\cos\beta}(\cos\phi\cos\theta\cos\alpha + \sin\theta\sin\alpha)$$
$$+q - \tan\beta(p\cos\alpha + r\sin\alpha)$$
$$\dot{\beta} = \frac{\cos\beta}{mV}(Y + mg\sin\phi\cos\theta) + p\sin\alpha - r\cos\alpha$$
$$-\frac{\sin\beta}{mV}(Z\sin\alpha + X\cos\alpha) - \frac{g\sin\beta}{V}(\cos\phi\cos\theta\sin\alpha - \sin\theta\cos\alpha) \qquad (2.2)$$

$$\dot{p} = \frac{I_{ZZ}}{I_{XX}I_{ZZ} - I_{XZ}^{\ 2}}(L - (I_{ZZ} - I_{YY})qr + I_{XZ}qp)$$
$$+\frac{I_{XZ}}{I_{XX}I_{ZZ} - I_{XZ}^{\ 2}}(\mathrm{N} + (I_{XX} - I_{YY})qp - I_{XZ}qr)$$
$$\dot{q} = \frac{1}{I_{YY}}(M - (I_{XX} - I_{ZZ})pr - I_{XZ}(p^2 - r^2))$$
$$\dot{r} = \frac{I_{XZ}}{I_{XX}I_{ZZ} - I_{XZ}^{\ 2}}(L + (I_{YY} - I_{ZZ})qr + I_{XZ}qp)$$
$$+\frac{I_X}{I_{XX}I_{ZZ} - I_{XZ}^{\ 2}}(\mathrm{N} + (I_{XX} - I_{YY})qp - I_{XZ}qr) \qquad (2.3)$$

$$\dot{\phi} = p + (q\sin\phi + r\cos\phi)\tan\theta$$
$$\dot{\theta} = q\cos\phi - r\sin\phi$$
$$\dot{\psi} = (q\sin\phi + r\cos\phi)\sec\theta \qquad (2.4)$$

$$
\begin{aligned}
X &= \frac{1}{2}\rho(z)V^2 S_{ref} C_X(\alpha,\beta,M,\underline{\delta}) + T_x \\
Y &= \frac{1}{2}\rho(z)V^2 S_{ref} C_Y(\beta,M,\underline{\delta}) + T_y \\
Z &= \frac{1}{2}\rho(z)V^2 S_{ref} C_Z(\alpha,\beta,M,\underline{\delta}) + T_z \\
L &= \frac{1}{2}\rho(z)V^2 S_{ref} b C_l(\beta,M,\underline{\delta}) \\
M &= \frac{1}{2}\rho(z)V^2 S_{ref} \overline{c} C_m(\alpha,\beta,M,\underline{\delta}) \\
N &= \frac{1}{2}\rho(z)V^2 S_{ref} b C_n(\beta,M,\mathrm{T},\underline{\delta})
\end{aligned}
\tag{2.5}
$$

While a 6DOF model more accurately represents the performance of a missile, a 3DOF model is often sufficient for optimal trajectory design [18].

3. 3DOF Dynamics Model

In order to simplify analysis, a 3DOF model is often used in lieu of the 6DOF equations of motion. The 6DOF model involves multiple assumptions. These assumptions necessarily hold true in the 3DOF model as well. Additional assumptions are made that set the necessary conditions where the 3DOF equations of motion represent the 6DOF model. All assumptions for the 3DOF model are described in the next section.

a. Model Assumptions

The first assumption that is made (in both the 6DOF and 3DOF models) is that the Earth is flat and is non-rotating. By assuming that the Earth is non-rotating, the Coriolis Effect that is caused by the rotating earth goes to zero. This model also makes the assumption that the missile is not traveling far enough of a distance for round-earth effects to be taken into account. Due to the fact that the Earth is not a perfect sphere, there are variations in the gravitational constant based on where you are located on the surface of the Earth. The model assumes that there is no variations in the gravity so the standard constant value is used.

It is also assumed that the missile has a constant mass. In the flight of an actual missile, the mass will change through the beginning stages of flight as the fuel is burned. For the problem being examined in this thesis, the missile is in the mid-to-terminal phase of flight and it is assumed that all the propellant has been burned. When the entire missile trajectory is taken into account, mass variations need to be considered. The missile is also treated as a rigid body vehicle. By assuming that the missile is a rigid body rather than a flexible body, it eliminates the distortional effects that occur due to the additional forces and moments cause by aeroelasticity in the structure (e.g., flutter of the wings and fins). Additionally, the cross-products of inertia are considered to be negligible.

Missiles are launched in many environments and regions in the world. For most areas over land, the ground is located above the sea level and when the missile impacts the ground is it not at a mean sea level of zero. The 6DOF and 3DOF models both assume that when $z = 0$, the missile is at sea level, in a standard atmosphere. In addition since the missile is symmetric about the roll axis, the roll rate is assumed to be fixed at zero. Side-slip results from side force that is produced from an unequal lift on the airframe wings from either untrimmed flight surfaces or relative wind [20]. For this model is also assumed that there is no sideslip. The assumptions that were made for the model are summarized in Table 5.

Table 5. Model Assumptions

Flat, non-rotating Earth
No wind
No gravity variations
No Coriolis effect
Rigid body vehicle
Constant mass
Negligible cross-products of inertia
Z = 0 is at sea level, standard atmosphere
No side-slip
Missile is symmetric about the roll axis

b. Dynamic Equations

For the 3DOF model dynamic equations, the variables that are used are defined in Table 6.

Table 6. 3DOF Dynamic Equation Variables

Name	Symbol	Units
Down-range distance	x	m
Cross-range distance	y	m
Altitude	z	m
Velocity	v	m/sec
Heading angle	σ	rad
Flight path angle	γ	rad
Angle of attack	α	rad
Bank angle	μ	rad
Thrust	T	N
Drag	D	N
Lift	L	N
Mass	m	kg

When the assumptions described above are applied to the 6DOF equations of motion, the equations are reduced as follows:

$$\begin{aligned}
\dot{x} &= v\cos\gamma\cos\sigma \\
\dot{y} &= v\cos\gamma\sin\sigma \\
\dot{z} &= v\sin\gamma \\
\dot{v} &= \frac{1}{m}(T\cos\alpha - D) - g\sin\gamma \\
\dot{\sigma} &= \frac{1}{mv}(T\sin\alpha + L)\frac{\sin\mu}{\cos\gamma} \\
\dot{\gamma} &= \frac{1}{mv}(T\sin\alpha + L)\cos\mu - \frac{g}{v}\cos\gamma
\end{aligned} \tag{2.6}$$

If it is assumed (as above) that the rocket motor is burned, thrust drops from the equations and Equation (2.6) can be further simplified. In this case the missile can be assumed to be in the mid-to-terminal phase of flight and the equations for the 3DOF model without the thrust terms reduce to:

$$\begin{aligned}
\dot{x} &= v\cos\gamma\cos\sigma \\
\dot{y} &= v\cos\gamma\sin\sigma \\
\dot{z} &= v\sin\gamma \\
\dot{v} &= \frac{-D}{m} - g\sin\gamma \\
\dot{\sigma} &= \frac{L}{mv}\frac{\sin\mu}{\cos\gamma} \\
\dot{\gamma} &= \frac{L}{mv}\cos\mu - \frac{g}{v}\cos\gamma
\end{aligned} \tag{2.7}$$

Equation (2.7) is the model that will be used in the remainder of this work.

B. AERODYNAMIC MODEL

1. Missile DATCOM Software

The actual coefficients of lift and drag for a missile are determined through flight testing of the vehicle. However, since the values are needed for the design and simulation prior to actual testing, there is a need for software that predicts the aerodynamic

characteristics of a missile based on the design configuration. There are several different models that can be used in order to determine the coefficients of lift and drag for a missile. The software that was used for this thesis was the Missile DATCOM software [17]. The Missile DATCOM software is an aerodynamic design tool that allows users to input the physical dimensions of a missile for a given configuration and based on this, provides output of the required aerodynamic coefficients.

The Missile DATCOM software is written in FORTRAN and allows the user to input the characteristics of the missile that they are interested in, in the form of a configuration file. The user is able to input the number of angles of attack that that they desire and the Mach number they are expecting the missile to fly at. For the simplicity of this thesis, only one Mach number was used. For a more complex and realistic model, a table of coefficients would need to be created in order to more accurately represent the aerodynamics. Dimensions of the missile are also needed which include the length of the nose section, diameter of the nose, number of fins and their location on the body, as well as dimensions of the fins. The program also allows for a trim setting to be applied and will output the associated coefficients if the missile is able to be trimmed for the given angle of attack.

Once the appropriate configuration data is entered into the Missile DATCOM software, the program outputs a table of coefficients for a given set of trim settings and angles of bank. In the 6DOF model, the force and moment equations, Equation (2.5), each require an aerodynamic coefficient. There are six different coefficients, which are listed in Table 6. Of note, the roll moment coefficient, C_l, should not be confused with the coefficient of lift, C_L.

Table 7. 6DOF Aerodynamic Coefficients

Name	Symbol
Axial Force Coefficient	C_X
Side Force Coefficient	C_Y
Normal Force Coefficient	C_Z
Roll Moment Coefficient	C_l
Pitch Moment Coefficient	C_m
Yaw Moment Coefficient	C_n

An example of one of the outputted aerodynamic coefficients is shown in Figure 18. For ease of comparison all of the plots for the coefficient data have been normalized. Figure 18 shows the relationship between the angle of attack and the axial force coefficient. These numbers were all calculated at the assumed maximum velocity of 639 m/s (1.863 Mach).

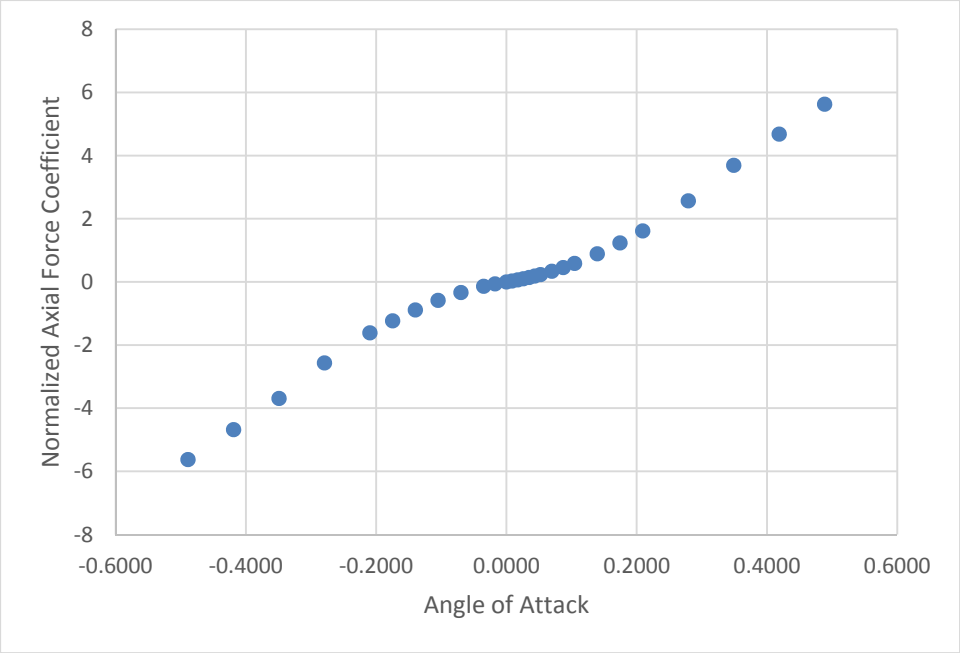

Figure 18. Normalized Axial Force Coefficient versus Angle of Attack

When using the simplified 3DOF model, Equation (2.7), the equations of motion only require the values for lift and drag. The equations for lift and drag depend on the lift and drag coefficients, C_L and C_D as follows:

$$L = \frac{1}{2}\rho v^2 S_{ref} C_L$$
$$D = \frac{1}{2}\rho v^2 S_{ref} C_D \tag{2.8}$$

The coefficients of lift and drag can be geometrically determined from the axial and normal force coefficients [18]. The resulting equations are:

$$C_D = -C_X \cos\alpha \cos\beta - C_Y \sin\beta - C_Z \sin\alpha \cos\beta$$
$$C_L = C_X \sin\alpha - C_Z \cos\alpha \tag{2.9}$$

Since the 3DOF model assumes that there is no side-slip and that all turns are done in a coordinated fashion where $\beta = 0$, the equations further reduce to:

$$C_D = -C_X \cos\alpha - C_Z \sin\alpha$$
$$C_L = C_X \sin\alpha - C_Z \cos\alpha \tag{2.10}$$

The relationship between the two sets of aerodynamic coefficients is shown in Figure 19, where $C_N = -C_Z$ and $C_A = -C_X$ and the side-slip is zero. The Missile DATCOM software determines the lift and drag coefficients automatically and outputs C_L and C_D values directly for the desired angles of attack.

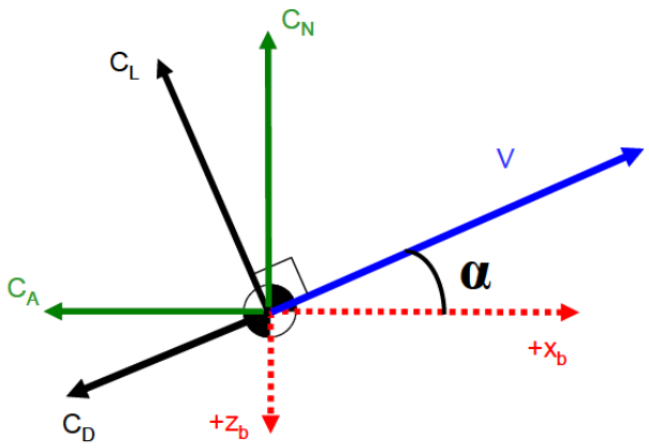

Figure 19. Relationship Between Aerodynamic Coefficients with $\beta = 0$

Source [18]: Bollino, K. P., 2006, "High-Fidelity Real-Time Trajectory Optimization for Reusable Launch Vehicles."

2. Range of Angle of Attack (AoA)

While the fidelity of the coefficient data will be discussed further in Chapter V, an issue that was discovered with regard to selecting the range of AoA selected will be discussed here. The resulting products in subsections *a* and *b* assume a 2nd degree curve fit of the aerodynamic data to provide an illustration for the discussion.

a. Initial AoA Range

One of the inputs the user can enter into the Missile DATCOM software is the number and range of angle of attack values that they want the software analysis to be run over. When the Missile DATCOM software was first run, it was done over a range of -2 to 28 degrees angle of attack. The data that is outputted produces the coefficients for only the specific angles of attack. For optimization, an equation where the coefficients can be determined for any given angle of attack is needed. The desired equation was produced by plotting the data points and applying different curve fits to the data. Figures 20 and 21 show the coefficients of lift and drag and their curve fits assuming a 2nd degree polynomial fit.

The R^2 value shown in the plots represents the correlation coefficient. This value describes how well the equation represents the data. If the equation fit the data perfectly, the R^2 value would be identically 1.

The trendlines that were applied to the data produced the following normalized coefficient equations.

$$C_L = 2.0809\alpha^2 + 1.1477\alpha - 0.0106 \tag{2.11}$$

$$C_D = 4.2284\alpha^2 - 0.2776\alpha + 0.1281 \tag{2.12}$$

These equations were originally used to obtain an optimal control solution over an extended range of α (i.e., beyond the $-2 \le \alpha \le 28$ range), shown in Figures 20 and 21. Note these plots only show data over a limited of attack range.

The curve fits for $-2 \le \alpha \le 28$, shown in Figures 20 and 21. This range was selected because it encompasses the expected autopilot limits. These curves are not symmetric as in Figure 18, because of the limited range in angle of attack selected for the data fits.

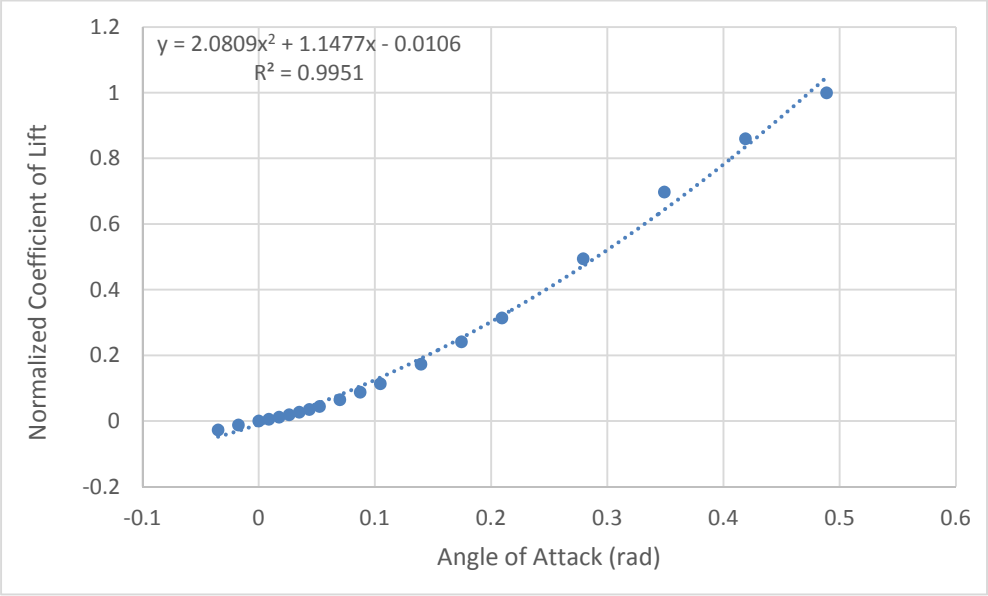

Figure 20. Coefficient of Lift with a 2nd Degree Polynomial Fit for $-2 \le \alpha \le 28$ versus AoA

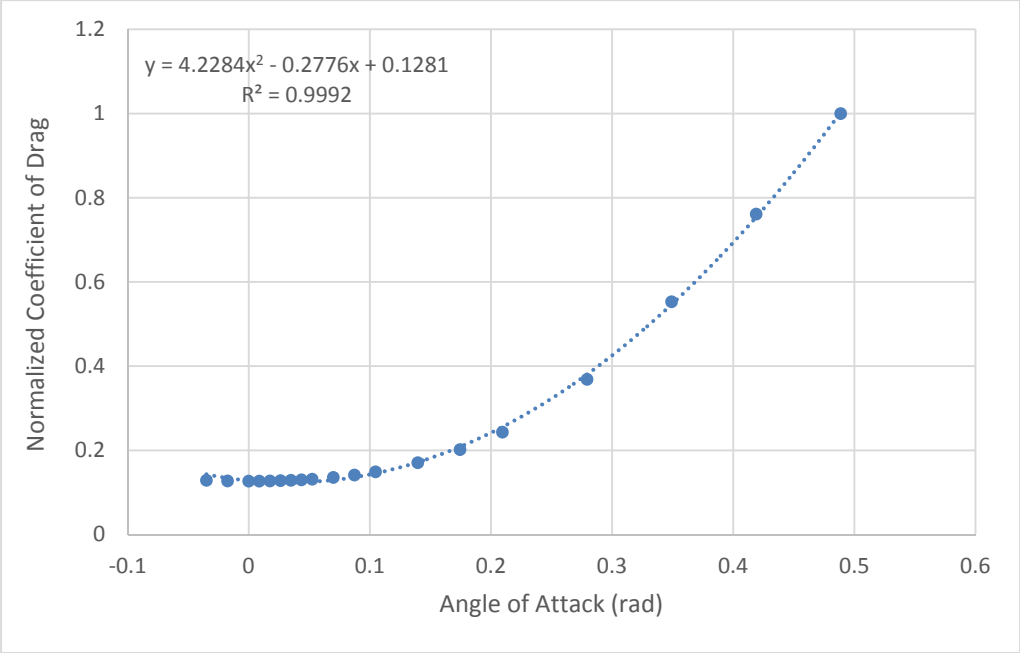

Figure 21. Coefficient of Drag with a 2nd Degree Polynomial Fit for $-2 \leq \alpha \leq 28$ versus AoA

b. Extended AoA Range

When Equation (2.11) was plotted against the entire range of angle of attacks used as bounds in the optimal control problem, the resulting plot (see Figure 22) showed increasing lift for negative angles of attack, which defies the laws of physics.

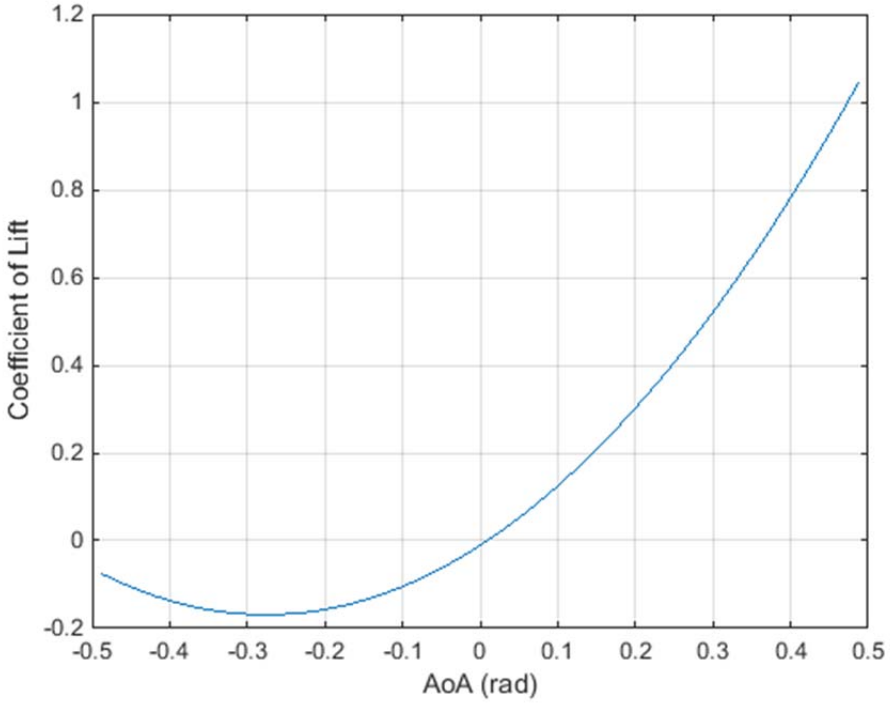

Figure 22. Coefficient of Lift versus Extended AoA for a 2nd Degree Fit

To correct this issue, the Missile DATCOM program was run again with an increased angle of attack range going from -28 to 28 degrees, to include a range of negative coefficients within the bounds used in the optimal control problem. Figures 23 and 24 show the new lift and drag plots with a new 2nd degree polynomial curve fit over the increased angle of attack range.

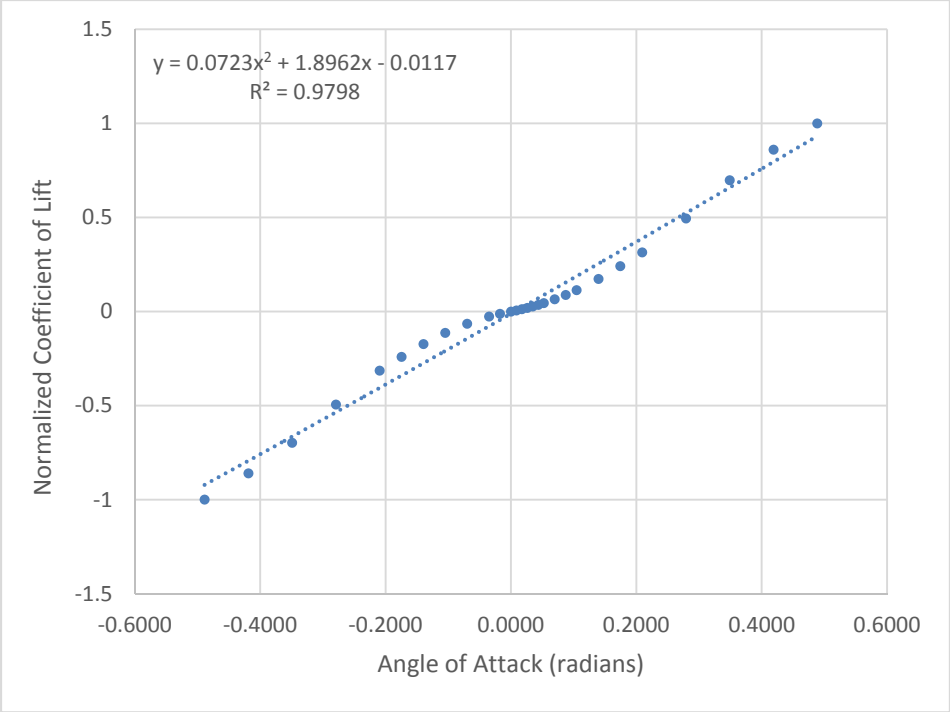

Figure 23. Coefficient of Lift with a 2nd Degree Polynomial Fit for $-28 \leq \alpha \leq 28$ versus AoA

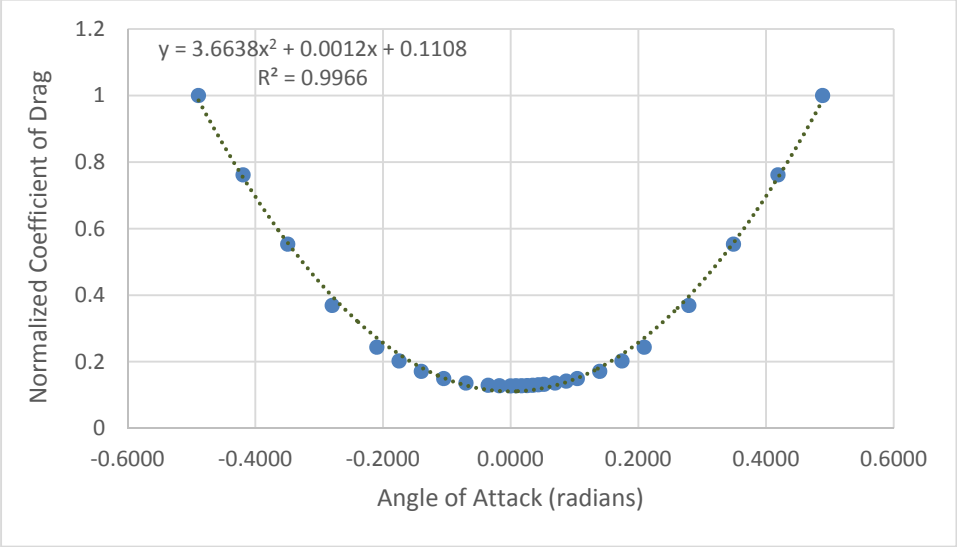

Figure 24. Coefficient of Drag with a 2nd Degree Polynomial Fit for $-28 \leq \alpha \leq 28$ versus AoA

The trendlines that were applied to the data produced the following normalized coefficient equations.

$$C_L = 0.0723\alpha^2 + 1.8962\alpha - 0.0117 \tag{2.13}$$

$$C_D = 3.6638\alpha^2 + 0.0012\alpha + 0.1108 \tag{2.14}$$

These updated equations were used for subsequent runs of the optimal control software.

The trendlines produced with the angle of attack range $-2 \le \alpha \le 28$, Equations (2.11) and (2.12), were different from the trendlines produced for the angle of attack range $-28 \le \alpha \le 28$, Equations (2.13) and (2.14). The two sets of equations were plotted against the full range of angles of attack and were compared. Figure 25 shows a comparison of the two equations for coefficient of lift. The blue line represents Equation (2.11) and the red line represents Equation (2.13). Figure 26 shows a comparison of the two equations for coefficient of drag. The blue line represents Equation (2.12) and the red line represents Equation (2.14). As can be seen, the problem of increasing lift for negative AoA has been corrected by extending the range of angle of attack data. The approximation of the drag coefficient is similar to before but with enhanced accuracy for negative AoA values.

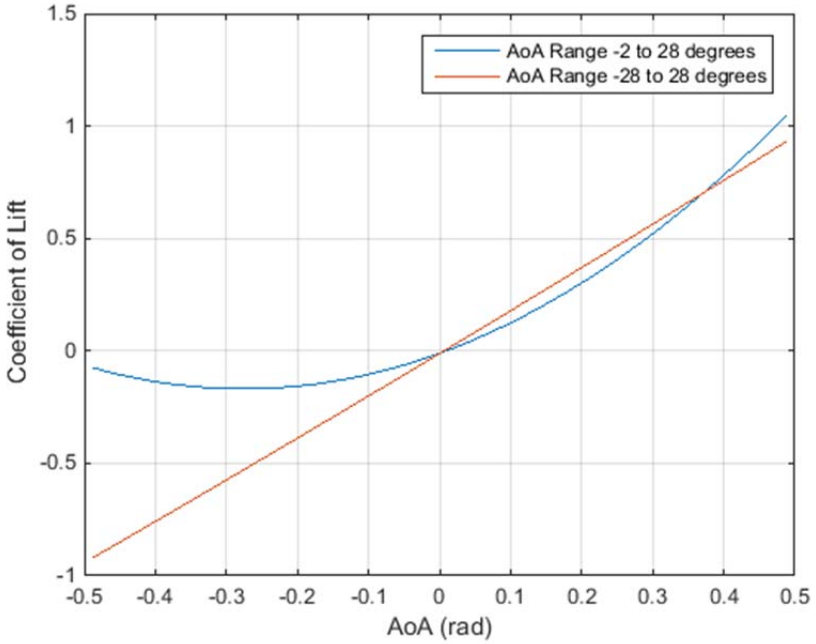

Figure 25. Comparison of C_L Equations

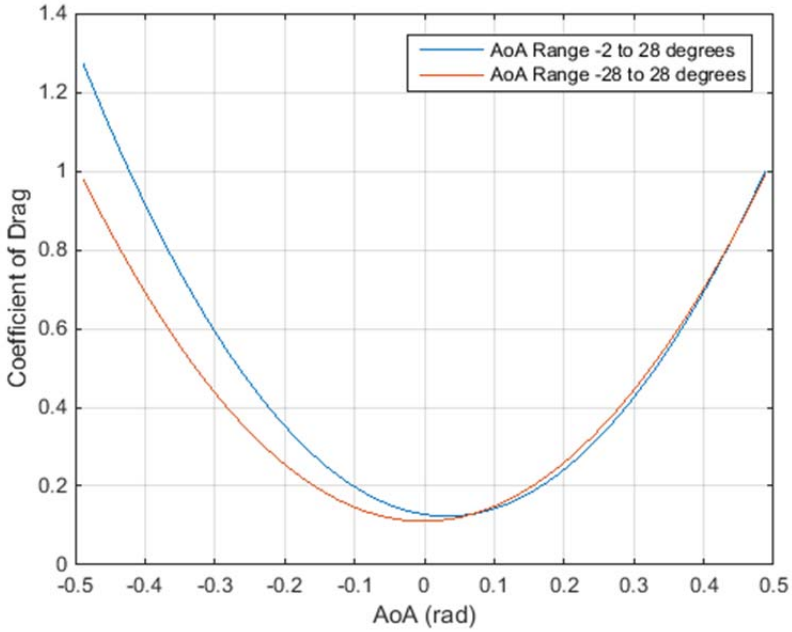

Figure 26. Comparison of C_D Equations

3. Issues on Fitting the Aerodynamic Data

Depending on the fidelity of the model that is being used, different curve fits may represent the data better than others. The curve fits are an estimate of the coefficients and are designed to be used for simulation since tables will later be developed from testing on the actual missile. Thus, a lower fidelity curve fit may be an appropriate choice for initial simulations and optimal control runs.

a. Coefficient of Lift

A linear, a 2nd degree polynomial, and a 3rd degree polynomial curve fit were applied to the extended coefficient of lift data. They are shown in Figures 27–29.

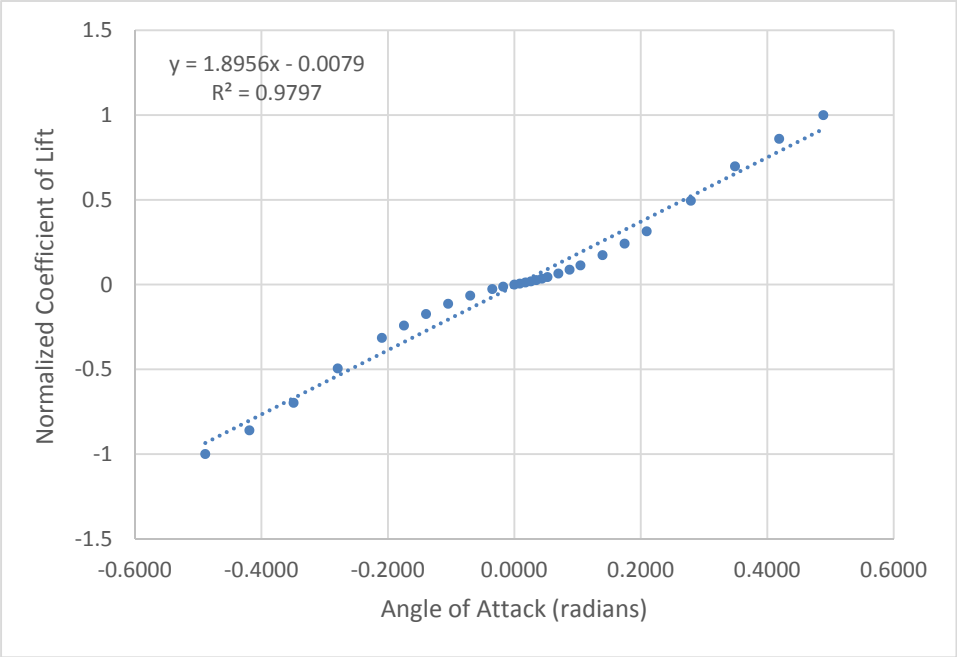

Figure 27. Normalized Coefficient of Lift with a Linear Curve Fit versus AoA

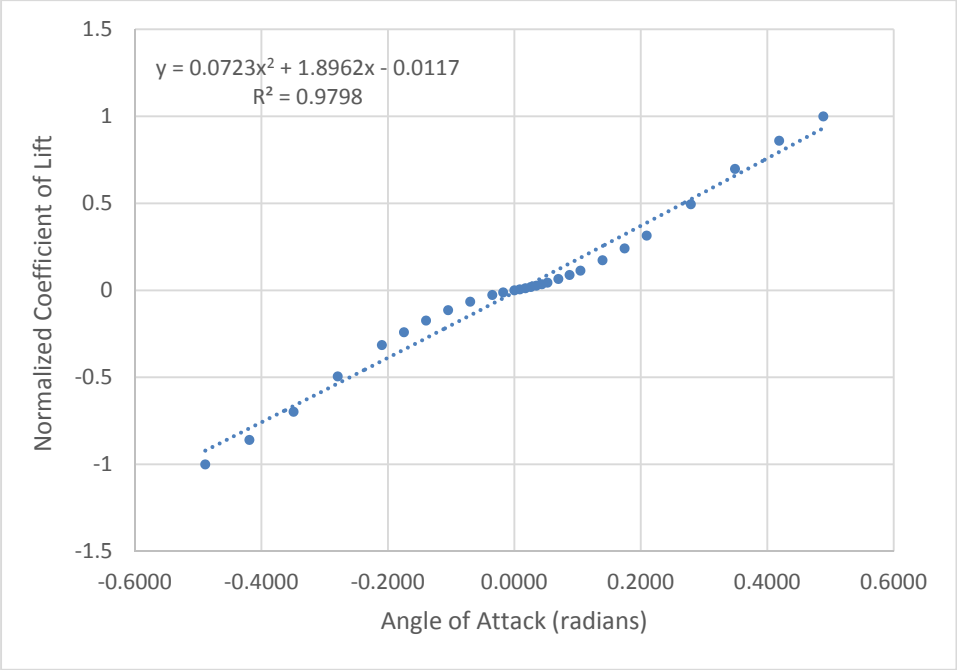

Figure 28. Normalized Coefficient of Lift with a 2nd Degree Polynomial Curve Fit versus AoA

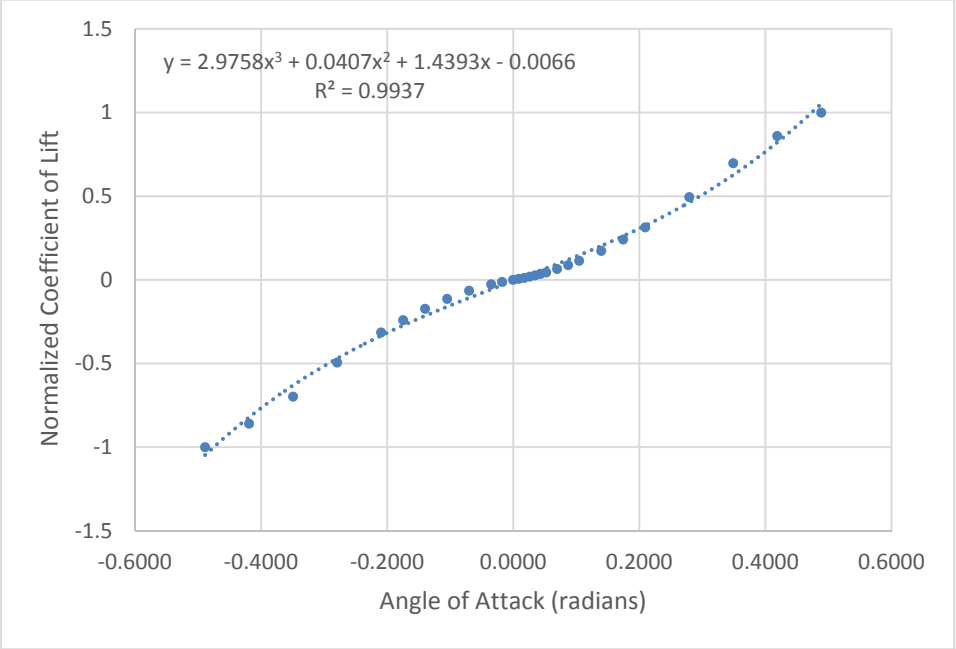

Figure 29. Normalized Coefficient of Lift with a 3rd Degree Polynomial Curve Fit versus AoA

b. *Normalized Equations for the Coefficient of Lift*

The resulting equations for the coefficient of lift are:

$$C_L = 1.89565\alpha - 0.0079 \tag{2.15}$$

$$C_L = 0.0723\alpha^2 + 1.8962\alpha - 0.0117 \tag{2.16}$$

$$C_L = 2.9758\alpha^3 + 0.0407\alpha^2 + 1.4393\alpha - 0.0066 \tag{2.17}$$

Any of equations (2.15) to (2.17) could be used to represent the coefficient of lift. In the remainder of this thesis, Equation (2.16) was used to represent the lift coefficient.

c. *Coefficient of Drag*

The same set of curve fits was applied to the coefficient of drag plots. Because the coefficient of drag is parabolic, a linear curve fit is a very poor fit for the coefficient of drag as shown in Figure 30. The 2nd and 3rd degree polynomial curve fits are better and these are shown in Figures 31 and 32. As is seen, the 2nd and 3rd polynomials are about the same, so either could be used to represent the coefficient of drag.

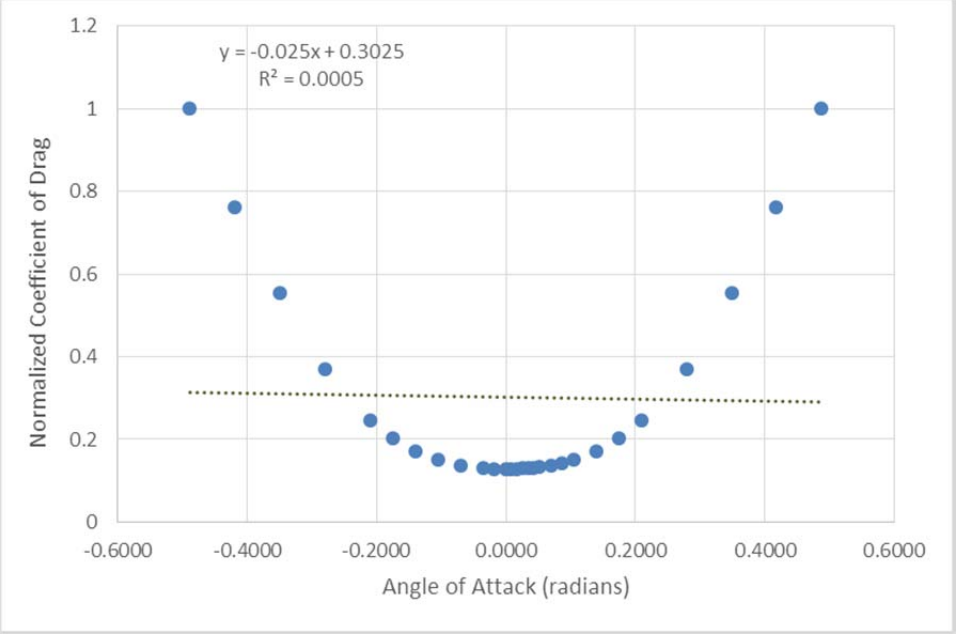

Figure 30. Normalized Coefficient of Drag with a Linear Curve Fit versus AoA

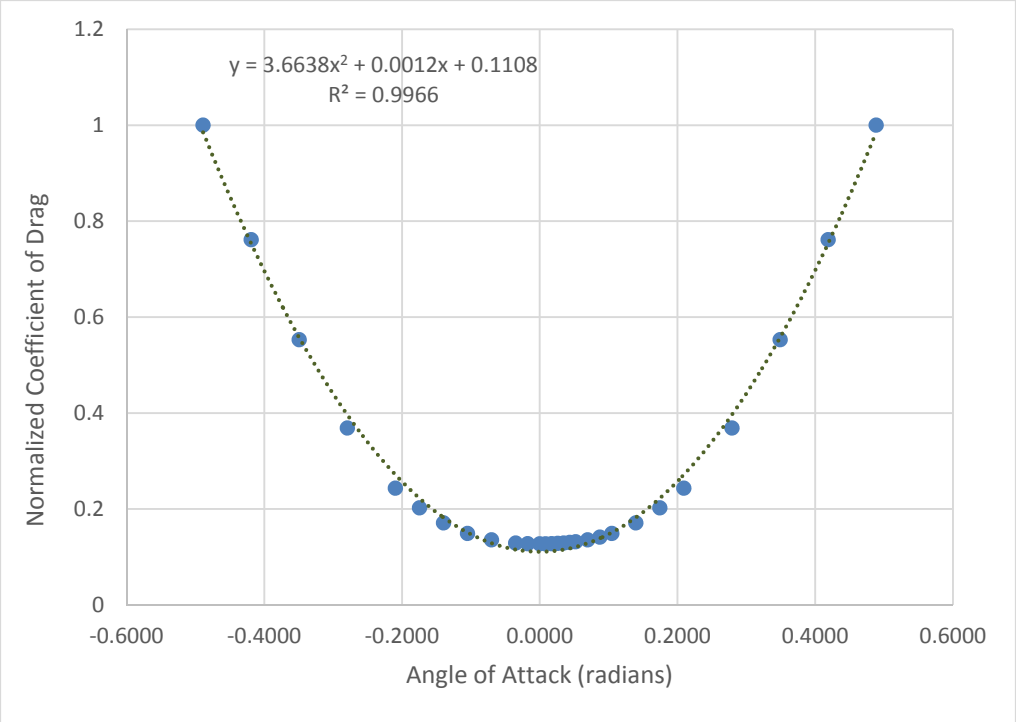

Figure 31. Normalized Coefficient of Drag with a 2nd Degree Polynomial Curve Fit versus AoA

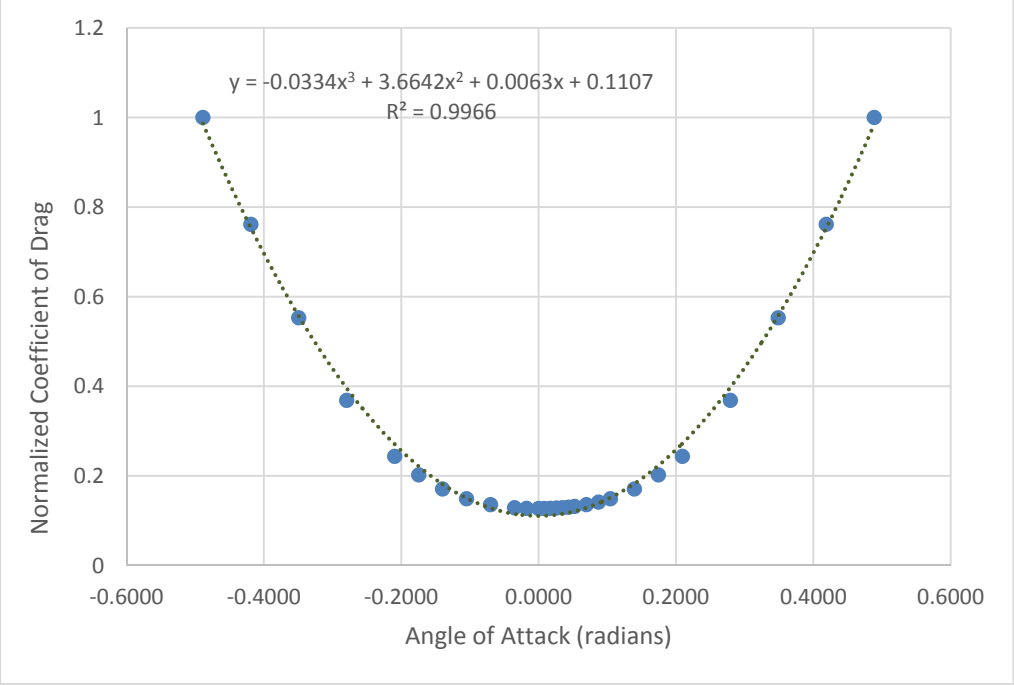

Figure 32. Normalized Coefficient of Drag with a 3rd Degree Polynomial Curve Fit versus AoA

d. Normalized Equations for the Coefficient of Drag

The resulting equations for the coefficient of drag are shown in the following equations.

$$C_D = -0.025\alpha + 0.3025 \tag{2.18}$$

$$C_D = 3.6638\alpha^2 + 0.0012\alpha + 0.1108 \tag{2.19}$$

$$C_D = -0.0334\alpha^3 + 3.6642\alpha^2 + 0.0063\alpha + 0.1107 \tag{2.20}$$

In the remainder of this thesis, Equation (2.19) was used to represent the drag coefficient. Since Equation (2.18) does not do a good job of approximating the parabolic nature of the drag data, it should not be used.

C. SUMMARY

This Chapter introduced the configuration and performance characteristics of the guided rocket model that is used in this thesis. The 6DOF and 3DOF models that can be used to represent the missile were introduced, as well as the assumptions for the models. The Missile DATCOM software used to derive the coefficients of lift and drag was described and the development of the coefficient of lift and drag equations was shown.

THIS PAGE INTENTIONALLY LEFT BLANK

III. CONVENTIONAL APPROACH FOR GUIDANCE

In order to determine the benefits of applying optimal control to the missile guidance problem, a baseline that the results of the optimal control solution can be compared to is needed. This baseline is determined using the conventional approach for missile guidance. This chapter introduces the standard guidance law, namely proportional navigation [7], that is currently used in guided missiles.

A. FUNDAMENTALS OF PROPORTIONAL NAVIGATION

The fundamentals of tactical missile guidance are described in detail in [7]. This section provides a summary of the ideas presented in [7] that are needed in order to have a basis of understanding of the conventional approach. Proportional navigation utilizes the line-of-sight between the missile and the target. The guidance law "issues acceleration commands, perpendicular to the instantaneous missile-target line-of-sight, which are proportional to the line-of-sight rate and closing velocity" [7]. Mathematically this can be described as:

$$n_c = N' V_c \dot{\lambda}, \tag{3.1}$$

where n_c is the acceleration command, N' is the effective navigation ratio, V_c is the missile to target closing velocity and λ is the line-of-sight angle. A diagram of the geometry in a two-dimensional plane is shown in Figure 33. In the Figure, R_{TM} is the range from the target to the missile, V_M is the velocity of the missile, and n_t is the target acceleration.

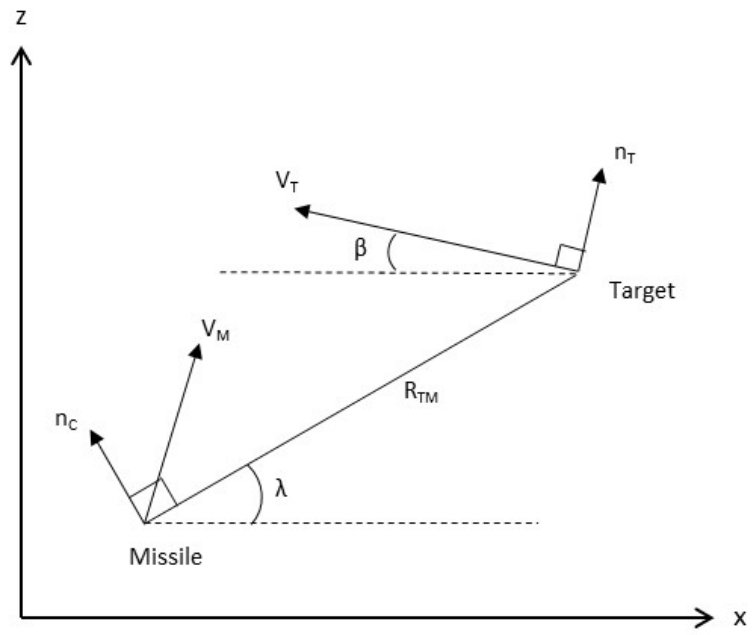

Figure 33. Two-dimensional Missile-Target Engagement Geometry

From [7]: Zarchan, P., 2007, "Tactical and Strategic Missile Guidance," American Institute of Aeronautics and Astronautics, Inc., Reston, VA.

From the geometry shown in Figure 33, the following relationships can be derived [7]. The velocity of the target can be split into two components based on the flight path angle of the target, β. The components become

$$\begin{aligned} V_{Tx} &= -V_T \cos\beta \\ V_{Tz} &= V_T \sin\beta \end{aligned} \tag{3.2}$$

The differential equations for the missile velocity and position from [7] are

$$\begin{aligned} \dot{R}_M &= \left[V_{Mx}, V_{Mz}\right] \\ \dot{V}_M &= \left[a_{Mx}, a_{Mz}\right] \end{aligned} \tag{3.3}$$

For the problem that is being examined in this thesis, the target is stationary and the maneuver is being conducted in the x-z plane (for maximum range). The separation between the missile and the target can therefore be found by

$$R_{TM} = \left[x_t - x,\ z_t - z\right], \tag{3.4}$$

where x_t is the position of the target and x is the current position of the missile. The same applies in the z-axis. Given the range from the target in both of the axes, the line-of-sight angle can then be found by simple geometry

$$\lambda = \tan^{-1} \frac{R_{TMz}}{R_{TMx}}. \tag{3.5}$$

If the target is moving, the relative velocity between the missile and the target is found by taking the difference between the velocity components in each axis.

$$V_{TM} = \begin{bmatrix} V_{Tx} - V_{Mx} & V_{Tz} - V_{Mz} \end{bmatrix} \tag{3.6}$$

Since the target is stationary in this problem, Equation (3.6) reduces to

$$V_{TM} = \begin{bmatrix} -V_{Mx} & -V_{Mz} \end{bmatrix} \tag{3.7}$$

From the relative velocities and ranges, the line-of-sight rate can be determined by

$$\dot{\lambda} = \frac{R_{TMx} V_{TMz} - R_{TMx} V_{TMz}}{{R_{TM}}^2}, \tag{3.8}$$

where the range from the target to the missile is found by applying the distance formula

$$R_{TM} = \sqrt{{R_{TMx}}^2 + {R_{TMz}}^2}. \tag{3.9}$$

Now that the range to the missile is known, the closing velocity can be determined as [7]

$$V_C = -\dot{R}_{TM} = \frac{-\left(R_{TMx} V_{TMx} + R_{TMz} V_{TMz} \right)}{R_{TM}} \tag{3.10}$$

Equation (3.10) provides the last variable that is needed to calculate the missile guidance command. Once the magnitude of the missile guidance command is known, the acceleration in each axis can be determined by

$$\begin{aligned} a_{Mx} &= -n_c \sin\lambda \\ a_{Mz} &= n_c \cos\lambda \end{aligned}. \tag{3.11}$$

B. MAXIMUM RANGE USING PROPORTIONAL NAVIGATION

In order to implement the equations listed in the section above, a SIMULINK model was created for the conventional model, shown in Figure 34. The first MATLAB function shown in Figure 34, titled PN, contains the missile guidance equations described in Section A of this Chapter. The resulting acceleration that is used to adjust the missile LOS is outputted. The second MATLAB function embedded in the SIMULINK model contains the dynamic equations for the 3DOF aerodynamic model. The acceleration that was commanded is compared to the acceleration is outputted from the missile_3DOF function block. The current states are inputted and an updated state vector is outputted along with the acceleration of the missile. The new position is used to determine the new line-of-sight angle and the process (control loop) continues until the missile impacts the ground stopping the simulation.

Due to the fact the problem assumes that the missile is already in flight and that the maneuver begins at the point when thrust turns off, the initial conditions had to be developed and set to match the flight profile. It was assumed that the missile would be flying in trimmed flight at the moment the maneuver begins. Appropriate initial conditions are given in Table 8.

Table 8. Initial Conditions for Conventional Maneuver

	Units	Value
x_o	m	0
y_o	m	0
z_o	m	661.1
v_o	m/s	514.5
σ_o	rad	0
γ_o	rad	0
α_o	rad	0.349
μ_o	rad	0

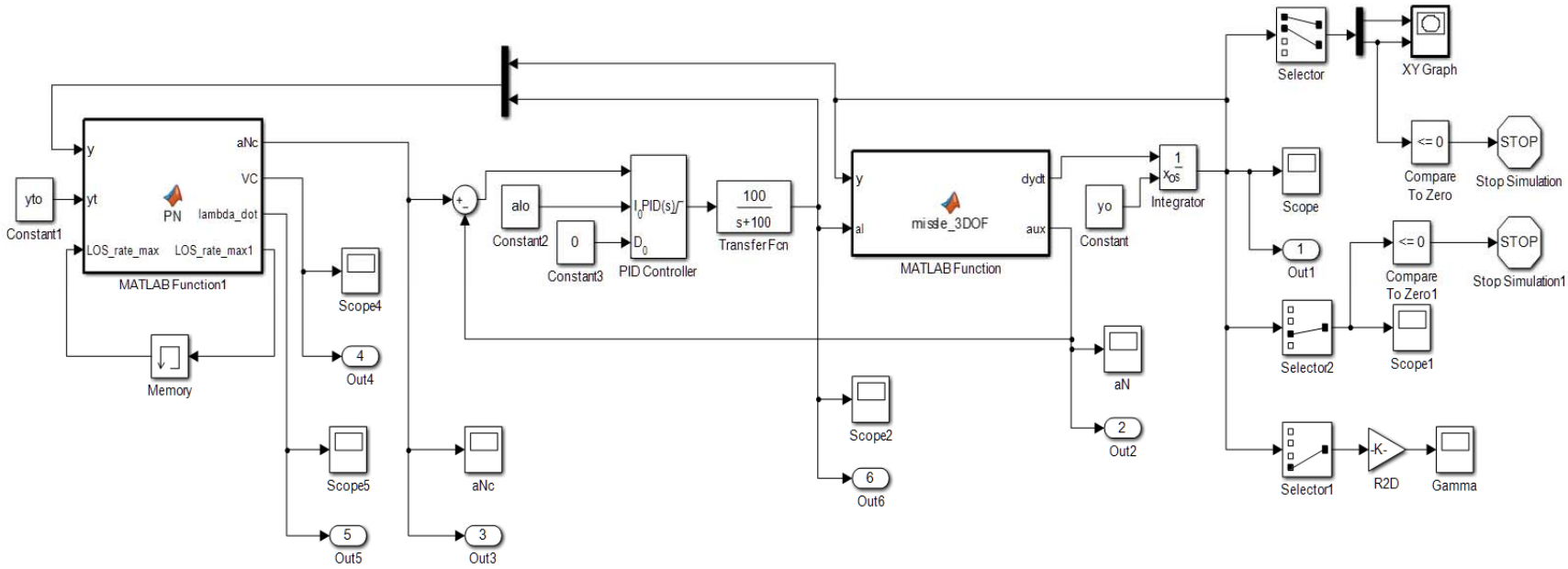

Figure 34. SIMULINK Block Diagram for Simulating Proportional Guidance

In order to find the maximum range of the missile using the SIMULINK model, the location of the target was adjusted further and further out until the missile could no longer hit the target and impacted the ground shy of the intended point. The maximum range of the missile using the conventional approach was determined to be 8637 m with a flight time of 32.3 seconds. The trajectory of the missile is shown in Figure 35. Due to the fact that the target is stationary, the trajectory that the missile follows is essentially a straight line. The velocity profile versus time of flight is shown in Figure 36.

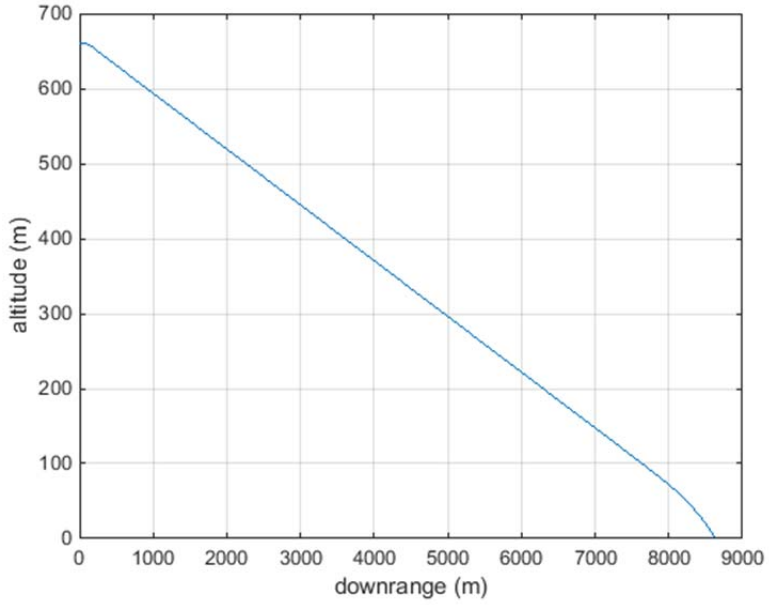

Figure 35. Trajectory of Missile for Conventional Guidance

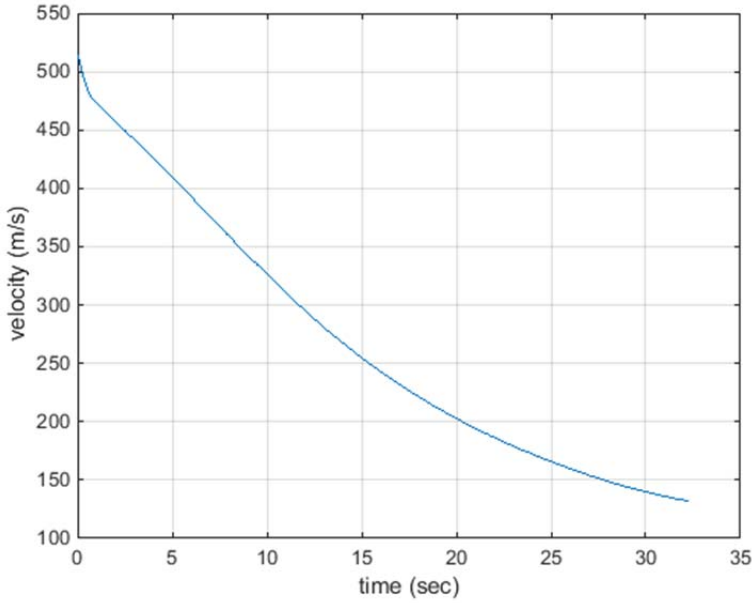

Figure 36. Missile Velocity for Conventional Guidance

Since the boost phase of the missile is completed prior to the start of the maneuver, gravity is the main force acting on the missile and it assumes a ballistic trajectory to intercept the target. The target trajectory for a ballistic missile is approximately a straight line as proven in reference [7]. Due to the nature of the ballistic trajectory, the line-of-sight angle for the missile remains constant for the majority of the flight. When missile is in close proximity to the target, the line-of-sight angle begins to change as the proportional navigation law adjusts the acceleration to zero line-of-sight error. This is shown in Figure 37. These results will be used later in the thesis to provide a baseline for comparison when the missile is flown using an optimal control solution.

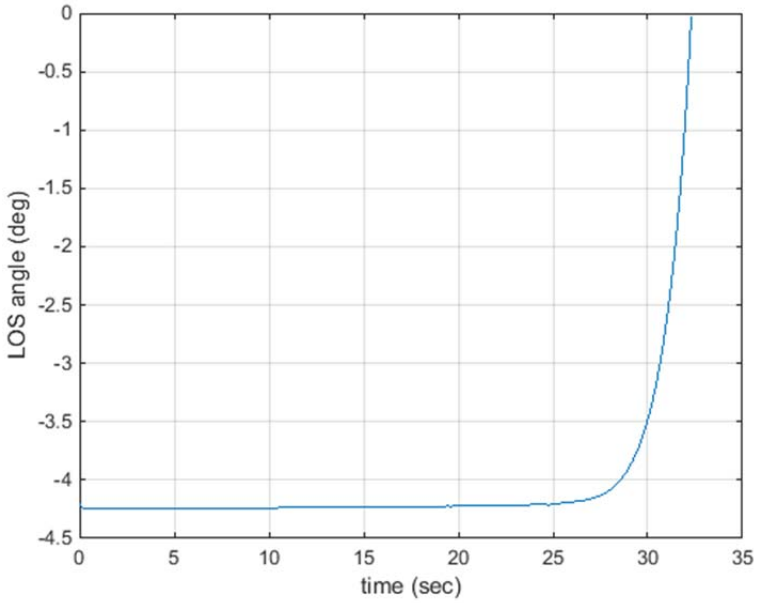

Figure 37. Line of Sight versus Time

C. SUMMARY

This chapter introduced the conventional proportional navigation approach that has long been used for guidance of rockets. In addition, a maximum range maneuver was simulated to establish a baseline performance that will be used to compare against the results achieved through optimal control.

IV. OPTIMAL CONTROL THEORY

There are multiple paths that a missile can take to reach the desired end state. Each path will require a different amount of resources, such as fuel or time. Optimal control theory looks to find the path that best minimizes or maximizes a given objective function with respect to the constraint set on the problem. For example, a user may want the quickest route. The objective function in this case is to minimize time of flight. Conversely, a user may want to extend the range of a missile so the objective is to maximize the distance travelled form the launch point. In either case, the optimal control solution will yield the path that optimizes the objective.

This chapter provides the basic background needed for this thesis in regard to optimal control theory. A more thorough discussion of optimal control can be found in [15]. References [18], [19], [21] also provide a good introduction to the basics of optimal control. This chapter contains a summary of the important concepts from these references. In order to solve optimal control problems and find the appropriate path for a given task, an optimal control software tool is typically used. This is because solving the problem analytically is often intractable. For this thesis, DIDO was used to obtain all the optimal control solutions. This chapter, therefore, also includes an introduction to the DIDO psuedospectral optimal control software.

A. THE OPTIMAL CONTROL PROBLEM

The generic optimal control problem as derived in [15], [18], is shown in Equation (5.1). Within this equation, J is the cost functional, E is the endpoint cost, F is the running cost. The value of the cost functional is subject to a set of state variables, x, and control variables, u. The equation $\dot{x} = f(x,u)$, in Equation (5.1), defines a set of dynamic equations for the problem. In addition e defines the set of end point constraints (boundary conditions) for the problem.

$$(P_o)\begin{cases} Minimize\, J\left[\mathbf{x}(\bullet), u(\bullet), t_f\right] = E(\mathbf{x}_f, t_f) + \int_{t_o}^{t_f} F(\mathbf{x}(t), u(t))dt \\ Subject\ to: \\ \dot{\mathbf{x}}(t) = f(x(t), u(t)) \\ \mathbf{x}(t_o) = \mathbf{x}^0 \\ t_o = t^0 \\ t_f = t^f \\ e(\mathbf{x}(t_f)) = 0 \end{cases} \tag{4.1}$$

Pontryagin's Principle is stated as follows: "Given an optimal solution to Problem P_o, there exists a covector function, $\lambda(\bullet)$, and a covector, ν, that satisfy the Hamiltonian minimization condition, the Hamiltonian value condition, the Hamiltonian evolution equations, the adjoint equations, and the transversality condition" [15]. These conditions lead to the formulation of a boundary value problem (BVP), which can be solved to find the optimal solution.

The first step in this process is to develop the Hamiltonian function which is defined as:

$$H(\lambda, x, u) = F(x, u) + \lambda^T f(x, u) \tag{4.2}$$

The Hamiltonian introduces the costates λ, which represent the adjoint covector. The covector has the same dimension as the state vector, *x*, but does not occupy the same space as *x* [15]. The adjoint dynamics are defined as:

$$\dot{\lambda}(t) = -\frac{\partial H}{\partial x} \tag{4.3}$$

According to Pontryagin's principle for the control function $u(\bullet)$ to be optimal, $u(\bullet)$ must globally minimize the Hamiltonian for every *t* from t_o to t_f, while holding λ and *x* constant at each instant in time [15]. This is known as the Hamiltonian Minimization Condition (HMC), which is defined as:

$$(HMC)\begin{cases}\underset{u}{\text{Minimize}} & \mathrm{H}(\lambda, x, u, t) \\ \text{Subject to} & \mathrm{u} \in \mathbb{U}\end{cases} \tag{4.4}$$

If the controls do not have any constraints, the HMC is reduced to the Euler-Lagrange equation which is given as:

$$\frac{\partial H}{\partial u} = 0 \tag{4.5}$$

In the presence of constraints on u, partial derivative $\frac{\partial H}{\partial u}$ must be interpreted as a switching function, that is:

$$S_u = \frac{\partial H}{\partial u} \ . \tag{4.6}$$

The sign of S_u then determines the value of the control variable at any instant in time.

The optimal control BVP should have $2N$ boundary conditions where N is the number of state variables. In order to find any missing boundary conditions, the Terminal Transversality Condition given in Equation (4.6) is used [15].

$$\lambda\left(t_f\right) = \frac{\partial \bar{E}}{\partial x_f} \ , \tag{4.7}$$

where $\bar{E}$ is the endpoint Lagrangian, defined as

$$\bar{E}(v, x(t_f)) = E(x(t_f)) + \upsilon^T e(x(t_f)) \tag{4.8}$$

While the Transversality condition provides N_x new equations, it also produces N_e unknowns. There is one final missing boundary condition which comes from the Hamiltonian Value Condition, given in Equation (5.8).

$$H\left[t_f\right] = -\frac{\partial \bar{E}}{\partial t_f} \tag{4.9}$$

Equations (4.7) and (4.9) provide the remaining needed boundary conditions in order to be able to construct and solve the boundary value problem (BVP) associated with

the optimal control problem. A challenge in solving the BVP is that it cannot typically be done analytically. Thus, a software tool is needed.

B. INTRODUCTION TO DIDO

DIDO is a MATLAB-based software package that was originally developed by Fahroo and Ross of the Naval Postgraduate School to solve complex optimal control problems [22]. DIDO was "originally developed to make it "easier to solve optimal control problems" by allowing the user to focus on defining the problem they want to solve as opposed to worrying about how to solve it" [23]. This tool takes the system dynamic equations and boundary conditions of the basic optimal control problem as described in Section A and develops a solution through use of pseudospectral optimal control theory. A more thorough discussion of the theories and mathematics behind DIDO can be found in [16].

DIDO requires the user to state the problem in a specific format that is encoded in four MATLAB m-files. The four function files are the "dynamics," "cost," "events," and "path"-files. The cost, dynamics, and event files are mandatory for every problem but the path file is optional. The cost function describes the endpoint cost and running cost for the problem. The cost for the problem is determined by the user and is set based on what the problem is intended to minimize (e.g., time) or maximize (e.g., range). The dynamics function contains the differential equations or state-space model to be optimized. In the event function m-file, all the known boundary conditions for the problem are entered. The path function allows the user to provide path constraints at the nodes. The path is an optional file and is only used if the problem has path constraints. The problem being examined in this thesis does not require use of the path function. However, a path constraint could be used if it is necessary to limit some aspect of the missile performance so that it is consistent with operational requirements, for example, bounding the maximum acceleration.

The m-file that is needed in order to be able to call DIDO in MATLAB is a main problem file. Within the main file, the upper and lower limits for the state variables, control variables, and clock times are defined. In addition, the number of nodes that will

be used to determine the solution (the computational grid) are also defined in the main file. The number of nodes determines the accuracy of the solution. One advantage to DIDO is that it can be used iteratively and a lower fidelity solution can be used and as a seed to refine the solution [21]. This provides a way to improve the accuracy of the solution quickly. The main file also allows the user to output any desired data or plots from the run. Once the cost, dynamics, events, and main files have been completed, DIDO can be run. DIDO performs analysis of the problem and if a solution is found, DIDO will output a message indicating that an extremal solution has been found. A solution is extremal if it is a minimizer for the HMC [22]. While Pontryagin's boundary value problem is not directly coded, DIDO provides data on the costates that can be used to check of the solution against Pontryagin's necessary conditions as part of a verification and validation (V&V) step.

For any extremal solution, it is important to verify and validate the results that were produced. This ensures that an optimal solution was in fact obtained and that the problem that was solved was indeed the one intended by the user. In addition to checking Pontryagin's necessary condition, the feasibility of the results should be checked by utilizing the built in MATLAB ODE tools. In this V&V test, the outputs from the DIDO run are propagated through the ODE function (dynamics) and the results compared in terms of their residual differences. An easy way to do this is by creating a simple comparison graph where both the outputs from the DIDO run and the propagation are plotted together. When the results are compared, if the optimal control results matches the results of the ODE propagation within some acceptable tolerance, the solution can be considered feasible.

1. Scaling the Problem

In any numerical algorithm, the scaling of the problem is also important. If the problem is badly scaled, the algorithm will be unable to solve the problem. This is typically seen in DIDO when the relative magnitudes of the states and the costates are large. This problem can be addressed by refining the solution through scaling. The scaling is accomplished through the use of "designer units" [23]. Equation (2.7) is the

dynamics equations for the 3DOF model. The dynamic model is formulated in state space and is given by $\dot{x} = f(x,u,t)$. In this state space, the control function u is the input into the dynamics equation to produce a response. The states for the model can be assembled into a vector as:

$$\bar{x}^T = \left[x, y, z, v, \sigma, \gamma\right] \tag{4.10}$$

The basic idea behind designer units is that each element in the state vector can be scaled by an arbitrary number selected by the user as shown in Equation (4.11),

$$\bar{x}^T = \left[\frac{x}{X}, \frac{y}{Y}, \frac{z}{Z}, \frac{v}{V}, \frac{\sigma}{\Sigma}, \frac{\gamma}{\Gamma}\right] \tag{4.11}$$

where *X*, *Y*, *Z*, etc., are the designer scale factors.

The same method of scaling applies to the control variable and the time units, which become:

$$\bar{u} = \left[\frac{\alpha}{\mathrm{A}}, \frac{\mu}{\mathrm{M}}\right] \tag{4.12}$$

$$\bar{t} = \frac{t}{T} \tag{4.13}$$

While the scaling factors are arbitrary, the goal is to pick "good" designer units. "A fundamental rule for scaling optimal control problems is to choose designer units in such a manner that the scaled states and costates are roughly the same order of magnitude" [23]. The reason it is important for the states and costates to be roughly the same order of magnitude is due to the relationship between the two.

$$\lambda \text{ UNITS} = \frac{\text{Cost UNITS}}{\text{State UNITS}} \tag{4.14}$$

For the 3DOF missile problem the scaled costate vector becomes:

$$\bar{\lambda}^T = \left[\lambda_x \frac{X}{T}, \lambda_y \frac{Y}{T}, \lambda_z \frac{Z}{T}, \lambda_v \frac{V}{T}, \lambda_\sigma \frac{\Sigma}{T}, \lambda_\gamma \frac{\Gamma}{T}\right] \tag{4.15}$$

Pontryagin's Principle and the Hamiltonian Value Condition do not change when the Hamiltonian is scaled which is why problem scaling is effective. For a practical problem, the scaling is applied within the MATLAB coding and a trial and error approach is used in order to find the values that produce a solution where and the states and costates at approximately the same order of magnitude [23].

2. Coding the Scaling in MATLAB

In order to apply scaling to the problem, several additional lines of code are required in the m-files that are to be used by DIDO. The first step is to create a global variable by the name of SCALES in the main file. This is done for convenience so that the scale factors can be easily shared between the different m-files. In the main file, the scales are then defined for each of the states, controls, and time variable as follows:

```
global SCALES;
SCALES.X = 1;
SCALES.Y = 1;
SCALES.Z = 1;
SCALES.V = 1;
SCALES.SIGMA = 1;
SCALES.GAMMA = 1;
SCALES.ALPHA = 1;
SCALES.MU = 1;
SCALES.T = 1;
```
(4.16)

In the dynamics file, in the preamble where the states, controls and nodes are defined from the primal data structure, the scaling factor for each variable is applied. Then when defining *xdot*, the vector is multiplied by the time scale factor and then each element of the vector is divided by its scaling factor returning the output to the original value. Thus, the dynamics are computed in engineering units but are operated on by the numerical algorithm in terms of designer units. In the main file, all of the bounds for the states, controls, time and events must also be divided by the scale for the appropriate value. Of note, the scaling used when running the program with lower nodes may need to

be refined as the results are stepped into higher node runs for increased accuracy. An additional benefit to the scaling is that it also allows for quicker run times.

As an example, for the optimal control problem that is solved in later Chapter V, when DIDO is run without any scaling the output for the states x and γ versus time are shown in Figures 38 and 39. As shown, the ranges of the two states differ by five orders of magnitude so scaling can be used to collapse this range.

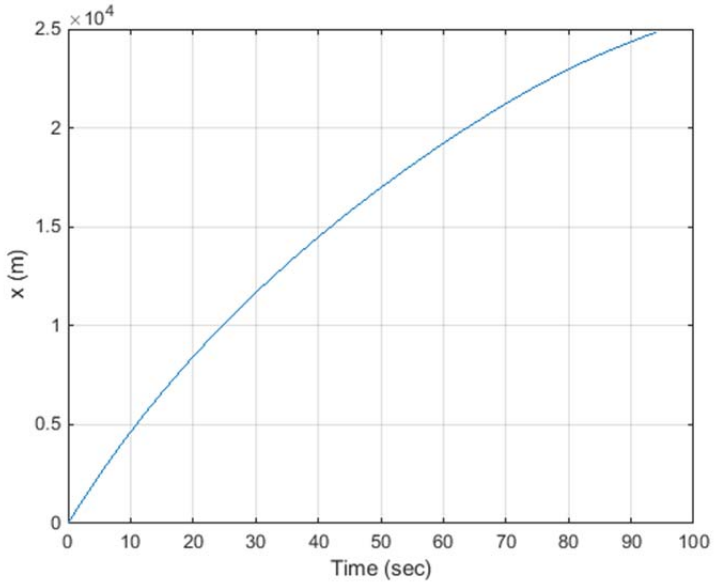

Figure 38. Down-Range Distance versus Time

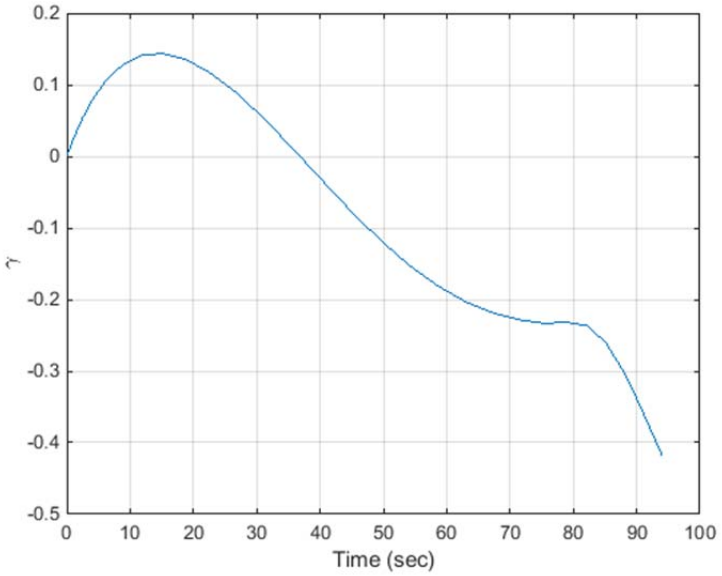

Figure 39. Flight Path Elevation Angle versus Time

The scaling not only applies to the relationship between the states, but also the relationship between the state and it's costate. The costates for x and γ versus time are shown in Figures 40 and 41. The range of x and λ_x differ by four orders of magnitude and the range of γ and λ_γ differ by three orders of magnitude. The ideal range between the states and costates is a 1:1 relationship with the range of both values being of the same order of magnitude.

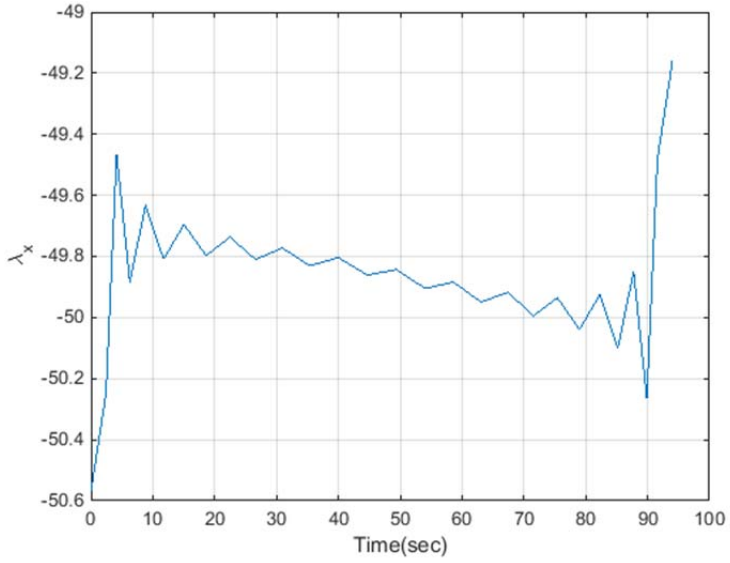

Figure 40. λ_x versus Time for Maximum Range Maneuver

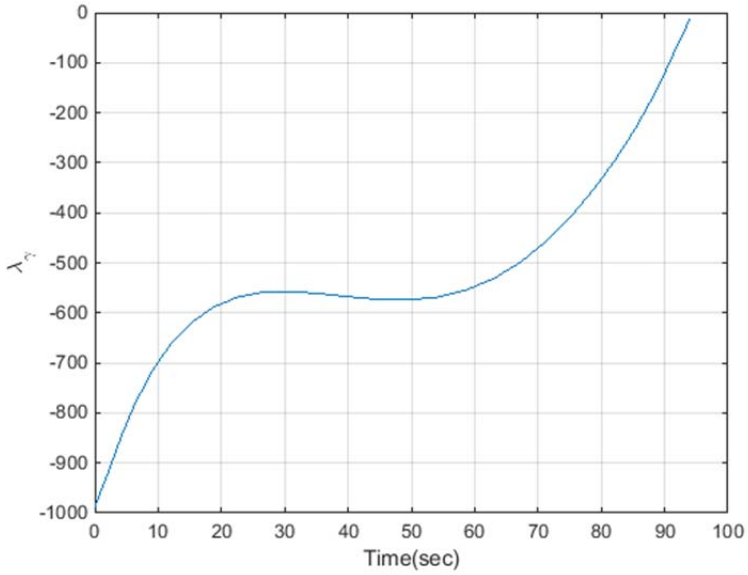

Figure 41. λ_γ versus Time for Maximum Range Maneuver

Designer units can be applied to these variables in the dynamics files as

```
x       = primal.states(1,:)*SCALES.X;
sigma   = primal.states(5,:)*SCALES.SIGMA;
```
(4.17)

This same principal is applied to all of the other states. Since the dynamics m-file must output the scaled dynamics (*xdot*) for the algorithm to operate on, the dynamics (calculated in engineering units) must be converted back to designer units. Converting the dynamics from engineering units to designer units is done as shown in Equation (4.18).

$$\begin{aligned} \text{xdot}(:,i) = \text{SCALES.T}*[\text{xDot}(i)./\text{SCALES.X}; \\ \text{sigmaDot}(i)/\text{SCALES.SIGMA}]; \end{aligned} \tag{4.18}$$

When DIDO is run with the scaling applied, the resulting scaled states and costates are shown in Figure 42. Referring to Figure 42, the scaled states and costates are now similar in order of magnitude, which improves the quality of the numerical solution.

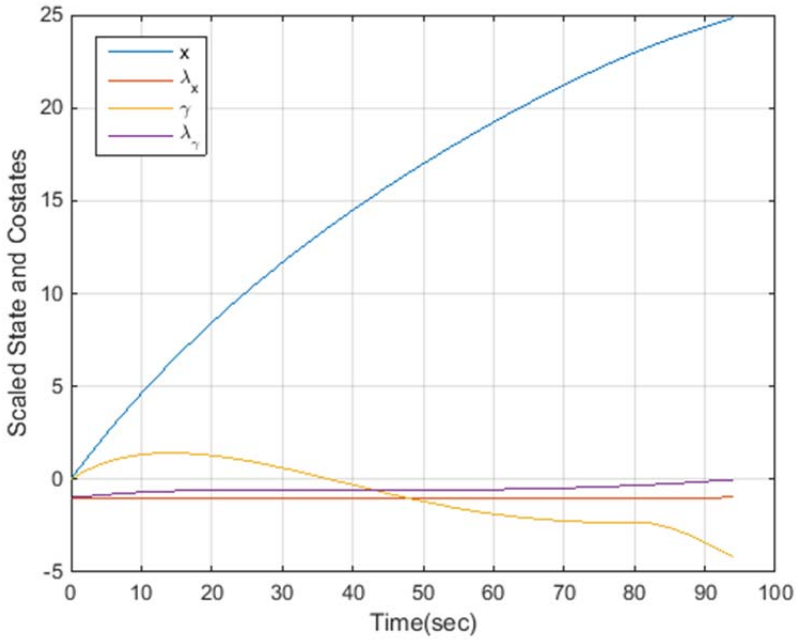

Figure 42. Scaled States versus Time for Maximum Range Maneuver

C. SUMMARY

This chapter provided the basic background needed for this thesis in regard to optimal control theory. This chapter also introduced the DIDO psuedospectral optimal control software, the software package used to solve the optimal missile trajectories in

this work. Issues related to numerical conditioning via scaling through designer units were also discussed. The optimal control framework will be applied to the missile problem in the next chapter.

V. MAXIMIZING THE RANGE OF A GUIDED ROCKET

In this chapter optimal control theory is used to obtain a guidance solution to maximize the range of the fictitious missile under study. The bounds and conditions that were used for the problem setup as well as development of the necessary conditions for optimality will be shown. The results of the solutions obtained using DIDO will be presented and discussed. The resulting maneuver will be compared to the conventional proportional navigation based solution. As will be seen, the application of optimal control theory allows the range of the missile to be enhanced significantly.

A. DESCRIPTION OF THE PROBLEM

The desired outcome of the optimal control problem studied in this chapter is to maximize the range that the missile is able to travel. In order to start building the optimal control problem formulation, the 3DOF equations developed in Chapter II will be used. As mentioned previously, for the scope of this thesis, the problem will consider a guided rocket traveling in the mid-to-terminal phase of flight only. Thus, it will be assumed that the problem begins once the rocket motor is burned. The 3DOF optimal control problem was set up utilizing the version of the dynamics equations shown in Equation (2.7). The state and control variables for the problem are repeated in Table 9 for convenience.

Table 9. Reduced 3DOF Model States and Controls

State	Symbol	Units
x-position (down-range distance)	x	m
y-position (cross-range distance)	y	m
z-position (altitude)	z	m
velocity (airspeed)	v	m/s
flight path heading angle	σ	rad
flight path elevation angle	γ	rad
Control	Symbol	Units
angle of attack	α	rad
bank angle	μ	rad

Since the missile's autopilot utilizes inner loop control logic, the control variables for the optimal control problem can be written as

$$\begin{aligned} \dot{\alpha} &= u_a \\ \dot{\mu} &= u_\mu \end{aligned}, \tag{5.1}$$

which allows the optimal control solution to accommodate the time constraints from the inner loop.

The maximum range problem is solved by minimizing the negative value of the final downrange position, x_f. Hence for the maximum range problem, there is an endpoint cost but no running cost. Problems with a specified crossrange are not considered. The maximum range optimal control problem is therefore stated as

$$
\left(P_{OC\ \text{Max. Distance}}\right)=\begin{cases}
\text{Minimize } J\left[\boldsymbol{x}(\bullet),u(\bullet),t_f\right]=-\boldsymbol{x}_f \\
\text{Subject to:} \\
\dot{x}=v\cos\gamma\cos\sigma \\
\dot{y}=v\cos\gamma\sin\sigma \\
\dot{z}=v\sin\gamma \\
\dot{v}=\dfrac{-D}{m}-g\sin\gamma \\
\dot{\sigma}=\dfrac{L}{mv}\dfrac{\sin\mu}{\cos\gamma} \\
\dot{\gamma}=\dfrac{L}{mv}\cos\mu-\dfrac{g}{v}\cos\gamma \\
\dot{\alpha}=u_\alpha \\
\dot{\mu}=u_\mu \\
\boldsymbol{x}\left(t_0\right)=\left[x_0,y_0,z_0,v_0,\sigma_0,\gamma_0\right] \\
t_0=t^0 \\
e(\boldsymbol{x}(t_f))=\left[z_f\right] \\
u_\alpha{}^L\le\left|u_\alpha\right|\le u_\alpha{}^U \\
u_\mu{}^L\le\left|u_\mu\right|\le u_\mu{}^U
\end{cases}
\tag{5.2}
$$

In Equation (5.2), $\boldsymbol{x}^0$ is a given vector that consists of the initial conditions for the states at time t_0. The values that comprise $\boldsymbol{x}^0$ are given in the next section in Table 10. Equation (5.2) also states that $e(\boldsymbol{x}(t_f))=\left[z_f\right]$ (i.e., the maximum range is reached when the missile impacts the ground). The numerical values that comprise the initial and final conditions are given in the next section in Tables 11 and 12, respectively. Since the problem statement does not include a running cost, the value is equal to zero at the final time.

B. APPLICATION OF THE OPTIMAL CONTROL THEORY

Now that the problem has been stated, the next step is to apply the process that was described in Section A of Chapter IV, in order to derive the necessary conditions for

optimality. The first step is the formulation of the Hamiltonian utilizing Equation (4.2). The Hamiltonian for the Problem (5.2) is

$$\begin{aligned} H(\lambda,x,u) &= \lambda_x\left[v\cos\gamma\cos\sigma\right]+\lambda_y\left[v\cos\gamma\sin\sigma\right]+\lambda_z\left[v\sin\gamma\right] \\ &+\lambda_v\left[\frac{-D}{m}-g\sin\gamma\right]+\lambda_\sigma\left[\frac{L}{mv}\frac{\sin\mu}{\cos\gamma}\right] \\ &+\lambda_\gamma\left[\frac{L}{mv}\cos\mu-\frac{g}{v}\cos\gamma\right]+\lambda_\alpha u_\alpha+\lambda_\mu u_\mu \end{aligned} \tag{5.3}$$

Taking the partial derivative of the Hamiltonian with respect to the control variables gives

$$\begin{aligned} \frac{\partial H}{\partial u_\alpha} &= \lambda_\alpha = 0 \\ \frac{\partial H}{\partial u_\mu} &= \lambda_\mu = 0 \end{aligned} \quad . \tag{5.4}$$

Thus, the Hamiltonian Minimization Theorem must be applied, where

$$(HMC)\begin{cases} \text{Minimize} & H(\lambda,x,u) \\ \text{Subject to} & u^L \le u \le u^U \end{cases}, \tag{5.5}$$

due to the fact that the control variables appear linearly in Equation (5.3). The equations in Equation (5.4) become switching functions, as shown in [19], where

$$S_\alpha = \begin{cases} \lambda_\alpha > 0 & u_\alpha = u_{\alpha_{\min}} \\ \lambda_\alpha < 0 & u_\alpha = u_{\alpha_{\max}} \\ \lambda_\alpha = 0 & u_{\alpha_{\min}} \le u_\alpha \le u_{\alpha_{\max}} \end{cases} \tag{5.6}$$

The same principal can be applied to the other control variable, which produces the second switching function

$$S_\mu = \begin{cases} \lambda_\mu > 0 & u_\mu = u_{\mu_{\min}} \\ \lambda_\mu < 0 & u_\mu = u_{\mu_{\max}} \\ \lambda_\mu = 0 & u_{\mu_{\min}} \le u_\mu \le u_{\mu_{\max}} \end{cases} \tag{5.7}$$

These switching functions given in Equations (5.6) and (5.7) can be utilized as an additional means for validation and verification of the optimal control solution. For example, λ_α and u_α can be plotted to check that if u_α is at the upper bound, then $\lambda_\alpha < 0$, etc. The same analysis can be performed with λ_μ and u_μ. If the trajectories obey the inequality for the switching function, then the necessary condition for optimality is satisfied. If not, then the solution may not be correct and the reason for the discrepancy must be isolated and corrected.

Because the adjoint equations are only being used for verification and validation rather than problem solving, ρ can be assumed constant in the drag and lift equations when the costate dynamics are derived. The application of Equation (4.2), the adjoint equation becomes

$$
\begin{aligned}
\dot{\lambda}_x(t) &= -\frac{\partial H}{\partial x} = 0 \\
\dot{\lambda}_y(t) &= -\frac{\partial H}{\partial y} = 0 \\
\dot{\lambda}_z(t) &= -\frac{\partial H}{\partial z} = 0 \\
\dot{\lambda}_v(t) &= -\frac{\partial H}{\partial v} = -\lambda_x \cos\gamma\cos\sigma - \lambda_y \cos\gamma\sin\sigma - \lambda_z \sin\gamma \\
&\quad -\lambda_v\left[\frac{1}{m}\rho v S_{ref} C_D\right] + \lambda_\sigma\left[\frac{1}{m}(\frac{1}{2}\rho S_{ref} C_L)\frac{\sin\mu}{\cos\gamma}\right] \\
&\quad +\lambda_\gamma\left[\frac{1}{m}(\frac{1}{2}\rho S_{ref} C_L)\cos\mu + \frac{g}{v^2}\cos\gamma\right] \\
\dot{\lambda}_\sigma(t) &= -\frac{\partial H}{\partial \sigma} = \lambda_x\left[v\cos\gamma\sin\sigma\right] - \lambda_y\left[v\cos\gamma\cos\sigma\right] \\
\dot{\lambda}_\gamma(t) &= -\frac{\partial H}{\partial \gamma} = \lambda_x\left[v\sin\gamma\cos\sigma\right] + \lambda_y\left[v\sin\gamma\sin\sigma\right] - \lambda_z\left[v\cos\gamma\right] \\
&\quad +\lambda_v\left[g\cos\gamma\right] - \lambda_\sigma\left[\frac{L}{mv}\frac{\sin\mu\sin\gamma}{\cos^2\gamma}\right] + \lambda_\gamma\left[\frac{g}{v}\sin\gamma\right] \\
\dot{\lambda}_\alpha(t) &= -\frac{\partial H}{\partial \alpha} = -\lambda_v\left[\frac{1}{m}\left(\frac{1}{2}\rho v^2 S_{ref}\left(C_x\sin\alpha + C_z\cos\alpha\right)\right)\right] \\
&\quad -\lambda_\sigma\left[\frac{1}{mv}\left(\frac{1}{2}\rho v^2 S_{ref}\left(-C_x\cos\alpha - C_z\sin\alpha\right)\right)\frac{\cos\mu}{\cos\gamma}\right] \\
&\quad -\lambda_\gamma\left[\frac{1}{mv}\left(\frac{1}{2}\rho v^2 S_{ref}\left(-C_x\cos\alpha - C_z\sin\alpha\right)\right)\cos\mu\right] \\
\dot{\lambda}_\mu(t) &= -\frac{\partial H}{\partial \mu} = -\lambda_\sigma\left[\frac{L}{mv}\frac{\cos\mu}{\cos\gamma}\right] + \lambda_\gamma\left[\frac{L}{mv}\sin\mu\right]
\end{aligned}
\tag{5.7}
$$

From Equation (5.7), since $\dot{\lambda}_x = \dot{\lambda}_y = \dot{\lambda}_z = 0$, the costates for the *x*, *y*, and *z* variables must be constant. This provides another piece of information that can be used to verify the DIDO outputs. If the numerical values of the costates are not constant, then the solution can be determined to be invalid.

The transversality condition is applied next. The Endpoint Lagrangian becomes

$$
\overline{E}(v, x(t_f)) = E\left(x_f\right) + \upsilon^T e(x_f) = -x_f + \upsilon_1 z_f, \tag{5.8}
$$

When partial derivative of the Endpoint Langrangian is taken with respect to each of the states (at t_f), the value of the costate at time t_f is obtained. These values, together with the behavior of the adjoint equations can also be used for verification and validation of the optimal control solution.

$$\begin{aligned}
\lambda_x\left(t_f\right) &= \frac{\partial \bar{E}}{\partial x_f} = -1 \\
\lambda_y\left(t_f\right) &= \frac{\partial \bar{E}}{\partial y_f} = 0 \\
\lambda_z\left(t_f\right) &= \frac{\partial \bar{E}}{\partial z_f} = \upsilon_1 \\
\lambda_v\left(t_f\right) &= \frac{\partial \bar{E}}{\partial v_f} = 0 \\
\lambda_\sigma\left(t_f\right) &= \frac{\partial \bar{E}}{\partial \sigma_f} = 0 \\
\lambda_\gamma\left(t_f\right) &= \frac{\partial \bar{E}}{\partial x_f} = 0
\end{aligned} \tag{5.9}$$

1. State and Control Variable Bounds

As mentioned in Chapter IV, Section B, the main program file for the DIDO problem contains the required bounds for each state variable. The constraints serve to provide a restrictive range to search for a feasible solution to the optimal control problem. While the goal is to limit the search range, the search range needs to be large enough that it encompasses the range in which a feasible solution can be found.

For the problem addressed in this thesis, the x-limit is based on having a range that allows the entire maneuver to be completed. The x-limit was adjusted until the final solution was inside the upper bound ensuring that the maximum range of the missile could be reached. The z-limit set the ceiling for the maneuver. The allowed cross-range was ±100 m. The velocity limits ranged from the maximum speed of the missile to 100 m/s which was estimated to be the minimum speed needed on missile impact at the target. The bounds for the states and controls are shown in Table 10.

Table 10. Bounds for the States and Controls for Maximum Range Maneuver

State	Lower Bound	Upper Bound	Units
x	0	30000	m
y	-100	100	m
z	0	3000	m
v	100	625	m/s
σ	-π/6	π/6	rad
γ	-π/6	π/6	rad
Control			
α	-0.349	0.489	rad
μ	-0.0872	0.0872	rad
u_α	-0.349	0.489	rad/sec
u_μ	-0.0872	0.0872	rad/sec

2. Initial Conditions

As stated above, the maximum range maneuver begins with the missile in-flight at the moment that the engine has burnt out and the thrust goes to zero. The missile is assumed to be in steady state controlled flight at the moment that the terminal maneuver begins. The known initial conditions are shown in Table 11. The initial conditions are the same conditions that were utilized for the conventional approach in order to be able to properly compare to the results from the OCP.

Table 11. Initial Conditions for Maximum Range OCP

	Units	Value
x_o	m	0
y_o	m	0
z_o	m	661.1
v_o	m/s	514.5
σ_o	rad	0
γ_o	rad	0
α_o	rad	0.349
μ_o	rad	0

In order to determine the initial value for the angle of attack, the fact that the rate of change of the flight path elevation angle would need to be zero for the missile to be in straight and level flight was used. From Equation (2.7) it is given that

$$\dot{\gamma} = \frac{L}{mv}\cos\mu - \frac{g}{v}\cos\gamma \tag{5.10}$$

Substituting the known values at the initial condition, the equation reduces to

$$\frac{L}{m} - g = 0\,, \tag{5.11}$$

where

$$L = \frac{1}{2}\rho v^2 S_{ref} C_L\,. \tag{5.12}$$

By substituting in the equation for C_L that was developed earlier in Chapter II, the angle of attack for straight and level flight was determined to be 0.349 rad (20 deg). For the optimal control model, the missile is being controlled through adjustment of the angle of attack. On the physical missile, however these changes are implemented through applying fin deflections to produce the desired results. Thus, for implementation of the optimal maneuver, an inner loop autopilot would need to be used.

3. Final Conditions

In addition to the initial conditions, the events function allows the user to input any known final or endpoint conditions. For this problem, the distance that the missile would travel was unknown as well as the velocity at the point of impact. In addition, the orientation of the missile with respect to the reference plain at the time of impact was not known. The only known endpoint condition was that missile would impact the ground, thus $z_f = 0$ as listed in Table 12.

Table 12. Known End Point Conditions for the Maximum Range OCP

	Units	Value
z_f	m	0

C. MAXIMUM RANGE SOLUTION

With all the data defined for the cost, event, dynamics, and main files, the problem case was coded and solved using DIDO.

1. Selection of Coefficient of Lift and Drag Fidelity

In Chapter II, equations for the coefficient of lift and drag were determined from the Missile DATCOM. Equations (2.15)–(2.20) provided three different curve fits that could be used for each of the coefficients. When DIDO was initially run, a third degree polynomial curve fit was used because it had the highest correlation value of the three fits. The results of these initial runs indicated that the problem was infeasible.

While the results from a DIDO run for an infeasible solution cannot be trusted as accurate, one observation that was noticed was that the costates were incredibly large, shown in Figure 43. This indicated that problem scaling was likely the reason why the problem was being determined infeasible.

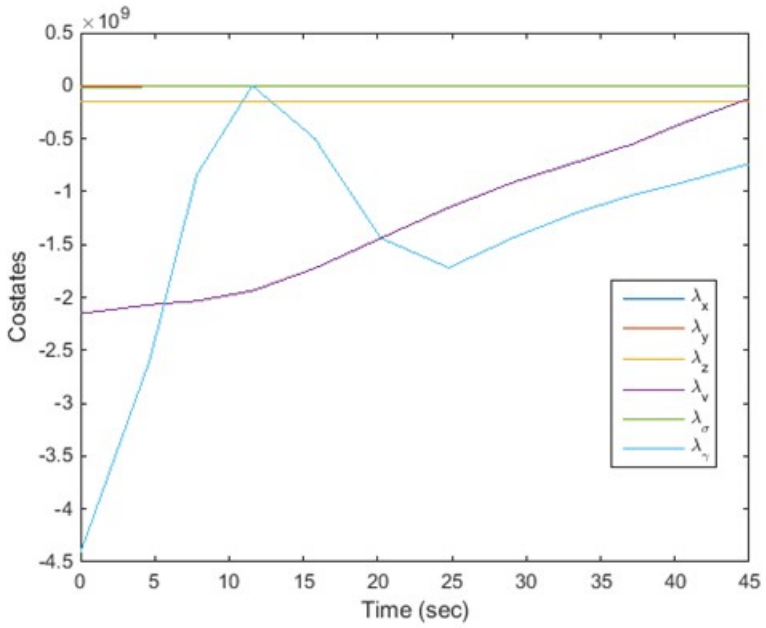

Figure 43. Costates versus Time for DIDO Run with a 3rd Degree Polynomial Curve Fit Applied to C_L and C_D

The two costates that were drastically larger than the other costates were the one for velocity and flight path angle. When examining the equations for the costates, Equation (5.5), it was noted that they were the only two costates that contained the coefficients of lift and drag. In addition, both equations had $\cos\gamma$ or $\cos^2\gamma$ in the denominator. For small angles of attack, the result of the angle of attack being cubed in the equation caused the value for gamma to approach $\pi/2$, which produced a very small number in the denominator causing the values of the costates to become quite large.

To test the theory, the problem was run with a linear curve fit for the coefficient of lift and drag equations and DIDO produced a feasible result with the costates all within the same order of magnitude. The problem was then run again with a second degree curve fit and DIDO once again produced a feasible result with the costates within the same order of magnitude. This process provided a valuable lesson learned. When utilizing a model, such as Missile DATCOM output, to produce equations for estimating the coefficients of lift and drag it is best to start with a lower fidelity model for initial simulation runs. Once the problem has been properly scaled, the fidelity can then be

increased incrementally the scaling adjusted appropriately at each increment. For the results that will be discussed later in the chapter, both the coefficient of lift and drag equations are the equations obtained for second degree polynomial curve fits.

2. Results

a. Scaling the Problem

When the problem was run with the 2nd order curve fits for the aerodynamic data (Equations 2.16, 2.19), a feasible solution could be obtained using $N = 16$ collocation nodes. However, the resulting costate for the flight path angle, Figure 44, was still several orders of magnitude greater than the other costates. In addition, the variation in the Hamiltonian, Figure 45, was large, which is inconsistent with the associated necessary condition. As stated in Chapter IV, Section B, the way to resolve these issues is through proper scaling.

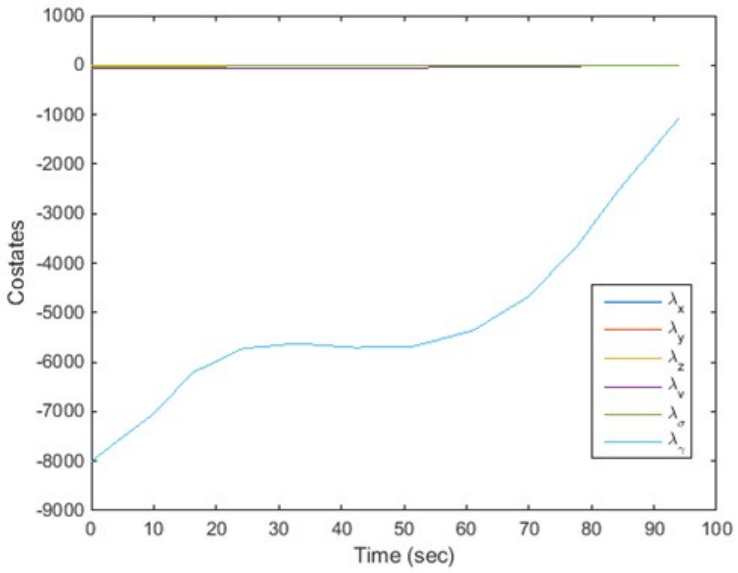

Figure 44. Costates versus Time for Unscaled Maximum Range Maneuver

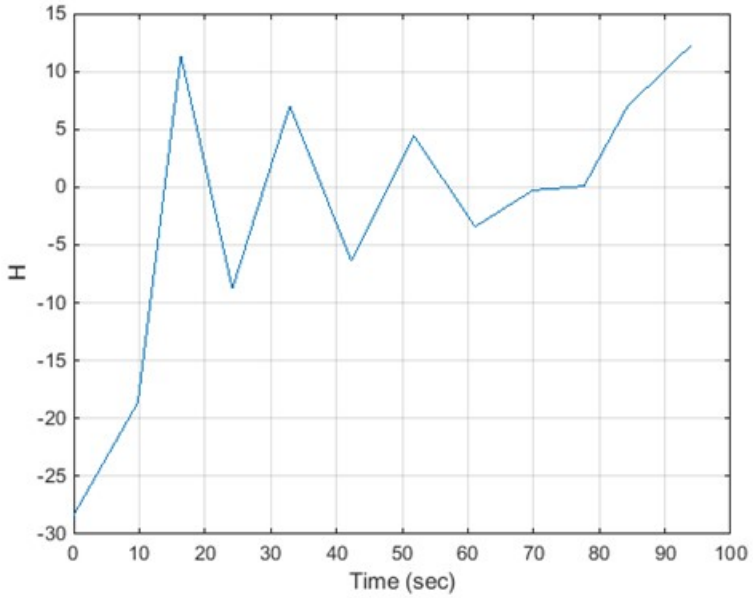

Figure 45. Hamiltonian for the Unscaled Maximum Range Maneuver

In order to determine the proper "designer units" for this problem, multiple trial run were conducted. The resulting scaling factors for the problem were determined as follows:

```
SCALES.X = 1000;
SCALES.Y = 50;
SCALES.Z = 100;
SCALES.V = 50;
SCALES.SIGMA = 1;                                    (5.13)
SCALES.GAMMA = 0.1;
SCALES.ALPHA = 1;
SCALES.MU = 1;
SCALES.T=1;
```

With these designer units the ranges of the states and costates became comparable (as will be shown next) and the problem run time improved.

b. Solutions for the Scaled Maximum Range Problem

The problem was then re-run and refined using N = 16, 24, and 32 collocation nodes utilizing the scaling factors developed in the previous section. After DIDO produced a feasible solution, the states, costates, controls, Hamiltonian, and cost for the problem were outputted. The position of the missile versus time is shown in Figure 46. Since the cross-range is zero (even though this condition was not specified), the results show that the range is maximized by flying in the x-z plane.

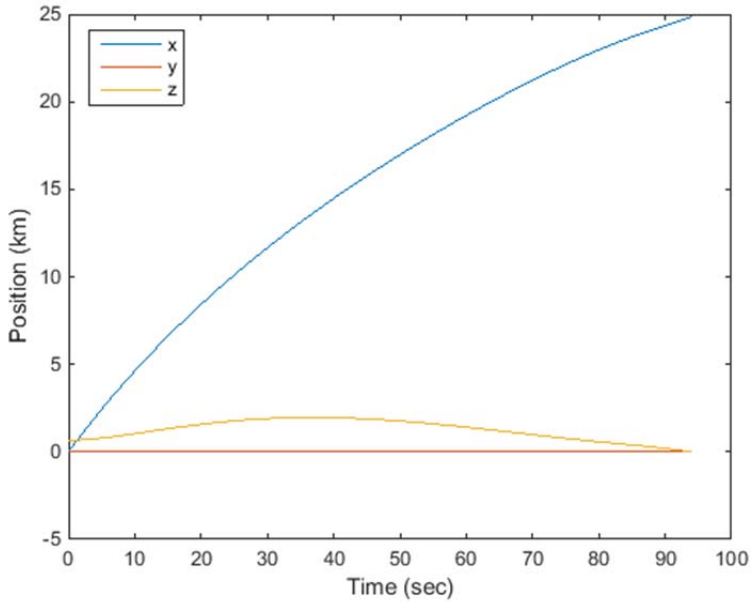

Figure 46. Position versus Time for the Maximum Range Solution

When the maneuver was initiated, the missile is seen to initially climb to an altitude of 1954 m before beginning its decent. The missile impacted the ground at a time of 94.02 seconds. The missile's altitude throughout the flight is shown more clearly in Figure 47. As mentioned above, the optimal trajectory for the missile was in the x-z-plane. The trajectory of the missile in this plane is shown in Figure 48.

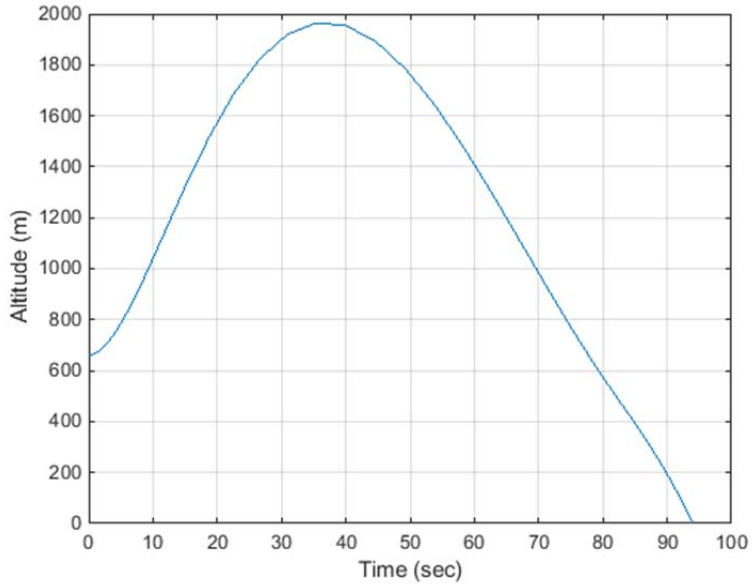

Figure 47. Altitude Profile for the Maximum Range Maneuver

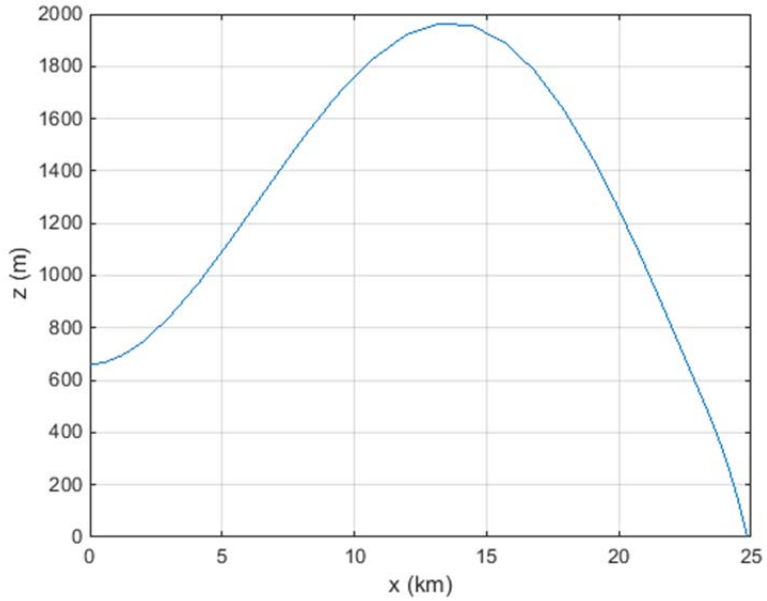

Figure 48. Trajectory of the Missile for Maximum Range Maneuver

The missile was traveling at a speed of 121.4 m/s when it impacted the ground, as shown in Figure 49, which exceeds the minimum required velocity of greater than 100 m/s for impact.

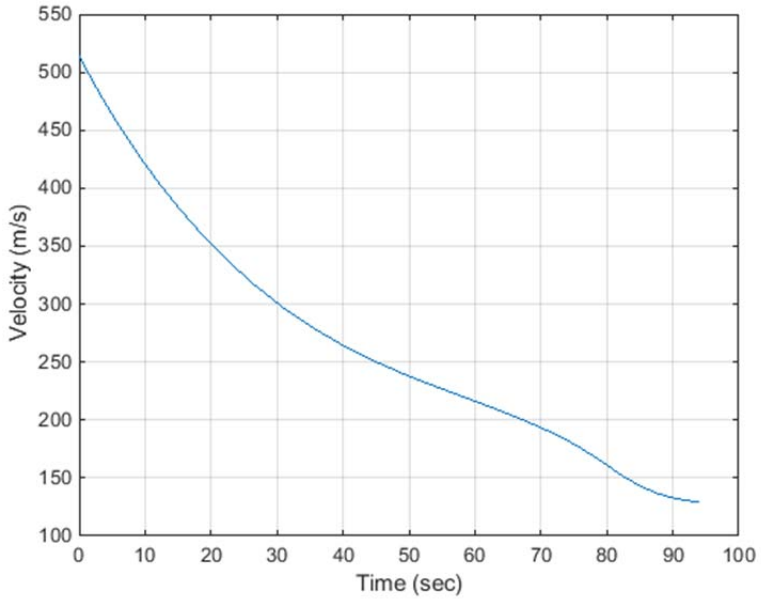

Figure 49. Velocity versus Time for Maximum Range Maneuver

The angle of attack for the missile was set with an upper limit of 0.489 rad (28 deg). The missile reaches the upper limit that was established near the end of the maneuver, shown in Figure 50. This behavior is similar to the conventional guidance approach which commands a large normal acceleration near the end of the flight in order to zero the line-of-sight error as shown previously in Figure 37. While the missile is climbing and then descending in this maneuver, the missile traveled in a zero crossrange path which resulted in negligible bank angles being applied to the missile, shown in Figure 51. If the desired maneuver required a turn or the missile was intercepting a moving target, this control would be utilized.

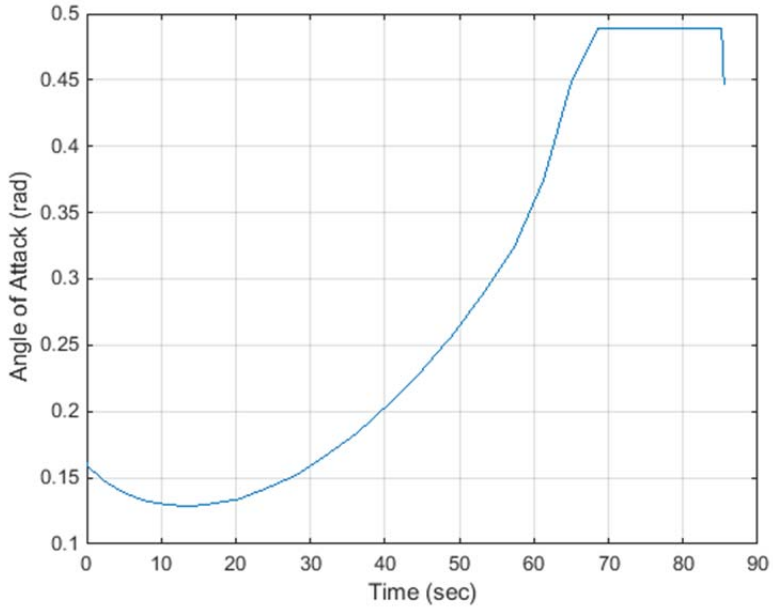

Figure 50. Angle of Attack versus Time for Maximum Range Maneuver

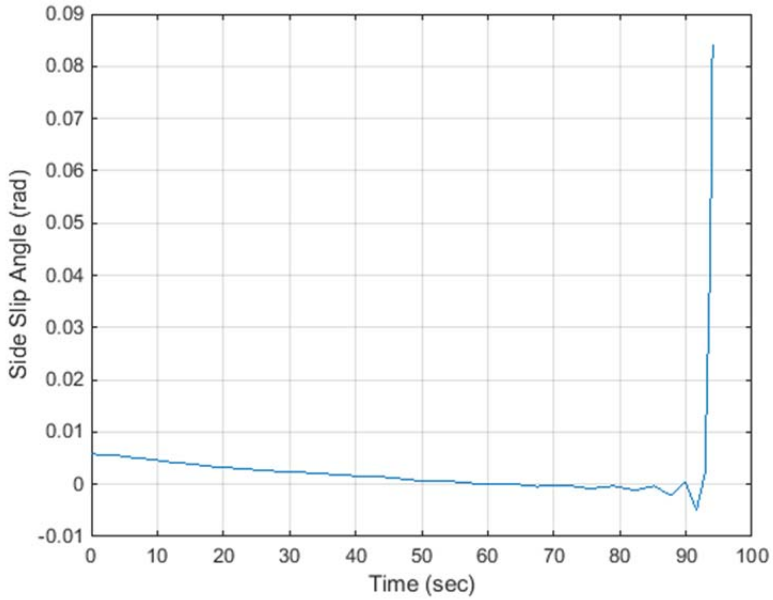

Figure 51. Roll Angle versus Time for Maximum Range Maneuver

The costates for the problem with scaling applied are shown in Figure 52. When compared to Figure 42, the effects of proper scaling on the costates can be clearly seen.

As mentioned above, Equation (5.7) showed that $\lambda_x, \lambda_y, \lambda_z$ should be constant. Figure 52, shows this to be true and is a validation point for the optimal control solution. When the costates listed above are plotted against time, Figure 52, the values are not exactly constant (due to numerical tolerances) but are within an acceptable level of error. As the fidelity of the model is increased through the bootstrapping to a higher number of nodes, the costate becomes smoother and settles towards being a constant value. However, even with infinite precision there will still be some error in the model. The costates for the other states are shown in Figure 53. As noted earlier, the behavior of these costates is complex so these trajectories are not useful as far as V&V is concerned. However, trasversality provides some conditions that can be checked. (Rachel pls. confirm that the behavior of the remaining costates (at the end time) is correct with respect to the transversality conditions.. For example, Equation (5.9) states that $\lambda_x\left(t_f\right) = -1$, and that $\lambda_\gamma\left(t_f\right) = 0$, etc. The results obtained from the optimal control solver are consistent with these equations.

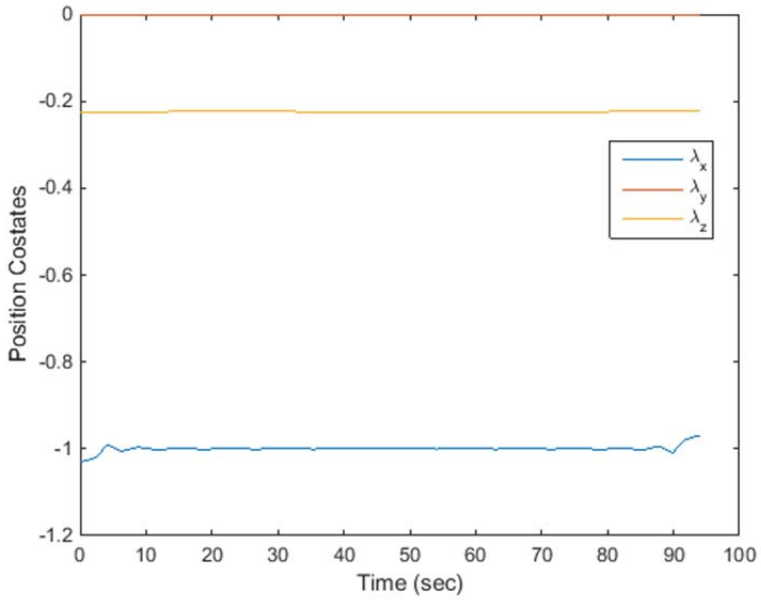

Figure 52. Scaled Position Costates versus Time for Maximum Range Maneuver

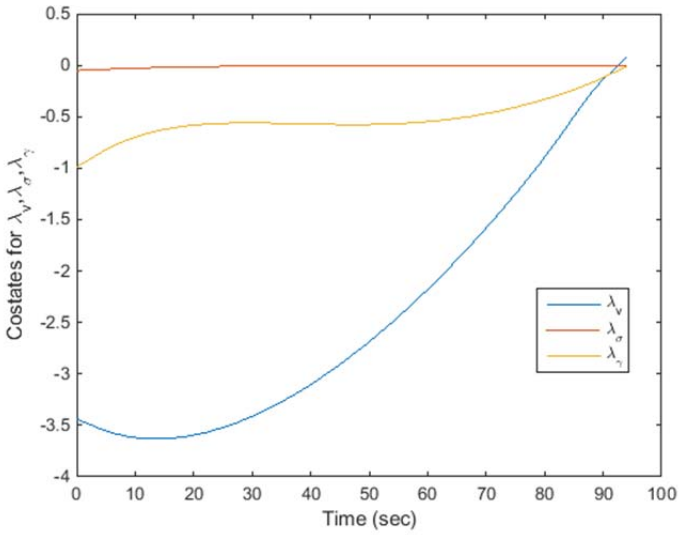

Figure 53. Scaled Costates for Velocity and Flight Path Angles versus Time for Maximum Range Maneuver

The Hamiltonian for the scaled problem is shown in Figure 54. The variation in the Hamiltonian is nearly zero, as required. The fact that the solution satisfies these necessary conditions allows one to conclude that an optimal solution has indeed been found and that the missile's range has been maximized per to problem limits and constraints.

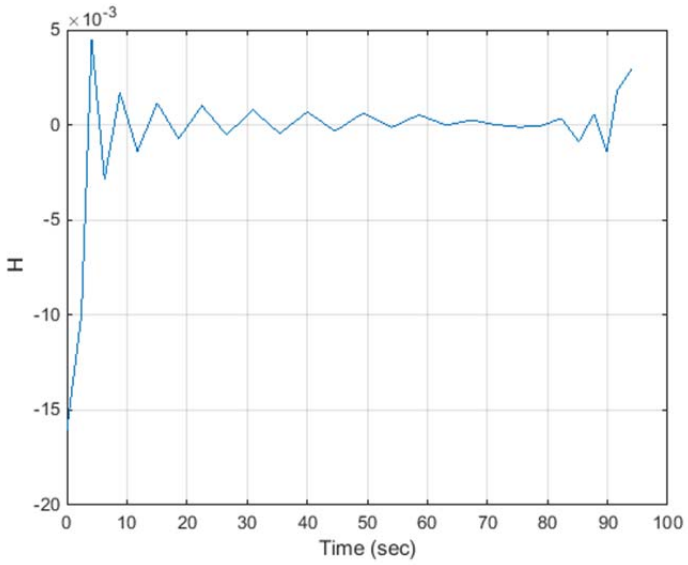

Figure 54. Hamiltonian versus Time for Maximum Range Maneuver

c. Verification and Validation

In order to verify that the optimal control solution is indeed a dynamically feasible solution, the next step was to perform a propagation test [15]. The optimal controls that were produced were propagated through the dynamic equations for the problem, Equation (2.7), using the ODE45 solver in MATLAB. The algorithm uses the control and time values associated with the nodes and interpolates to find the value for the control needed at a specific time. The results of the propagation were plotted against the optimal control solution for all of the states, shown in Figures 55–58. As can be seen the propagated solution closely matches the solution obtained from DIDO. Thus, the solution is feasible for implementation.

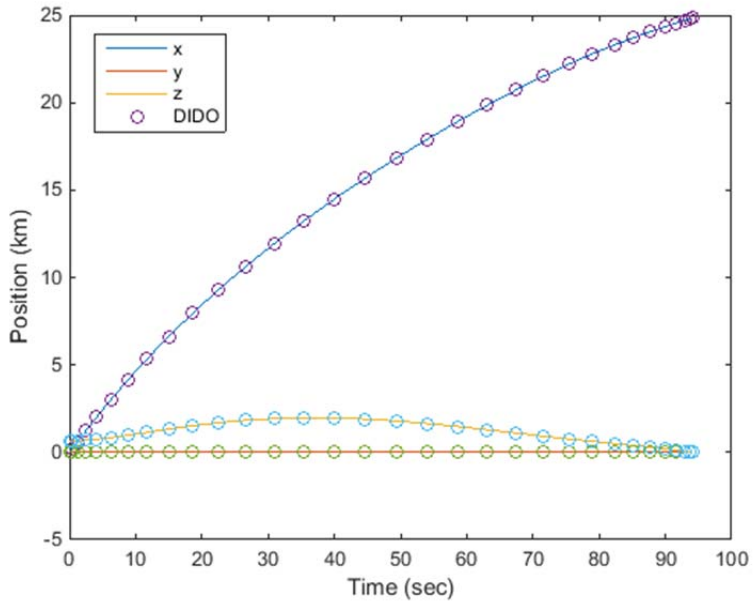

Figure 55. Verification of Position versus Time along the X-, Y- and Z-Axis for Maximum Range Maneuver

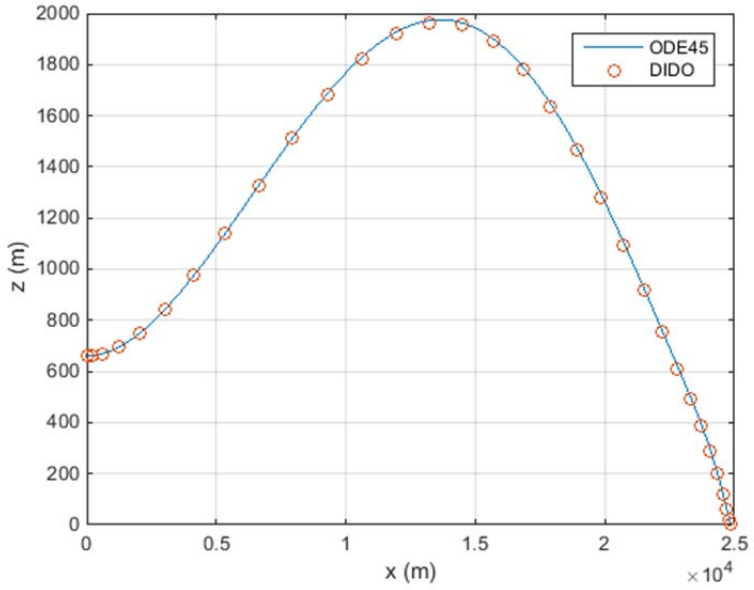

Figure 56. Verification of Missile Flight Path for Maximum Range Maneuver

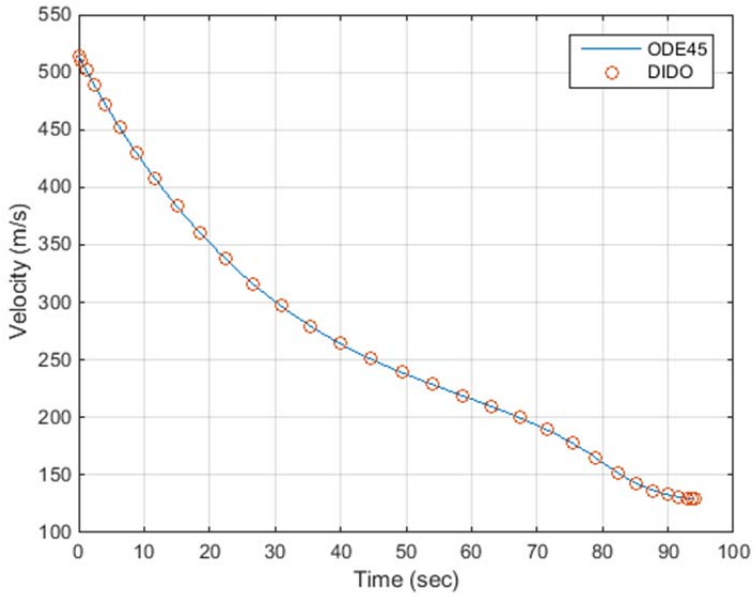

Figure 57. Verification of Velocity Vector for Maximum Range Maneuver

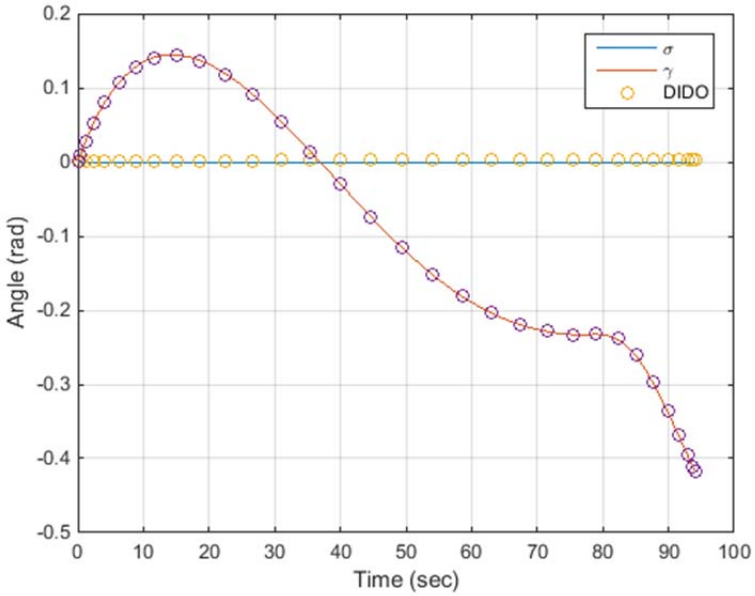

Figure 58. Verification of Flight Angles for Maximum Range Maneuver

d. Impact of AoA Range

In Chapter II, Section B, Paragraph 2, the range of AoA used to determine the coefficient of lift and drag plots within the MissileDATCOM was discussed. To show the impact that the incorrect range (and hence incorrect aerodynamic data) can have on the final solution, the results of the optimal control problem using Equations (2.10) and (2.11) are compared to the results obtained using Equations (2.12) and (2.13), shown in Figure 55.

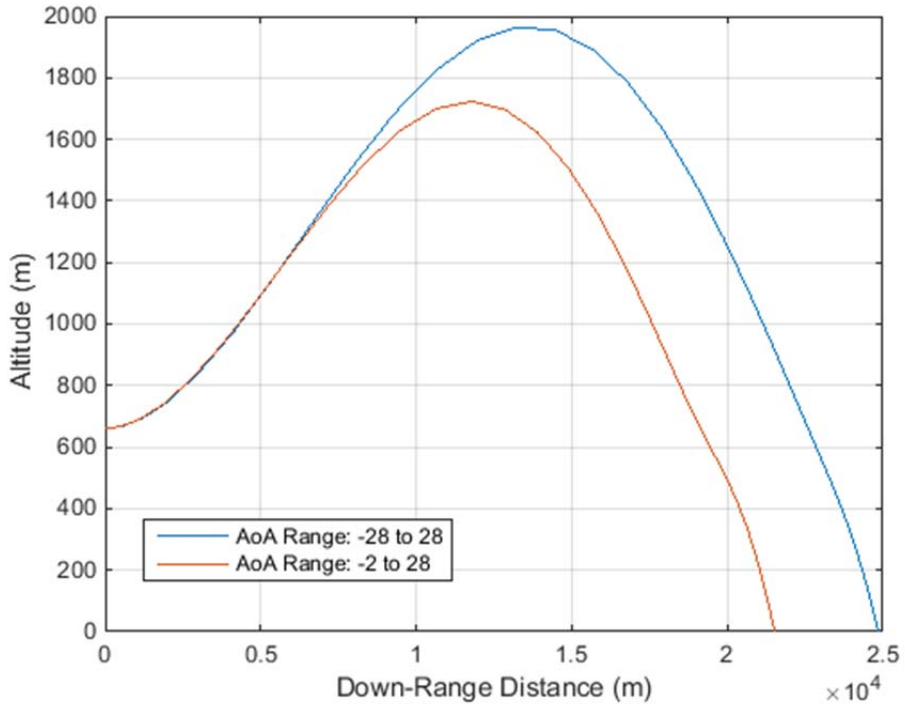

Figure 59. Comparison of Missile Trajectory Utilizing Curve Fits Derived from Different AoA Ranges

When the increased range of angles of attack to include the full range of the negative angles of attack, the distance the missile traveled increased significantly. Utilizing the incorrect solution resulted in underestimating the missile range by 3328 m. This result is included to be utilized as a lessoned learned for future work on this topic.

e. Setting Upper Bounds for AoA

In the results shown in subsection b, Figure 48, the angle of attack trends toward the upper bounds limit toward the end of the flight. As mentioned in Section B, the upper bound was set to 0.489 rad (28 deg). It was assumed that to ensure penetration of the target, the angle of attack would need to be less than 30 degrees when impacting the ground. Nonetheless, the effect of the upper bounds of the angle of attack was examined to determine the effect these limits could have on the optimal solution. The trajectories of the missile utilizing four different angle of attack limits are shown in Figure 60.

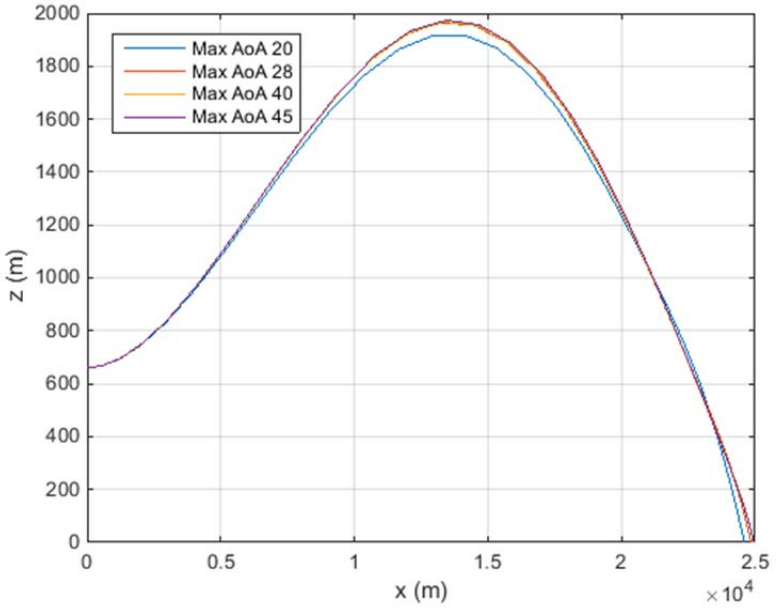

Figure 60. Trajectories of the Missile for a Maximum Range Maneuver with Various AoA Limits

The trajectories were all very similar and the path the missile follows (shown in Figure 60) appears to be nearly the same for all four angle of attack limits. When the point of impact for the missile is zoomed in on the graph (see Figure 61) it is seen that there is a difference of 350 m between the maximum angle of attack at 0.349 rad (20 deg) and 0.785 rad (45 deg). Depending on the situation, the extra 350 m in range could be a factor that warrants the consideration of adjusting the AoA limit to a larger value. This

decision, however, will depend on the constraints on missile effectiveness, aspects that are not considered here.

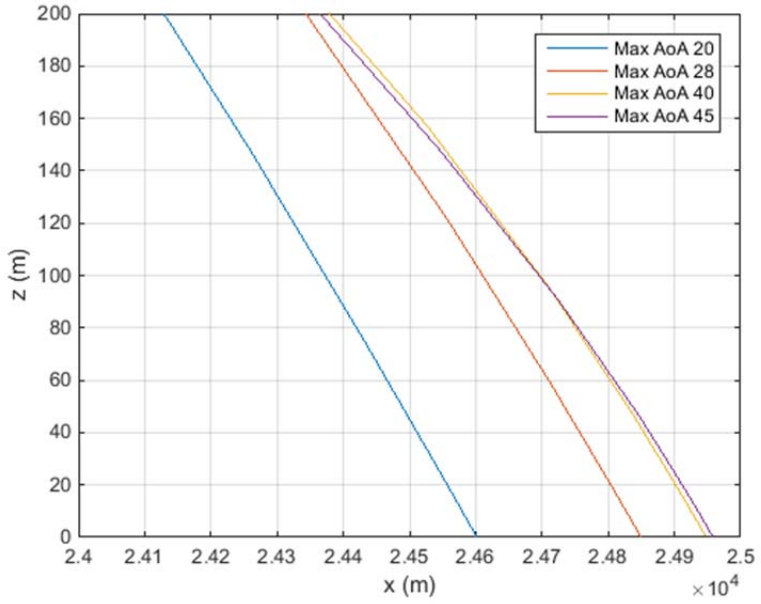

Figure 61. Trajectory of Missile in Last Portion of Flight

While the differences in the range of the missile are rather small compared to the overall range in the terminal phase, the impact of the maximum angle of attack bound can be seen the most in the velocity at the end of the flight, shown in Figure 62. When the maximum angle of attack is limited to 0.349 rad, the final velocity at the point of impact is 159.8 m/s, while a maximum angle of attack at 0.785 rad the final velocity is at the lower bound at 100 m/s and the time of flight is only a few seconds shorter.

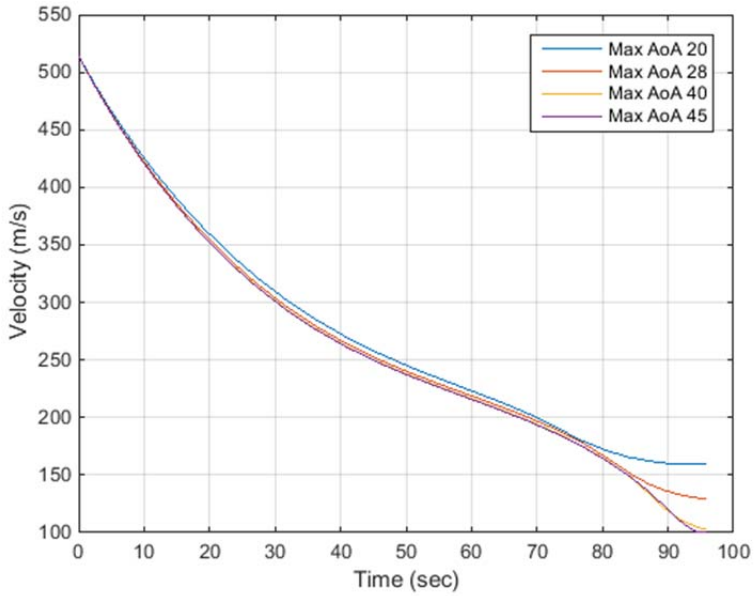

Figure 62. Velocity versus Time for Varying Maximum AoA

Depending on the target that is selected, a slightly (350 m) shorter range with a higher (+60 m/s) impact velocity may be desired over the increased range and slower impact speed. The higher velocity may allow the missile to penetrate further prior to detonation if the desired target is a building or bunker. If a shallower angle of attack on impact and decreased velocity is permissible, then the increased range may be the desired effect.

The comparisons shown above were done using the coefficient of lift and drag equations that were developed over a range of $-28 \le \alpha \le 28$. In aerodynamic flight, the attack angle produces an increase in lift until the angle of attack has increased to a point where the relative surface area of the missile to produce lift has decreased enough that the lift for the body begins to decrease. The larger angle of attacks examined may be beyond this point which would result in even further decreased ranges and impact velocities. The effect described above was not reached within the bounds for the optimal control problem and determination of the angle where this begins to occur is outside the scope of this thesis.

D. COMPARISON OF CONVENTIONAL AND OPTIMAL SOLUTIONS

1. Maximum Range Maneuver

When the trajectories of the missile are plotted against each other for both methods, shown in Figure 63, the difference between the two flight paths is substantial. Both of the problems began with the missile in the same steady flight condition but the fundamentals behind each approach make a significant difference in the outcome. The conventional approach is driven by a simple law involving the line-of-sight and range to the target. In the terminal phase of flight, this results in the missile assuming a ballistic trajectory. The optimal control solution, on the other hand, causes the missile to initiate a climb in the beginning of the maneuver utilizing the initial airspeed of the missile to gain altitude.

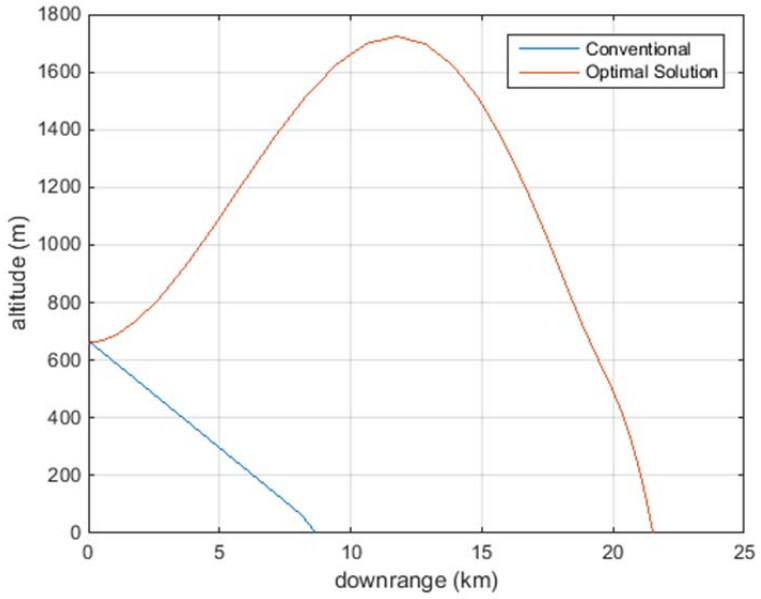

Figure 63. Comparison of the Missile Trajectory for Conventional and Optimal Control Method for Maximum Range Problem

The maximum downrange distance that could be achieved by the conventional approach to missile guidance with the given initial conditions was 8637 m. By utilizing the optimal control solution, the maximum range of the missile increased to 24850 m.

This was an improvement in range of 16213 m (8.75nm) which is nearly a 300% increase in the maximum range of the missile over the conventional proportional navigation based approach.

The time of flight was also significantly different from the conventional to optimal solution, shown in Figure 64. The time of flight for the missile using the conventional approach was 32.3 seconds, while the time of flight for the missile utilizing the optimal control solution was 94.02 seconds. This was an increase in the overall time of flight by a factor of 2.91. The increased range and time of flight allows the missile to be fired from further away and provides increased time for the aircraft firing the missile to get clear of the area. Both of these benefits can potentially improve the chances of mission success.

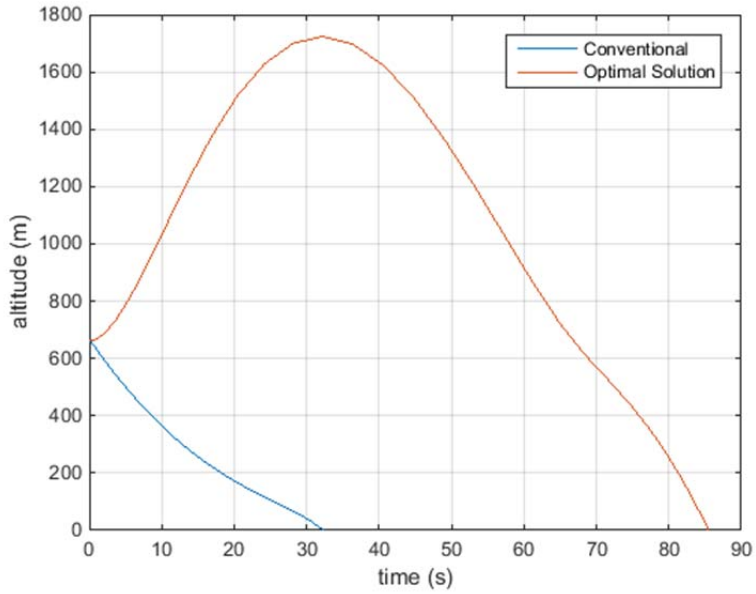

Figure 64. Time of Flight Comparison for Conventional and Optimal Control Methods for Maximum Range Problem

For both the conventional and optimal control approach, the velocity was plotted against time, shown in Figure 65. While the conventional approach has a much steeper, almost linear decrease in velocity, the optimal control solution has a gradual decrease

with the velocity leveling out slightly as the missile was at the top of the parabolic path and began its decent. In addition, the impact velocity was similar for both the conventional and optimal control solution, which means that increasing the range did not have an adverse impact on the terminal kinetic energy of the missile.

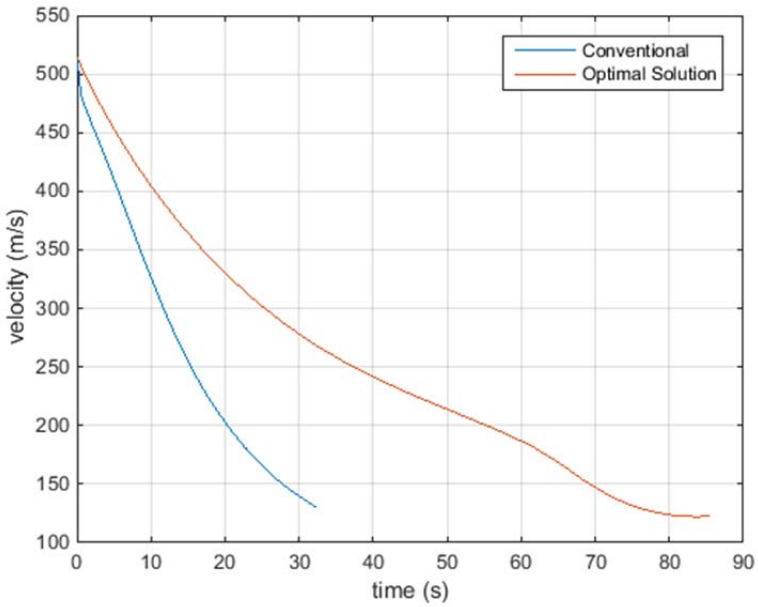

Figure 65. Comparison of Velocity versus Time for Maximum Range Problem

2. Minimum Time Solution

Because the maximum range produced with the optimal control solution was much greater than the maximum range that could be achieved by using the conventional approach, the range itself was the only aspect that could be clearly compared between the two approaches. To provide additional comparison of the two approaches for missile guidance, an additional optimal control problem was solved.

a. Problem Statement

For this problem, the desire was to minimize the time of flight to the same range obtained using the conventional approach. The second optimal control problem took the

same initial conditions as were used in the initial problem, shown in Table 11. However, an additional end point condition was added as shown in Table 12, by setting the downrange distance to the maximum range that was achieved by the conventional approach. The cost of the problem was also changed to minimize the time it would take for the missile to impact the target.

Table 13. Known End Point Conditions for Minimal Time OCP

	Units	Value
x_f	m	8637
z_f	m	0

The optimal control problem for the minimum maneuver is as follows:

$$\left(P_{OC\ \text{Min. Time}}\right)=\begin{cases}\text{Minimize } J\left[\boldsymbol{x}(\bullet),u(\bullet),t_f\right]=t_f\\ \text{Subject to:}\\ \dot{x}=v\cos\gamma\cos\sigma\\ \dot{y}=v\cos\gamma\sin\sigma\\ \dot{z}=v\sin\gamma\\ \dot{v}=\dfrac{-D}{m}-g\sin\gamma\\ \dot{\sigma}=\dfrac{L}{mv}\dfrac{\sin\mu}{\cos\gamma}\\ \dot{\gamma}=\dfrac{L}{mv}\cos\mu-\dfrac{g}{v}\cos\gamma\\ \dot{\alpha}=u_\alpha\\ \dot{\mu}=u_\mu\\ \boldsymbol{x}(t_0)=\left[x_0,y_0,z_0,v_0,\sigma_0,\gamma_0\right]\\ t_0=t^0\\ e(x(t_f))=\left[x_f-8637,z_f\right]\\ u_\alpha{}^L\le\left|u_\alpha\right|\le u_\alpha{}^U\\ u_\mu{}^L\le\left|u_\mu\right|\le u_\mu{}^U\end{cases} \tag{5.14}$$

The bounds of the states and controls were also adjusted for the new maneuver as shown in Table 13.

Table 14. Bounds the States and Controls for Minimum Time Maneuver

State	Lower Bound	Upper Bound	Units
x	0	10000	m
y	-100	100	m
z	0	2000	m
v	100	625	m/s
σ	-π/6	π/6	rad
γ	-π/6	π/6	rad
Control			
α	-0.349	0.489	rad
μ	-0.0872	0.0872	rad
u_α	-0.349	0.489	rad/sec
u_μ	-0.0872	0.0872	rad/sec

This problem was then solved utilizing the procedures described in Section C of this chapter. The problem produced a feasible result and was then scaled by utilizing the following designer units to refine the solution:

```
SCALES.X = 100;
SCALES.Y = 100;
SCALES.Z = 100;
SCALES.V = 50;
SCALES.SIGMA = 1;
SCALES.GAMMA = 0.1;
SCALES.ALPHA = 1;
SCALES.MU = 1;
```
(5.15)

b. Verification and Validation

As with the maximum range OCP, the results for the minimum time problem were verified against the necessary conditions (omitted for brevity) and propagated through the dynamics equations for the problem, Equation (2.7), using the ODE45 solver in MATLAB. The results of the propagation were plotted against the DIDO solution for all of the states. The data are shown in Figures 66–69.

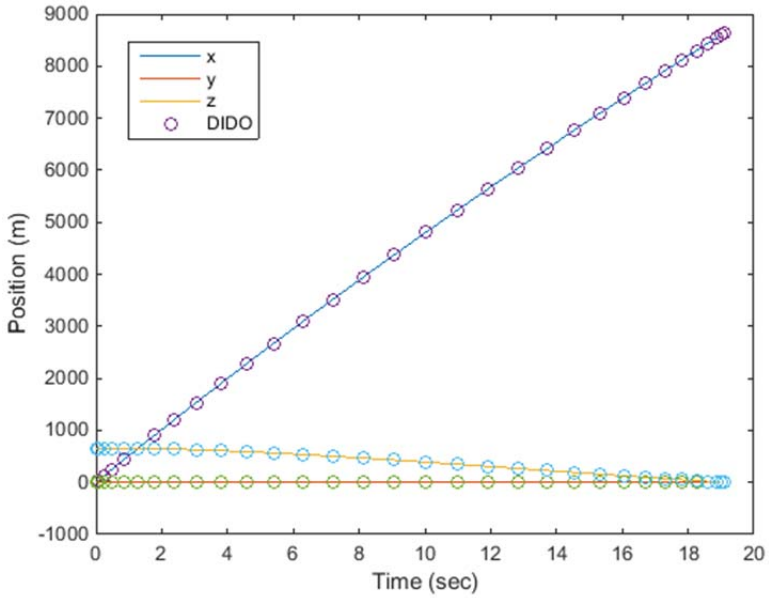

Figure 66. Verification of Missile Trajectory for Minimum Time Maneuver

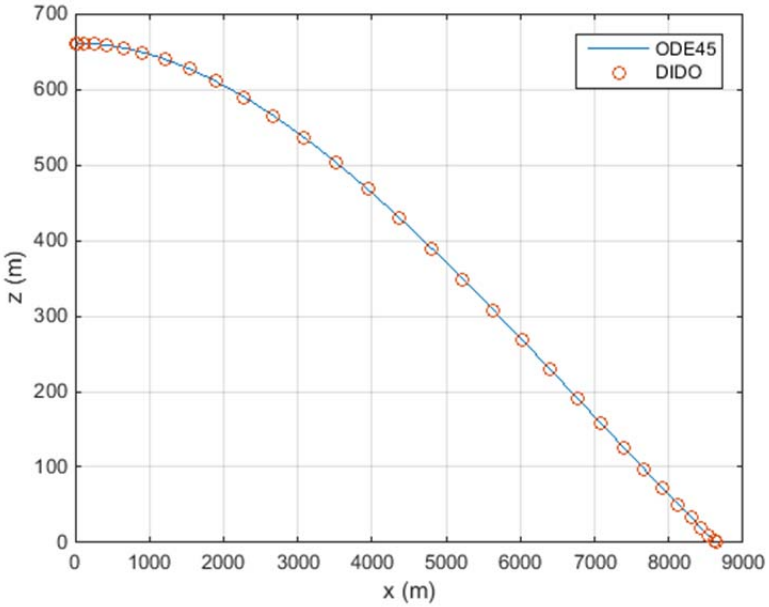

Figure 67. Verification of Missile Trajectory for Minimum Time Maneuver

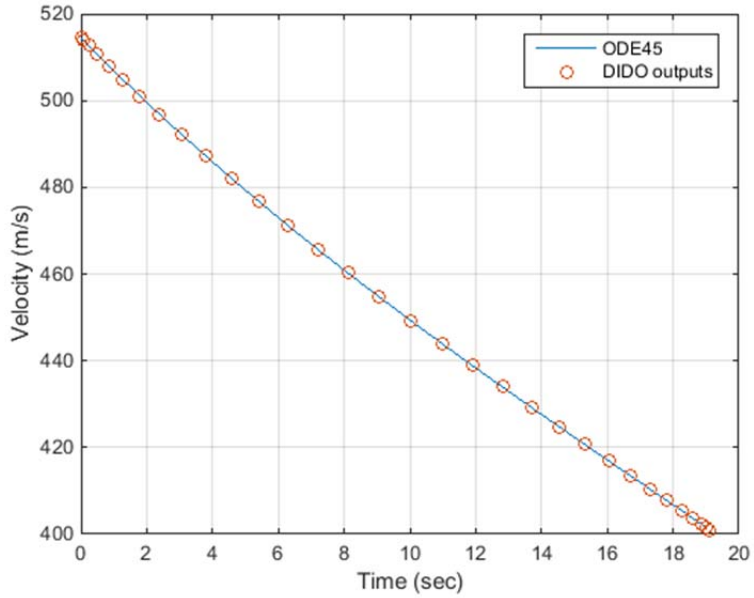

Figure 68. Verification of Velocity Vector for Minimum Time Maneuver

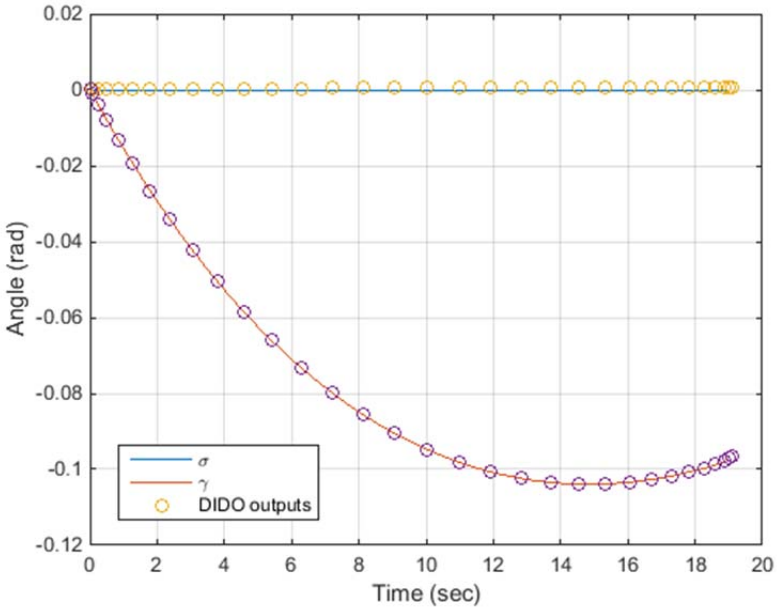

Figure 69. Verification of Flight Angles for Minimum Time Maneuver

The propagated states for the minimum time problem shown in the Figures above were obtained by propagating the controls for the maneuver shown in Figure 70.

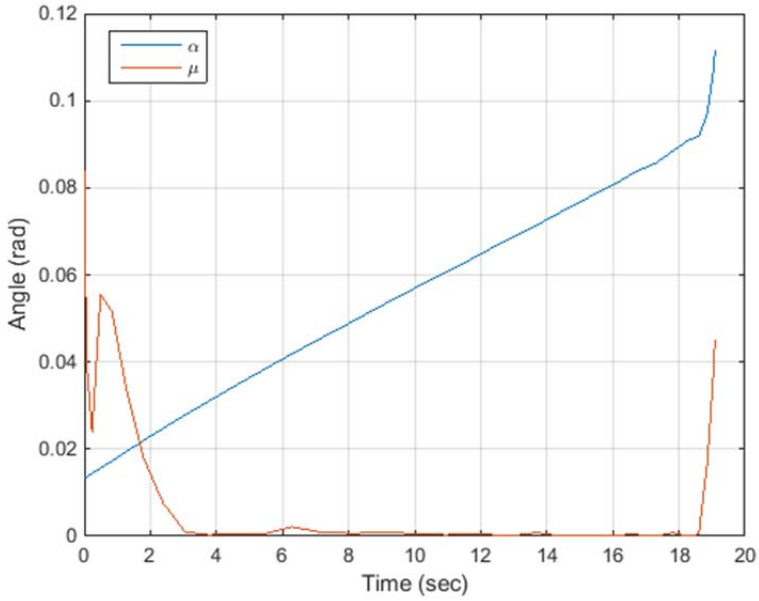

Figure 70. Controls versus Time for Minimum Time Maneuver

c. Comparison of the Results

Once the results are verified as in the previous section, they can be compared to the conventional approach. When the trajectories of the missile are plotted against each other for both methods, shown in Figure 71, the differences between the two paths can be seen. While the conventional approach produced a mostly linear response, the optimal control solution caused the missile to fly on a more parabolic trajectory.

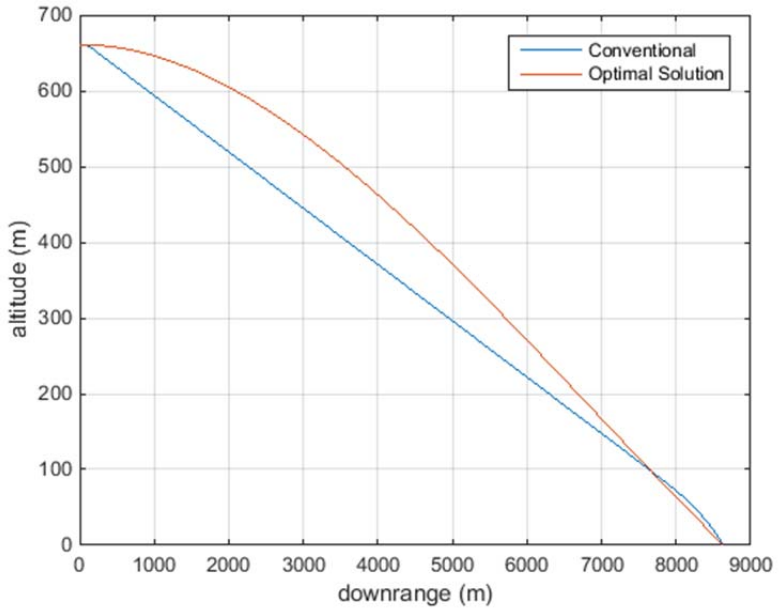

Figure 71. Comparison of Missile Trajectory for Conventional and Optimal Control Methods for Minimum Time Problem

While the trajectories show the two different paths that the missile takes to arrive at the same point, they do not provide any useful metric for comparing the two results. When the time of flight is plotted for both of the solutions, Figure 72, the effects of the different trajectories can be seen. As mentioned earlier in this chapter, the missile impacts the ground at a time of 32.3 seconds when using the conventional proportional guidance based control. When the missile is flown utilizing the optimal control solution, the missile is able to reach the target in a time of 19.1 seconds. The optimal control solution

results in a reduction of about 40% of the flight time required for the conventional approach, which can provide an advantage for the warfighter.

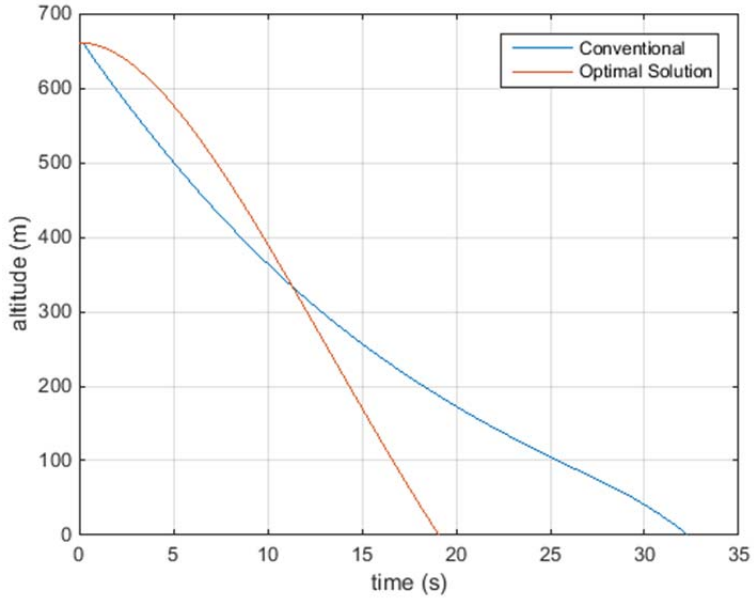

Figure 72. Time of Flight Comparison for Conventional and Optimal Control Methods for Minimum Time Problem

The last comparison that was done for the minimum time problem was a comparison of the final velocity upon impact, shown in Figure 73. The conventional approach produces a final velocity of 130.2 m/s on impact, while the optimal control solution produced a final velocity of 401.0 m/s on impact. The optimal control solution velocity is greater than the conventional approach velocity by a factor of approximately 3. Depending on the desired target, an increase in the maximum velocity may allow the missile to penetrate targets that had previously been impenetrable using conventional means.

The terminal velocity obtained using optimal control is significantly larger than proportional navigation. To determine whether the increase is possible on the real missile (without violating other unmolded constraints), a more detailed simulation study must be performed, including a 6DOF simulation and analysis of structural loads. If the solution

developed using the reduced order model is feasible for flight implementation a significant tactical advantage may be possible simply by updating the missile flight paths.

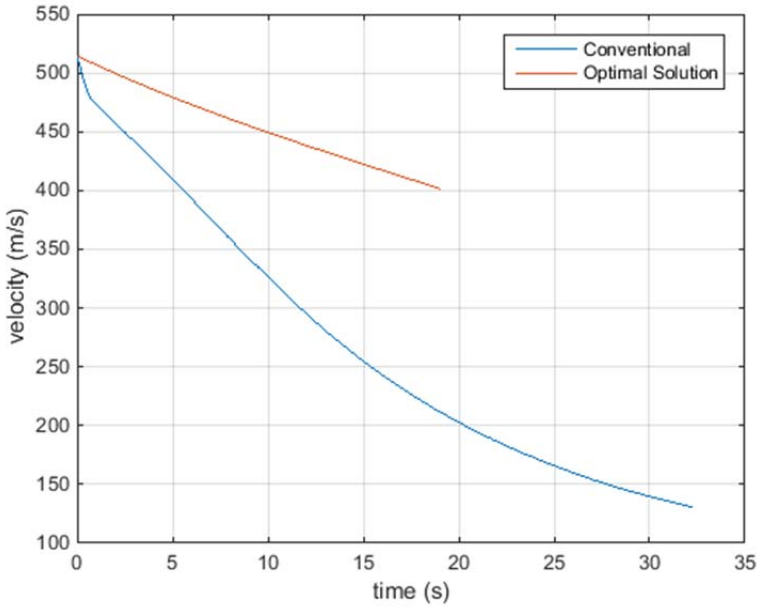

Figure 73. Comparison of Velocity versus Time for the Minimum Time Maneuver

E. SUMMARY

In this chapter optimal control theory was used to obtain a guidance solution to maximize the range of the fictitious missile under study. The bounds and conditions that were used for the problem setup as well as development of the necessary conditions for optimality were shown. The results of the solutions obtained using DIDO were presented and discussed. A minimum time maneuver of the fictitious missile was also obtained and the results of the solution obtained by DIDO were presented and discussed. The resulting maneuvers were compared to the conventional proportional navigation based solution and significant enhancements of the missile performance were observed using the optimal control-based approach.

THIS PAGE INTENTIONALLY LEFT BLANK

VI. CONCLUSIONS AND FUTURE WORK

A. CONCLUSIONS

The intent of this thesis was to apply advances in optimal control theory, namely pseudospectral optimal control, to improve the range of a missile without changing any of the physical characteristics of the missile or its hardware. This software only approach could be used to replace conventional guidance logic, which has not changed in over 50 years. Additionally, this thesis was intended to contribute useful research that can be built on for other applications such as intercontinental ballistic missiles and related space systems.

A reduced-order 3DOF model with simplifying assumptions was used to generate an optimal missile trajectory that provided nearly 300% increase in the maximum range of the missile over the conventional proportional navigation-based approach. The newest variants of the medium-range air-to-ground missiles in the United States Order of Battle have a ranges that tend to fall from 80–100nm. An increase in range in the terminal phase of flight by 8.75 nm is therefore a significant improvement in the reach of the missile.

In a minimum time maneuver, it was shown that the time of flight could be reduced by about 40% over conventional proportional navigation. While the optimal control solutions could be obtained in a reasonable amount of time, the MATLAB based process could not produce the solution in real time. Nonetheless, computing an optimal trajectory prior to flight allows for the optimal trajectory to be implemented by storing the appropriate commands. Moreover, it may be possible to obtain real-time solutions if a specialized code is developed for these problems, which would increase the utility of the optimal control-based approach for missile guidance.

B. FUTURE WORK

The work that was done in this thesis provides a good starting point for continued work on this problem. This thesis was limited to investigating only the mid-to-terminal phase of a missiles flight path, once the rocket motor was burned out. Expanding the flight profile to include the other stages of flight will provide a more complete picture on

the advantages that can be obtained through use of optimal control. The results that were found when examining just the final stage of flight, suggest that if the optimal control is applied throughout the entire flight of the missile, the range of a missile could be further increased or other performance benefits obtained. In addition, it would be helpful to explore the range of conventional mid-course guidance algorithms as compared to optimal control-based solutions.

The problem examined in this thesis assumed the missile would intercept a stationary target. One of the obvious next steps is to apply optimal control theory to a missile intercept problem involving a moving target. The principles of finding an optimal path to intercept a moving target can not only impact the guidance of missiles but can impact the other area where proportional navigation type laws are used, such as aircraft intercepting moving targets or satellites performing close proximity rendezvous.

LIST OF REFERENCES

[1] Anonymous 2010, "Rockets and Missiles," 2015(Oct 15), www.wsmr.army.mil/PAO/WUAWS/Pages/Rocketsandmissiles.aspx.

[2] United States Bureau of Naval Personnel, 1959, "Principles of Guided Missiles and Nuclear Weapons," Washington, DC.

[3] United States Department of the Air Force, 1958, Guided Missiles: Operations, Design, and Theory, McGraw-Hill Book Company Inc., New York.

[4] Haeussermann, W., 1981, "Developments in the Field of Automatic Guidance and Control of Rockets," Journal of Guidance, Control and Dynamics, 4(3), pp. 225–239.

[5] Warbirds Resource Group, "Fi-103/V-1 "Buzz Bomb," 2015(Nov 12), http://www.warbirdsresourcegroup.org/LRG/v1.html.

[6] Arkell, H., 2014, "Death from Above without Warning: 70 Years After the First One Fell, Interactive Map Reveals just Where Hitler's V2 Rockets Killed Thousands of British Civilians in Final Months of WW2," Daily Mail, 2015(Nov 13), http://www.dailymail.co.uk/news/article-2750353/Interactive-map-reveals-hundreds-sites-Hitler-s-V2-rockets-killed-thousands-British-civilians-final-months-WW2.html.

[7] Zarchan, P., 2007, "Tactical and Strategic Missile Guidance," American Institute of Aeronautics and Astronautics, Inc., Reston, VA.

[8] Fossier, M. W., 1984, "The Development of Radar Homing Missiles," The Journal of Guidance, Control, and Dynamics, 7(6), pp. 641–651.

[9] Parsch, A., "Lark," Encyclopedia Astronautica, 2015(Nov 14), http://www.astronautix.com/lvs/lark.htm.

[10] Lockheed Martin, 2014, "Trident II D5 Missile Reaches 150 Successful Test Flights," 2015(Nov 13), http://www.defencetalk.com/trident-ii-d5-missile-reaches-150-successful-test-flights-59786/.

[11] Sax, L. R., 2015, "U.S. Army Acquires APKWS™ Laser-Guided Rockets for Immediate Deployment," 2015(Nov 13), http://www.baesystems.com/en-us/article/u-s--army-acquires-apkws--laser-guided-rockets-for-immediate-deployment.

[12] Hawley, P. A., and Blauwkamp, R. A., 2010, "Six-Degree-of-Freedom Digital Simulations for Missile Guidance, Navigation, and Control," John Hopkins APL Technical Digest, 29(1), pp. 71–84.

[13] Lange, A. W., 1998, "Hellfire: Getting the most from a Lethal Missile System," Armor, Jan-Feb, pp. 25-30.

[14] Lin, C. F., 1987, “Analytical Solution of Optimal Trajectory-Shaping Guidance,” Journal of Guidance, Control, and Dynamics, 10(1), pp. 60–66.

[15] Ross, I. M., 2015, “A Primer on Pontryagin’s Principle in Optimal Control,” 2ed., Collegiate Publishers, Carmel, CA.

[16] Ross, I. M., and Karpenko, M., 2012, "A Review of Pseudospectral Optimal Control: From Theory to Flight," Annual Reviews in Control, 36, pp. 182-197.

[17] Air Force Research Laboratory, 2011, “Missile DATCOM Software.”

[18] Bollino, K. P., 2006, “High-Fidelity Real-Time Trajectory Optimization for Reusable Launch Vehicles,” Ph. D dissertation, Naval Postgraduate School, Monterey, CA.

[19] Savage, M. K., 2012, “Design and Hardware-in-the-Loop Implementation of Optimal Canonical Maneuvers for an Autonomous Planetary Aerial Vehicle,” MS thesis, Naval Postgraduate School, Monterey, CA.

[20] Barnard, R.H., and Philpott, D.R., 1995, "Aircraft Flight," Longman Group Limited, Essex, England.

[21] Arledge, R. K., 2014, “Conventional Implementation of Optimal Controls for Pointing Problems,” MS thesis, Naval Postgraduate School, Monterey, CA.

[22] Ross, I. M., and Karpenko, M., 2011, “AE4850: Astrodynamic Optimization Course Notes,” Naval Postgraduate School, Monterey, CA.

[23] Ross, I. M., 2007, “A Beginner’s Guide to DIDO- A MATLAB Application Package for Solving Optimal Control Problems,” Elissar LLC, Monterey, CA.

[24] Karpenko, M., 2014, “DIDO Tutorial: Scaling & Refining Solutions,” Naval Postgraduate School, Monterey, CA.

INITIAL DISTRIBUTION LIST

1. Defense Technical Information Center
   Ft. Belvoir, Virginia

2. Dudley Knox Library
   Naval Postgraduate School
   Monterey, California